Master's thesis and Internship : Coordinating Transmission And Distribution System Operators Through Secure Operating Envelopes.

Auteur : Maio, Anthony
Promoteur(s) : Ernst, Damien
Faculté : Faculté des Sciences appliquées
Diplôme : Master : ingénieur civil en génie de l'énergie à finalité spécialisée en Energy Networks
Année académique : 2025-2026
URI/URL : http://hdl.handle.net/2268.2/26142

Coordinating Transmission And Distribution System Operators Through Secure Operating Envelopes

Maio Anthony

Thesis presented to obtain the degree of:
Master of Science in Energy Engineering

Thesis supervisor:
Ernst Damien

Academic year: **2025 - 2026**

Preface

This thesis was carried out as part of my master's studies in Energy Engineering and focuses on improving the coordination between transmission and distribution system operators. It was conducted within the Smart Grid Lab of the Montefiore Institute (University of Liège), in the context of a collaboration between the Smart Grid Lab and French industrial partners, namely Réseau de Transport d'Electricité (RTE), i.e, the French transmission system operator, and Gérédis Deux-Sèvres, a French distribution system operator.

The developments proposed in this manuscript build upon a research article to which I contributed and that I co-authored. This research article, which can be found in [1], presents the formalization of a new coordination framework relying on the concept of operating envelopes. This concept and, more generally, the coordination framework, are detailed in chapter 3. Scientific contributions of [1] form the basis for the models, methodologies, and analyses developed in this thesis.

The present document aims to consolidate and extend these contributions. This thesis reflects the outcomes of this research and is primarily intended for professionals and researchers in power system operation, while remaining accessible to readers with a general engineering background.

Acknowledgments

First of all, I would like to express my deepest gratitude to my supervisor, Pr. Damien Ernst, who has been my mentor for more than two years. As an undergraduate student, I discovered the exciting world of research within his research lab, the *Smart Grid Lab* of the Montefiore Institute, where I have always felt welcome. Under his guidance, I have grown as a scientist but also as a citizen.

I also want to thank my co-authors with whom I had the opportunity to work on multiple scientific publications related to this Master Thesis. In particular, I want to thank Victor Dachet, Maurizio Vassallo, Adrien Bolland, and Raphael Fonteneau for their guidance and their patience in teaching me *the art of research* alongside Pr. Damien Ernst.

I am thankful to all the industrial partners with whom I interacted to bring this work to fruition: Olivier Bronckart (Elia, Belgium), Vincent Barbesant and Julien Callec (RTE, France), Sebastien Haye and Dorian Fourniret (Geredis, France). Their extensive understanding of the industry greatly helped me enhanced the practical application of this work.

Finally, I want to thank my parents who always believed in me and gave me the strength to always move forward.

"*Finding is nothing. The difficulty is to add to oneself what one finds.*"
Paul Valery, 1896.

Summary

Motivation and Objectives

The growing penetration of renewable and distributed energy resources (DERs) within electrical networks, including photovoltaic systems (PVs), electric vehicles, and battery energy storage systems, has significantly increased the complexity of power system operation. This increased complexity has led to more frequent violations of security constraints, such as voltage excursions or congestion, across multiple network levels, requiring local operators to implement corrective actions more frequently. These local interventions can impact other parts of the system and potentially induce operational limits violations elsewhere, which must then be addressed by other operators. This growing interdependence between network levels results in more complex control processes, which typically necessitate extensive data exchange between system operators. To tackle these issues, there is a need for coordination methods between different system operators.

This thesis presents a coordination method between operators that ensures static network security when grid operation is distributed across interconnected subnetworks operated by independent entities that follow a hierarchy. This coordination method is formalised in [1], a scientific article to which I contributed as co-author. In this thesis, a variant of this coordination procedure is presented. The hierarchy consists of a parent network (typically the transmission network) connected to child networks (typically the distribution networks). The coordination of these hierarchical networks is based on power and voltage magnitude ranges at their interfaces. The voltage magnitude ranges, called voltage operating envelopes (VOEs), are first agreed upon, and the power limits, called power operating envelopes (POEs), are then computed to ensure local security for all operating conditions on the children's networks.

In this thesis, this coordination approach is detailed and particularized to TSO/DSO coordination, where the TSO computes POEs at the interface with DSOs, based on agreed VOEs. An optimisation problem is proposed to compute POEs at TSO/DSO interfaces, defining admissible operating regions that DSOs must respect during operation. As long as DSOs respect the POEs, there exists a set of control actions in the TSO's network such that its network remains secure. In the proposed optimisation problem, phase-shifters' set-point modifications and the generators' re-dispatch are considered as control actions. The power flows are modeled through a quadratic convex approximation of the AC power flow equations. At the end, POEs and VOEs enable coordination among operating entities while maintaining a low level of data exchange among them.

Results

Unlike classical OPF-based approaches that determine a single optimal operating point, the proposed approach identifies intervals of secure operating points, thereby increasing operational flexibility and reducing computational and data-sharing requirements. Nevertheless, it is observed that the sizes of operating envelopes might differ drastically from one TSO/DSO interface to another, showcasing a need for regulation to ensure fairness among DSOs.

Résumé

Motivation et objectifs

La pénétration croissante des énergies renouvelables et des ressources énergétiques distribuées (systèmes photovoltaïques, véhicules électriques, stockage par batteries) au sein des réseaux électriques a considérablement accru la complexité de leur opération. Elle entraîne des violations récurrentes des contraintes de sécurité sur le réseau (excursions de tension, congestions), contraignant les opérateurs à des actions correctives plus fréquentes. Ces interventions locales peuvent affecter d'autres parties du système et y engendrer à leur tour de nouvelles violations, qui doivent être traitées par d'autres opérateurs. Cette interdépendance croissante entre réseaux voisins complexifie les processus de contrôle et requiert d'importants échanges de données entre opérateurs, d'où la nécessité de développer des méthodes de coordination entre ces derniers.

Cette thèse présente une méthode de coordination garantissant la sécurité statique du réseau lorsque son exploitation est répartie entre des sous-réseaux interconnectés gérés par des entités indépendantes hiérarchisées. Cette méthode de coordination est formalisée dans [1], un article scientifique auquel l'auteur a contribué en tant que co-auteur. Dans cette thèse, une variante de cette procédure de coordination est présentée. La hiérarchie repose sur un réseau parent (typiquement le réseau de transport) connecté à des réseaux enfants (typiquement les réseaux de distribution). La coordination repose sur des plages de puissance et de tension à leur interface : les plages de tension, ou enveloppes opérationnelles de tension (VOEs), sont convenues en premier lieu ; les plages de puissance, ou enveloppes opérationnelles de puissance (POEs), le sont ensuite afin de garantir la sécurité locale des réseaux enfants dans toutes leurs conditions d'exploitation.

Cette méthode de coordination est détaillée puis particularisée à la coordination TSO/DSO : le TSO calcule les POEs à l'interface avec les DSOs sur la base des VOEs convenues. Un problème d'optimisation est formulé à cet effet, définissant des régions d'exploitation admissibles que les DSOs doivent respecter. Tant qu'ils le font, il existe un ensemble d'actions de contrôle dans le réseau du TSO tel que ce dernier demeure sécurisé. Dans le problème d'optimisation proposé, les modifications du point de fonctionnement des déphaseurs et le redispatching des générateurs sont considérés comme actions de contrôle, et les flux de puissance sont modélisés par une approximation quadratique convexe. POEs et VOEs assurent ainsi la coordination tout en limitant les échanges de données entre opérateurs.

Résultats

Contrairement aux approches classiques fondées sur l'OPF, qui déterminent un unique point de fonctionnement optimal, l'approche proposée identifie des intervalles de points de fonctionnement sécurisés, augmentant la flexibilité opérationnelle et réduisant les besoins en partage de données. On observe néanmoins que la taille des enveloppes peut varier considérablement d'une interface TSO/DSO à l'autre, soulignant la nécessité d'un cadre réglementaire pour garantir l'équité entre DSOs.

Contents

List of Figures

List of Tables

List of Symbols

ACER	Agency for the Cooperation of Energy Regulators
AC	Alternating Current
ANM	Active Network Management
BESS	Battery Energy Storage System
BRUGEL	Régulateur Bruxellois pour l'Énergie
CAPEX	Capital Expenditures
CREG	Commission de Régulation de l'Électricité et du Gaz
CWaPE	Commission Wallonne pour l'Énergie
DC	Direct Current
DER	Distributed Energy Resource
DRA	Demand Response Aggregator
DR	Demand Response
DSO	Distribution System Operator
EV	Electric Vehicle
HC	Hosting Capacity
HV	High Voltage
ICT	Information and Communication Technology
IEEE	Institute of Electrical and Electronics Engineers
LACPF	Linearised AC Power Flow
LEM	Local Energy Market
LP	Linear Programming
LV	Low Voltage
MILP	Mixed-Integer Linear Programming
MISOCP	Mixed-Integer Second-Order Conic Programming
ML	Machine Learning

MV	Medium Voltage
OE	Operating Envelope
OPEX	Operational Expenditures
OPF	Optimal Power Flow
p.u.	Per Unit
P2P	Peer-to-Peer
POC	Point of Connection
POE	Power Operating Envelope
PV	Photovoltaic
QC	Quadratic Convex
RTE	Réseau de Transport d'Électricité
SCADA	Supervisory Control and Data Acquisition
SCOPF	Security-Constrained Optimal Power Flow
SC	Synchronous Condenser
SDP	Semidefinite Programming
SOCP	Second-Order Conic Programming
SOC	Second-Order Cone
SOGL	System Operation Guideline
SVC	Static Var Compensator
TSO	Transmission System Operator
UTOPF	Unbalanced Three-Phase Optimal Power Flow
VOE	Voltage Operating Envelope
VREG	Vlaamse Regulator van de Elektriciteits- en Gasmarkt

Chapter 1

Introduction

1.1 Motivation

Global warming has emerged as a major threat to our societies [6]. In an effort to reduce anthropogenic emissions, which have been proven to be the main driving force behind climate change [7], governments have encouraged the development of renewable production and flexible loads. The growing integration of renewable and distributed energy sources (DERs) such as photovoltaic (PV) systems, electric vehicles (EVs), and battery energy storage systems (BESSs) into our power systems has led to a significant increase in their operational complexity. The Iberian blackout in April 2025 is a reminder that this increased complexity can lead to widespread system outages [8, 9].

Historically, electricity generation was primarily provided by large synchronous generators connected to the transmission network. Power flows were therefore largely predictable, from transmission to distribution systems. With the increasing penetration of DERs in distribution networks, this paradigm has changed. Power flows have become more uncertain, significantly increasing the operational complexity of our electrical network. As a result, challenges such as balancing issues, voltage excursions, and network congestion occur more frequently. Distribution system operators (DSOs) are now required to take more control actions to preserve the continuity and quality of electricity supply for consumers.

However, actions taken at the distribution level might directly affect the transmission system. Despite this growing interdependence, transmission system operators (TSOs) and DSOs still do operate their networks with full independence.

To address these issues, an active field of research seeks to implement coordination approaches between TSOs and DSOs. Existing approaches typically rely on centralized optimal power flow (OPF) formulations, extensive data exchange, and detailed system models, resulting in large-scale, nonlinear optimisation problems that remain difficult to solve and deploy in practice.

As existing approaches do not seem scalable enough, the objective of this thesis is to develop coordination methods based on limited data exchange. More specifically, this thesis proposes a decoupled power system operation framework that guarantees the static operational security of power systems operated by multiple independent entities. In the developed framework, power and voltage magnitude ranges are imposed at the interface between TSOs and DSOs to ensure the secure operation of the network. These ranges are referred to as power operating envelopes (POEs) and voltage operating envelopes (VOEs), respectively.

1.2 Scientific Contributions

This section summarizes the scientific contributions of this work. The starting point of this thesis is the coordination framework and its mathematical formalisation introduced in [1], a scientific article to which the author contributed as co-author. The present thesis consolidates, extends, and validates that framework in several directions, and its original contributions are the following:

1. This thesis presents a variant of the coordination procedure developed in [1]. In this thesis, VOEs are not computed but rather assumed to be agreed upon through a negotiation process, prior to POE computation. The rest of the coordination procedure remains unchanged. The parent network and its child networks coordinate through voltage and power ranges at their interfaces. This coordination procedure is detailed and positioned with respect to the existing literature on TSO/DSO coordination.

2. This thesis extends the POE computation model of [1] in three directions: (i) phase-shifting transformers are included as an additional controllable asset, with an associated operational cost term; (ii) generator P-Q capability regions are modelled through elliptical second-order cone constraints, replacing the simplified box constraints of the original model; and (iii) the linearised AC power flow model is replaced by a quadratic convex (QC) relaxation, providing a tighter convex approximation of the AC power flow equations.

3. The extended POE computation model is implemented and validated on two test networks, namely a modified IEEE 14-bus network and the PandaPower Multi-Voltage network. The influence of phase-shifters on envelope quality is assessed, a sensitivity analysis of the model parameters is carried out, and the results are compared against a DC-based benchmark model.

1.3 Document Organization

This thesis is divided into several chapters, each focusing on a particular aspect of the research. The manuscript is therefore organized as follows:

Chapter 2: Literature Review. This chapter reviews the different existing approaches in the literature for coordinating TSOs and DSOs. The concept of operating envelopes, as defined in the literature, is also presented.

Chapter 3: Coordination procedure. This chapter provides the proposed coordination procedure for the operation of hierarchical power systems based on operating envelopes.

Chapter 4: Model Developments and Experimental Methodology. This chapter extends the POE computation model by integrating additional model features. Moreover, it presents the test networks used to validate the approach.

Chapter 5: Results and Discussion. This chapter describes the results obtained through the application of the POE computation model to the test networks. This chapter also discusses sensitivity analyses of the model's parameters.

Chapter 6: Future Perspectives. This chapter provides potential future research directions and, in particular, discusses additional POE computation model enhancements.

Chapter 7: Conclusions. The final chapter highlights the main findings of this thesis.

Chapter 2

Literature review

2.1 Preliminaries

This master's thesis is dedicated to developing a novel approach for the coordination between TSOs and DSOs using a mathematical object called Dynamic Operating Envelopes (DOEs), which corresponds to a set of acceptable power flow exchanges generally applied at the point of connection (POC) between an end-user (e.g, consumer, prosumer) and the public grid. This thesis is on the frontier between these two research topics (i.e, TSO/DSO coordination and DOEs). The first chapter of this thesis is dedicated to a state-of-the-art review of both topics. More specifically, section 2.2 explores the differences in terms of operation between TSOs and DSOs, motivates the need for increased coordination, and discusses different methods to coordinate TSOs and DSOs proposed in the literature. On the other hand, section 2.3 investigates the current applications for DOEs as well as the computation methods used to determine DOEs.

2.2 Coordination Methods between TSOs and DSOs

2.2.1 Preliminaries

Network operation is generally shared between TSOs and one or multiple DSOs. Their common goal is to ensure the secure, reliable, and efficient operation of their network while maintaining power quality and respecting operational constraints (e.g, current and voltage magnitude limits). However, their control strategies to reach these goals might differ significantly.

On the one hand, TSOs typically perform large-scale security-constrained OPF computations. Early formulations were introduced in [10], while more comprehensive surveys of OPF methods were later provided by authors in [11]. These approaches are widely used to support both long-term planning and near-real-time operation decisions, as discussed in [12].

On the other hand, DSOs increasingly rely on centralized active network management (ANM) to coordinate DERs. Authors in [13] show how ANM can help maintain the distribution network within operational limits in quasi-real-time by performing, among other control actions, Volt-VAR control and active power curtailment. More recently, authors in [14] and [15] illustrate that ANM techniques can significantly increase hosting capacity while limiting the need for grid reinforcement.

In both transmission and distribution systems, OPF-based formulations remain a key tool for translating forecasts and measurements into control actions that ensure secure operation, such as respecting current and voltage magnitude limits. The increasing penetration of DERs is, however, leading to more frequent security issues across multiple network levels. Authors in [2] highlight how this trend requires local operators to undertake an increasing number of corrective actions, which may in turn affect other parts of the network and generate new security constraints. This growing interdependence between network levels results in more complex control processes and substantial data exchanges among grid operators.

2.2.2 Coordination methods: a classification

To cope with these challenges, an active field of research aims at developing TSO/DSO coordination approaches. As the number of developed approaches is numerous, several literature reviews have been proposed to classify them. These reviews identify some common requirements for efficient coordination between TSOs and DSOs. In particular, they emphasize that DSOs must adopt a more proactive role in the operation of their networks. This implies shifting away from the classical *fit-and-forget* approach and investing in automation, smart metering, and data analytics to improve network observability and enable a more flexible grid, as mentioned in [16].

Therefore, as highlighted in [2], the adoption of any coordination model will increase both capital and operational expenditure (CAPEX and OPEX) of distribution networks. On the other hand, an increased availability of DER services will, in turn, allow the TSO to increase its reliance on DER, potentially reducing cost for the whole system in the long term.

A reference TSO/DSO coordination approaches classification is the one proposed by the authors in [2], where three core TSO-DSO coordination models for the provision of DER services, from the many proposed in the literature, are identified. These core models rely on TSO-managed, TSO-DSO hybrid-managed, and DSO-managed approaches. The classification in [3] only separates centralized and decentralized models. In practice, unification between these classifications exists. For example, the TSO-managed model corresponds to centralized models. The unified classification is depicted in Figure 2.1, relying on the works of both [2] and [3].

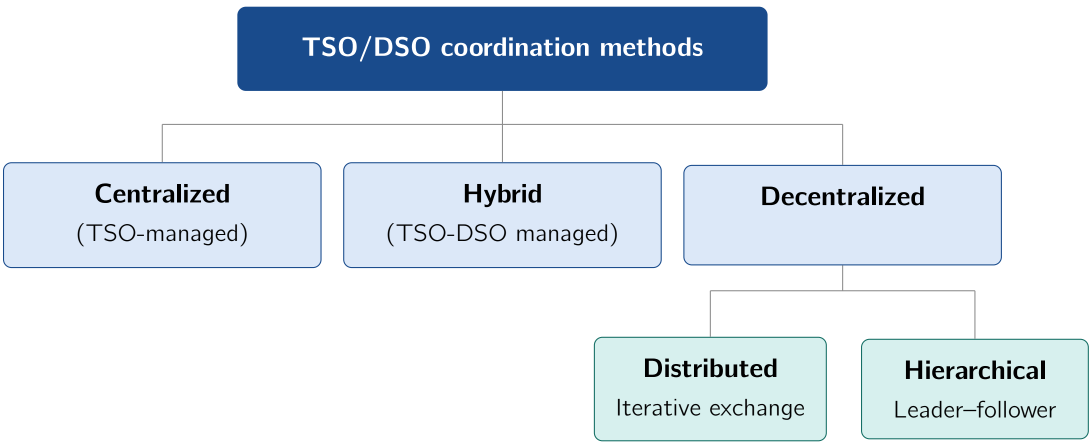

Figure 2.1: Unified classification of TSO/DSO coordination methods, adapted from [2] and [3].

TSO-managed or centralized approach. In this coordination approach, a single entity (i.e, the TSO) is responsible for performing a fully centralized dispatch considering both transmission and distribution network constraints. This includes, among other actions, managing on-load tap-changer or phase-shifter setpoints, active and reactive power generation setpoints, shunt reactors, and capacitor bank activation/deactivation within all network levels.

In this approach, DSO's responsibilities remain limited and consist mainly of providing real-time operational data to the TSO and performing maintenance. Proposals for this centralized approach often involve solving a single large-scale optimisation model, as illustrated in [17–20].

TSO-DSO hybrid-managed approach. In this intermediate coordination approach, the TSO is still responsible for the centralized dispatch, but the DSO is required to validate DER injection/withdrawal estimates, called bids, beforehand, such that the distribution network remains secure. In other words, DERs send their bids directly to the TSO for a given period, and the DSO is required to check the consistency of these bids with network security. The bids are then sent to the TSO. Finally, the TSO performs the dispatch and sends the dispatch commands to the DERs.

Compared to the first approach, there is no need for the TSO to verify bid consistency with distribution network constraints, as this is managed by the DSO. Specific instantiations of this general approach are presented in [21, 22].

Decentralized approach. In this last approach, the large-scale optimisation problem is decomposed into smaller subproblems, each of which is solved separately. Decentralized coordination methods are typically classified into either *distributed* or *hierarchical* schemes.

In *distributed* schemes, TSOs and DSOs solve their own optimisation subproblems by decomposing the problem along boundary bus variables, and iteratively exchange results with one another until convergence to an equilibrium is reached, as illustrated in [23–26]. For example, distributed optimisation methods that aim to preserve operator sovereignty are explored in [27].

In *hierarchical* schemes, by contrast, coordination follows a leader–follower structure, where the leader solves its optimisation problem first and communicates the resulting decisions to the followers, who then optimise their own subproblems subject to those decisions as fixed parameters. This sequential, top-down structure preserves a clear chain of authority between operators while avoiding the iterative communication rounds required by distributed schemes. An instance of this coordination paradigm is investigated in [28].

The presented classification is performed depending on the level of centralization of the coordination. Alternative classifications can also be defined, for example, according to whether models are deterministic or stochastic/robust, or whether they are linear/convex or non-convex.

For instance, authors in [29] propose a deterministic decentralized TSO/DSO operational method based on a Lagrangian relaxation of the power flow balance constraints at the interfaces between the TSO and DSOs. The idea behind this method is to decompose the optimisation problem into manageable subproblems and to coordinate subproblem solutions through the iterative update of Lagrangian multipliers, until convergence, i.e., until power flow balance constraints at the interfaces are respected. This method can therefore be classified as a *distributed* approach.

However, deterministic optimisation approaches, which do not account for parameters' uncertainty, have shown clear limitations in the case of a large-scale DER penetration. They have thus been gradually replaced by stochastic and robust approaches. In fact, researchers have been gradually focusing on stochastic and robust approaches for the coordination between TSOs and DSOs.

In [30], the authors investigate reactive power support from the DSOs to the TSO via a stochastic AC-OPF optimisation problem. For that, the uncertainty of DERs is modeled by scenarios for which a certain probability is associated. In [31], the authors solve a stochastic TSO/DSO coordinated security-constrained unit commitment problem. Authors in [32] even propose a coordinated expansion planning problem using second-order conic programming (SOCP). The results show that the coordinated planning framework outperforms conventional independent methods by decreasing expansion investment.

2.2.3 Limitations of coordination methods

Even though many coordination models have been proposed in the literature, a large majority of these approaches fail to reach the pilot stage. An extensive review of the main barriers to the practical implementation of TSO/DSO coordination methods has been proposed by authors in [4] and [5]. This section aims to highlight the main findings of these works and, in particular, to classify the main limitations of current coordination approaches.

According to these works, limitations arise due to *technical*, *economic* and/or *regulatory* challenges, as depicted in Figure 2.2.

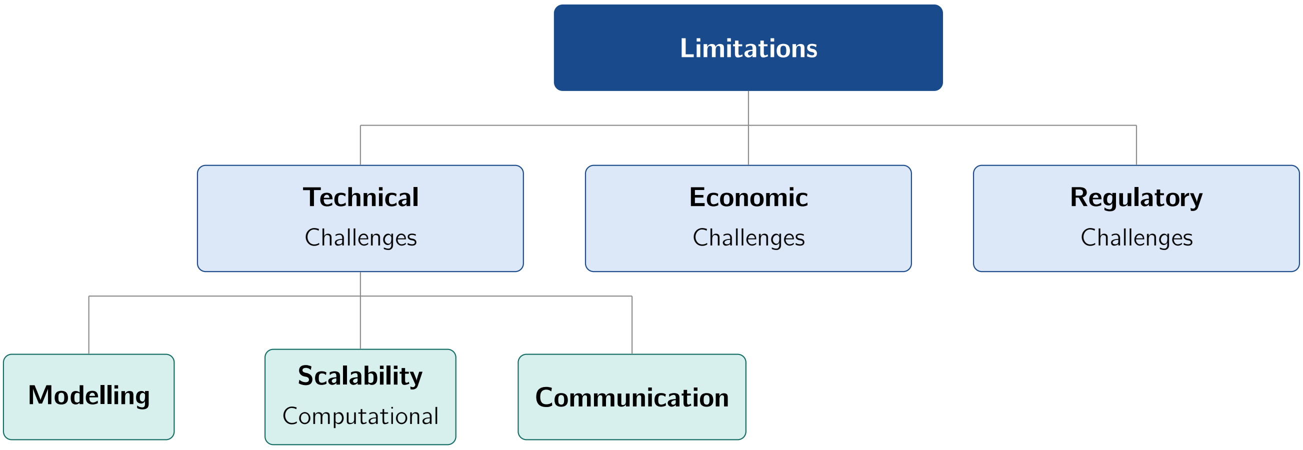

Figure 2.2: Classification of the main limitations of TSO/DSO coordination methods reported in the literature [4, 5].

Technical limitations. These limitations arise as the early-stage reasons for the implementation failure of coordination methods. Technical limitations include *modelling*, *scalability*, and *communication* challenges. *modelling* challenges refer to the difficulties of precisely modelling electrical networks. It is well-known in power systems that the steady-state three-phase power flow equations are highly nonlinear [33, 34] and can, in general, not be exploited as such. In general, power flow modelling involves relaxation and linearization, which is practical but might fail to accommodate real-network constraints.

Scalability challenges arise from the sheer size of modern power systems: detailed network models covering both transmission and distribution levels lead to very large optimisation problems with high computational requirements.

Finally, *communication* challenges refer to the inadequate information and communication technology (ICT) infrastructure currently available in many grid operators' systems and the high cost of upgrading it. Beyond infrastructure, the lack of willingness to share data across system boundaries is a recurring obstacle: reactive power forecasts, for example, are typically not exchanged between operators. The coexistence of different and incompatible ICT systems across TSO and DSO boundaries also introduces additional security risks and increases the likelihood of erroneous alarms during operations.

Economic limitations. Even when a coordination approach is technically feasible, its deployment is frequently hindered by economic barriers [5]. A first challenge is the absence of established market mechanisms for the procurement and remuneration of flexibility services at the TSO/DSO interface. In existing markets, the limited experience with such products leads to cautious behaviour from potential participants and high perceived financial risks.

A related issue is the divergence in price expectations between flexibility buyers (system operators) and sellers (aggregators, prosumers), which makes it difficult to reach mutually acceptable clearing prices. Furthermore, the economic viability of aggregators as business models remains unclear in the absence of a dedicated regulatory framework: without guaranteed revenues, aggregators face uncertainty regarding the profitability of investing in the required infrastructure. A further obstacle is the absence of financial incentives for reactive power provision in current incentive regulation schemes: beyond minimum technical grid-connection requirements, operators have little motivation to offer reactive power services across system boundaries.

Regulatory limitations. Regulatory barriers are often the most difficult to overcome, as they require coordinated action across multiple legislative levels [5]. A first challenge is the slow adaptation of regulatory frameworks. Whether at the European, national, or regional level, the legislation evolves at a pace that is generally insufficient to keep up with the rapid development of coordination concepts. This leaves the operators in a legal grey area when attempting to deploy new approaches.

A second challenge concerns the regulatory viability of new business models. The roles of aggregators and other intermediary actors at the TSO/DSO interface are not yet clearly defined or protected by regulation, creating uncertainty that discourages investment. A related issue is the risk of strategic bidding. In emergency situations, flexibility providers may submit inflated bids to exploit the operator's urgent need, which would lead to a reduction in social welfare.

The limitations discussed above are further substantiated by a recent literature review [4], which extends the classification of deployment barriers beyond the three categories above. Specifically, the authors propose a five-dimensional framework: *modelling*, *operation*, *validation*, *communication*, and *regulation*. This five-dimensional framework is applied to 47 selected publications spanning journal articles, conference papers, pilot project reports, and technical reports. Unlike reviews that classify coordination schemes by architecture or market design alone, this framework is oriented towards deployment readiness, providing a structured basis for identifying the gap between research-oriented development and real-world implementability.

Modelling.

From a modelling standpoint, the literature has consistently prioritised computational efficiency at the expense of physical accuracy [4]. Transmission networks are typically represented through linearised DC approximations, whereas distribution networks tend to rely on convexified AC power flow models. Most studies further simplify the problem by assuming, for example, a perfect three-phase balance system. These assumptions can lead to an overestimation of the flexibility actually available in practice.

Real-world pilot projects have not escaped this tension between computational tractability and physical realism. The CoordiNet project [35], for instance, adopted a two-step strategy in which a simplified DC representation is used at the market clearing stage, followed by an AC feasibility check. This choice illustrates the following practical constraint. No matter how accurate and detailed some models may be, operational deployment imposes computational constraints that require some degree of approximation.

Operation.

A recurring pattern in the reviewed literature concerns how time is treated in coordination models. The predominant choice of one-hour time steps is poorly suited to the timescales at which grid security constraints actually bind. Voltage fluctuations, for example, unfold over seconds to minutes, well below the resolution that hourly snapshots can represent. As a result, the ability of DERs to provide fast-response services tends to be ignored.

A second and related issue is the treatment of uncertainty. Rather than explicitly accounting for the variability inherent in renewable generation and flexible demand, most coordination frameworks are built around a single deterministic approach. Coordination approaches designed under this assumption may appear robust in simulation while failing to respect network constraints under realistic, uncertain conditions. The review in [4] finds that neither issue is specific to academic work. Pilot projects exhibit the same temporal and stochastic simplifications.

Validation.

The networks on which coordination methods are tested bear little resemblance to those on which they would need to operate. Most studies rely on small or medium-scale test networks, chosen for their convenience rather than their representativeness. Testing on realistic, large-scale networks is the exception.

When the SmartNet pilot project [36] attempted to do so, the computational cost of jointly simulating transmission and distribution systems proved prohibitive, forcing the development of simplified equivalent models. This illustrates the difficulty of validating a TSO/DSO coordination approach at scale. A coordination scheme that performs well on a small benchmark test network provides limited evidence of its behaviour on a real network with thousands of nodes and stochastic injections.

Communication.

Despite ICT being widely recognised as the backbone of future smart grids, it seems to have attracted little attention in TSO/DSO coordination. Data standardisation and privacy compliance are largely absent from the academic literature, and interoperability between the ICT systems of different operators is rarely addressed. Pilot projects have consistently exposed the inadequacy of existing data frameworks. For example, both SmartNet [36] and PLATONE [37] required the deployment of supplementary hardware and dedicated secure communication protocols to enable coordination in practice.

Regulation.

Regulatory and market-related aspects remain among the least addressed dimensions despite being critical for real-world deployment. A first structural issue is that TSOs and DSOs may compete for the same DER resources. Indeed, actions that are beneficial for transmission-level balancing can simultaneously induce the violation of local distribution constraints. This situation creates incentive misalignment that no purely technical solution can resolve [19].

Furthermore, existing regulatory frameworks provide insufficient incentives for DSO participation. Regulated tariffs typically compensate capital expenditures but not the operating expenses incurred when procuring flexibility services [35, 38].

Finally, strategic behaviour, e.g, inflated bids from flexibility service providers in emergency situations, is almost entirely neglected in the literature, where cooperative actors are routinely assumed. This assumption renders many proposed mechanisms vulnerable to manipulation when deployed in a real market environment [5].

Pilot versus non-pilot studies.

A key finding of the review is the asymmetry between pilot and non-pilot studies. In the modelling and operation dimensions, both categories exhibit negligible differences. Real-world implementations do not rely on fundamentally more advanced mathematical representations and operate under the same simplifying assumptions as theoretical work.

In contrast, notable differences emerge in the validation, communication, and regulation dimensions. Pilot projects are forced to navigate data interoperability issues, stakeholder conflicts, and regulatory misalignment that theoretical studies abstract away. This asymmetry leads to coordination mechanisms that perform well under idealized simulation conditions, but that may face major practical challenges upon deployment, as highlighted in [4].

From pilot projects to commercial deployment.

Even when coordination approaches have been sufficiently convincing in pilot projects, the step towards full commercial deployment has consistently proved elusive. Regarding the pilot projects reviewed in [4], a set of recurring frictions that academic work had not anticipated has been highlighted.

Beyond these individual frictions, none of the reviewed pilot projects has demonstrated sustained, reliable operation under conditions representative of a real power system: unbalanced distribution feeders, sub-minute power variations driven by inverter-connected resources, or degraded communication links. Pilots are therefore better understood as proofs of concept than as evidence that a given approach can be deployed at scale with acceptable robustness.

Closing the gap to commercial deployment will most likely demand simultaneous progress across all dimensions identified in this review, including those such as modelling and temporal resolution, where the academic literature may give the impression of relative maturity.

Technical barriers remain significant but are increasingly well understood. It is the validation, communication, and regulatory dimensions that represent the principal bottlenecks to deployment. This observation directly motivates the coordination approach developed in the remainder of this thesis, which prioritises minimal data exchange, preserves operator independence, and is designed to remain computationally tractable at the scale of real TSO/DSO networks. This decoupled coordination relies on the concept of operating envelopes defined in section 2.3.

2.3 Operating Envelopes in Power Systems

Another active field of research consists of leveraging the concept of Operating Envelopes (OEs). Based on the definition given in [39], (Dynamic) Operating Envelopes (DOEs) are power limits ensuring power flows remain within safe limits at each DER or customer connection point. The dynamical aspect of these limits comes from their real-time adaptability to some factors, such as the time of day, location, and network conditions.

The advantages of using DOEs at DER connections are numerous. Among others, DOEs enable the improvement of the use of existing infrastructure while ensuring compliance with network constraints. Different practical applications of DOEs are studied in subsection 2.3.1, while subsection 2.3.2 reviews the state-of-the-art methods to compute them.

2.3.1 Applications of DOEs

The literature showcases that operating envelopes can be suitable for different applications. A first application of DOEs is in Local Energy Markets (LEMs), where they act as guarantees of fair access to network capacity for prosumers. Typically, including DOEs into the LEM framework enables prosumers to trade energy more efficiently while respecting network constraints, minimizing curtailment, and preserving the privacy of prosumers' data. Indeed, in this framework, prosumers can manage their assets individually within their assigned DOEs to trade in the LEM using their own bidding strategy. This framework is illustrated in [40], where the authors propose the following strategy to operate a LEM without violating any network constraint for a given time slot.

First, prior to delivery, prosumers, who are equipped with PVs and/or EV chargers, compute their expected net demands (imports) or net generations (exports), and submit these values to the DSO. The DSO verifies whether the reported imports and exports lead to any network constraint violations. If no violations are detected, the proposed values are accepted for prosumer trading. Otherwise, the DSO solves an optimisation problem to determine DOEs. Prosumers then update EVs' charging/discharging setpoints for the given time slot based on the assigned DOEs. Prosumers can generate bids to participate in peer-to-peer energy trading, which is carried out by a market operator.

Along the same line of research, the authors also propose in [41] a double auction-based peer-to-peer energy trading based on DOEs, which focuses on computational efficiency and economic fairness. Authors in [42] extend the concept of DOE-based LEM to a peer-to-peer-to-grid framework, where DOEs are not predetermined solely by the DSO but are the results of a negotiation process between the DSO and prosumers participating in peer-to-peer trading.

Other authors propose game-theory-based approaches that exploit DOEs. These approaches leverage collaboration between prosumers to maximize collective profits, as explained in [43, 44].

Alongside local-market-based applications, DOEs have also been leveraged for demand response (DR). DR is defined in [45] as *changes in electric usage by end-use customers from their normal consumption patterns in response to changes in the price of electricity over time, or to incentive payments designed to induce lower electricity use at times of high wholesale market prices or when system reliability is jeopardized.* In [46], the authors propose a two-stage, coordinated approach for residential DR participation in electricity markets under the DOE framework.

More specifically, the approach relies on the coordination between different actors, namely a DSO, demand response aggregators (DRAs), and end-users. The DSO is responsible for ensuring the safe operation of the distribution network and computing the DOEs based on its data regarding the topology and electrical parameters of the distribution network.

In this framework, all end-users are not required to adopt DOEs, only those who participate in DR. The DRA, whose role is to aggregate controllable DERs owned by end-users for the provision of DR services, has to ensure that DOEs are respected while modifying power consumption/injection setpoints of controllable DERs. The paper focuses on air-conditioning systems as controllable DER. The DRA thus has to ensure the preservation of end-user thermal comfort. Additionally, it is supposed that end-users are equipped with PV panels, which are not controllable. The sequence of actions is as follows:

1. The DSO computes DOEs for all DR-participating end-users, called DOE-customers.

2. DOEs are communicated to these customers.

3. The DRA provides DR in real-time by controlling the consumption of air conditioning loads belonging to DOE-customers.

Simulation results suggest that DR can be effectively implemented in the low-voltage network without breaching network constraints, such as voltage magnitude limits. This is promising for the deployment of DOEs in the context of DR. Regarding the computation of DOEs in this paper, it relies on an unbalanced three-phase load flow formulation. The different methods proposed in the literature to compute DOEs are further developed in subsection 2.3.2.

2.3.2 DOE Computational Methods

As mentioned in [39], DOE's computation relies mostly on OPF-based optimisation models, where the objective function might differ. Some authors account for fairness in the objective function for the allocation of DOEs (i.e, maximize the smallest DOE) [47, 48]. Others prefer minimizing the DOE's deviation from the forecasted setpoint [49]. OPF-based models often rely on relaxations of non-linear AC-OPF formulation and can even account for imbalances between phases, which is called unbalanced three-phase OPF (UTOPF) models [50].

The choice of the OPF-based model depends on the level of modelling detail required by the authors, knowing that DOEs are more likely to represent the effective hosting capacity limitations using detailed network modelling.

A limitation of the deterministic formulations described above is their sensitivity to forecast errors. In practice, both demand forecasting and impedance modelling in distribution networks are subject to uncertainty. The load forecasts may indeed be inaccurate due to, for instance, the available generation of PV systems or the charging demand of EVs, which may deviate substantially from predicted values. When such uncertainty is ignored, the resulting DOEs may be infeasible in real time, as the power injections actually realised by DERs can violate the network constraints that the DOEs were designed to enforce.

To address the issues related to uncertainty, robust and stochastic extensions of the DOE computation problem have been proposed. Robust formulations seek envelopes that remain valid for any realisation of uncertain parameters, e.g, load forecasts and impedance values, within a defined uncertainty set [50, 51]. Stochastic approaches, in contrast, relax the hard feasibility requirement and instead enforce constraint satisfaction with a prescribed probability, typically using chance-constrained or scenario-based OPF formulations [48, 52]. Both approaches incur a higher computational cost than their deterministic counterparts, and tractability typically requires the use of linearised or convex-relaxed power flow models.

A further dimension of complexity arises from the temporal structure of the problem. The adjective *dynamic* in DOE reflects the fact that the limits are time-varying. Rather than remaining fixed over long periods, they are recomputed at regular intervals, typically on a day-ahead or intraday basis. Recomputing DOEs enables the consideration of updated demand and generation forecasts, or even changes in network topology. This time-varying character introduces a multi-period dimension to the DOE computation problem.

In the most general formulation, a separate set of envelope limits must be determined for each time step of the planning horizon, subject to inter-temporal constraints arising from storage devices or ramp-rate limitations of generators [52]. The resulting problem is significantly larger than its single-period counterpart, and practical implementations often decouple the temporal dimension by solving a sequence of independent single-period OPF problems, one per time step, at the cost of ignoring inter-temporal constraints.

These extensions, i.e, robust and stochastic formulations, and multi-period horizons, substantially increase the computational burden of DOE computation. For large distribution networks with many DER connection points, even linearised formulations may become intractable when all extensions are applied simultaneously. This observation motivates the use of approximations and decomposition strategies, and represents one of the main open challenges highlighted in the literature [39].

By leveraging the concept of DOEs, which have initially been developed in distribution feeders, this thesis aims to expand this concept to the coordination between TSOs and DSOs.

Chapter 3

Coordination Procedure

3.1 Preliminaries

This thesis explores a coordination procedure of interconnected electrical networks, as first mentioned in chapter 1. Detailed explanations about the approach can be found in [1], a paper that I co-authored during my thesis and that I extend in this manuscript. The current section summarizes the main requirements to understand the approach, including some basic knowledge about power systems and a comprehensive overview of the coordination procedure. The POE computation model, which is at the core of the coordination procedure, is detailed in section 3.2. It is followed by the instantiation of the objective function, the security constraints, and the control actions in section 3.3, section 3.4, and section 3.5, respectively.

3.1.1 Electrical grid modelling and operation

An electrical grid is composed of different elements enabling power to flow from generating plants to end-users. These elements ensure that electricity is supplied continuously, efficiently, and within acceptable security limits. The grid is therefore not a single entity, but rather a complex system composed of multiple assets.

The main elements of an electrical grid and their respective roles are summarized as follows:

- **Generating Plants**: Facilities where electrical energy is produced from primary energy sources such as fossil fuels, nuclear energy, or renewable sources (e.g., wind, solar, hydro). These plants inject power into the grid at various voltage levels [53].
- **Transmission Lines**: High-voltage lines designed to transport large amounts of electrical power over long distances with minimal losses [54].
- **Substations**: Nodes within the grid where voltage levels are changed using transformers, power flows are monitored, and different parts of the network are interconnected (e.g, transmission and distribution networks). Substations also house protection devices and switchgears [55].
- **Transformers**: Electrical devices used to step voltage levels up or down. Step-up transformers increase voltage (e.g, at the point of connection between a generator and the transmission grid), while step-down transformers reduce voltage for distribution and end use [56].
- **Distribution Lines**: Medium- and low-voltage lines that deliver electricity from substations to residential and commercial consumers [57].
- **Switchgear**: Equipment such as circuit breakers, switches, and fuses, used to control, protect, and isolate sections of the grid [58].

- **Protection Systems**: Systems that detect abnormal conditions (e.g., faults or overloads) and automatically trigger protective actions such as opening circuit breakers to prevent asset damage [59].
- **Control Systems**: Monitoring infrastructures (e.g., SCADA systems) that allow operators to supervise grid conditions in real time and make operational decisions [60].
- **End-users**: Consumers of electrical energy, including households, industries, and commercial facilities. Their demand patterns strongly influence grid operation and planning. Some end-users/consumers are becoming more active in power generation and are called prosumers, i.e, customers who produce electricity primarily for their own needs but can also inject part of their production into the distribution grid [61].

These elements form a highly complex system, whose operation is inherently challenging due to the need to continuously balance supply and demand, respect network security constraints, e.g., voltage magnitude limits, or thermal constraints, and ensure energy supply under a wide range of operating conditions and uncertainties. The large-scale and highly interconnected nature of modern power systems, combined with the increasing integration of DERs and prosumers, further amplifies this complexity.

In practice, the electrical grid is not operated as a single entity but can be decomposed into several interconnected subnetworks, each operated by a specific actor, which may correspond to different individuals or legal entities. Typically, the grid is divided into multiple voltage levels connected to each other at a substation, where power exchanges between these subnetworks are enabled. The decomposition may follow geographical or political boundaries, as in the case of interconnected national grids, or reflect the responsibilities of different network operators.

A particularly important and widely adopted decomposition is the distinction between transmission and distribution systems, which are operated by TSOs and DSOs, respectively. TSOs are generally responsible for the operation of high-voltage networks, ensuring long-distance power transport and system-wide balance, while DSOs manage lower-voltage networks that deliver electricity to end-users. Both are increasingly facing the integration of DERs, including PV generation and batteries. In the rest of this thesis, parts of the grid operated by distinct operators are referred to as *operational networks*.

3.1.2 Coordination between operational networks

As mentioned in the previous subsection, a power system is typically operated by multiple independent actors, each responsible for managing the grid elements within its own operational network. TSOs and DSOs jointly share the responsibility of ensuring the secure operation of the overall electrical grid [62]. In this thesis, the notion of security is restricted to *static security*, which is defined as the ability to maintain voltage magnitudes and line flows within their prescribed operating limits under normal operating conditions. Dynamic stability and N-1 contingency requirements are deliberately excluded from the security requirements studied in this thesis.

To maintain static security [63], each operator has access to a set of corrective control actions. These actions are not equivalent in terms of cost. Actions with limited financial impact, such as topology reconfiguration or shunt reactor switching, are prioritised, while more costly interventions, such as active power curtailment or generation redispatch, are reserved as last-resort measures.

Although each operator acts within the boundaries of its own network, the electrical grid is a physically interconnected system governed by physical laws. As a result, any control action taken by one operator, such as redispatch, modifying network topology, or adjusting reactive power output of a generator, can influence power flows, voltages, and loading conditions in neighboring operational networks. These interactions may, in turn, lead to the violation of security constraints outside the operator's operational network.

The responsibility of maintaining a secure grid operation is thus inherently collective, and reaching a certain level of coordination among operators might help to tackle the challenges related to the integration of DERs within the electrical network.

The key idea of this work relies on the assumption that the interaction between a given operational network and the rest of the grid can be fully characterized by a limited set of interface variables, namely the active and reactive power flows exchanged at the interconnection points, as well as the corresponding voltage phasors.

Once these interface quantities are specified, the detailed network modelling of the external system becomes irrelevant for assessing the static secure operation of the considered operational network. This abstraction enables a decoupled coordination of interconnected systems.

Based on this idea, the concept of *operating envelopes* (OEs) can be defined as a range of power committed in advance by an operator to a customer at a connection point. As long as the customer stays within the range, the operator guarantees static security in a preventive manner, without any operator action and without considering contingencies.

The definition of OEs can be extended, such that OEs (i) can be used as limits at the interface between operational networks, and (ii) account for corrective actions that can be taken by each operator. This leads to the definition of two complementary types of interface limits. *Power operating envelopes* (POEs) are defined as complex power limits at the interface between operational networks. *Voltage operating envelopes* (VOEs) are defined as voltage magnitude limits agreed bilaterally at interfaces between the operational network and the rest of the grid.

The goal of this work is to provide each operator with a set of interface variable ranges, i.e, the power and voltage operating envelopes, such that, as long as these envelopes are respected during operation, the static security of the network can always be restored through available corrective actions whose cost does not exceed a prescribed maximum.

POEs and VOEs provide a compact yet complete framework for coordinating decentralized operation while preserving local security. Within this framework, each operator can take corrective actions independently as long as they ensure that interface variables are within the bounds of the envelopes.

3.1.3 Coordination procedure for a practical use of POEs/VOEs

The process through which POEs and VOEs are established at the interface between subnetworks is referred to as the *coordination procedure*. This procedure provides a framework that enables multiple operators to manage their respective *operational networks* independently.

It is assumed that the grid is partitioned into several interconnected operational networks, each controlled by a distinct operator. It is also supposed that there exists a hierarchy between these subnetworks such that a parent network (in general, the transmission system) and one or multiple child networks (the distribution systems) can be identified. The interconnection structure is assumed to form a tree topology: each operational network is connected to at most one upstream (parent) network and to zero, one, or multiple downstream (child) networks. The importance of this hierarchy will be clarified during the coordination procedure explanation.

The coordination procedure consists of the following sequence of steps:

1. **Negotiation of VOEs:** Operators first agree on admissible voltage ranges at their interfaces for a specified future period. These VOEs define acceptable deviations of voltage magnitudes around nominal values, and their existence is a necessary non-unique condition to ensure that child networks can be operated in a secure way without requiring detailed knowledge of the parent network's operating conditions. It is assumed that the VOEs are first assigned at the parent node and then at child nodes.

2. **Estimation and Communication of Power Injections/Withdrawals:** Given the agreed VOEs, each operator computes a prediction of the net active and reactive power it expects to exchange with its parent network at the interface. These estimates depend not only on local conditions but also on the expected behavior of child networks. As a result, this step is performed recursively, in a *bottom-up* manner: each operator aggregates the power requests received from its children and sums them up with its internal forecasts (e.g., internal expected demand and/or generation) to determine its net interface power.

3. **Computation of POEs:** In the final step, operators compute admissible ranges for active and reactive power exchanges at their interfaces with child networks. These POEs must be such that, for any feasible realization of power exchanges within these bounds and under the previously agreed VOEs, the operator can maintain the static security of its own network through available corrective actions. In contrast to the previous step, this step is handled in a *top-down* manner, as the POE that the operator of the operational network received from its parent network needs to be respected, whatever the exchange of power with its own child networks within computed POEs.

In operation, the parent commits to keeping the interface voltage within the VOE. Each child commits to keep the interface power exchange within a POE. In other words, an operational network's operator is required to maintain the voltage magnitude of its child nodes within the agreed VOE, and the power exchange with its parent node should remain within the POE. To respect these agreements and ensure the static security of its own network, the operator should take corrective actions in operation.

For sake of clarity, let us consider a practical example of the coordination procedure. Let us consider the operational network depicted in Figure 3.1. It is characterized by one parent node and three child nodes. As mentioned in the procedure, it is first supposed that the operator of the studied network agrees on voltage magnitude limits at its parent and child nodes. The maximum acceptable voltage magnitude range in the N-state and N-1 state is generally between 90% and 110% of the nominal voltage magnitude (i.e, $V_{min} = 0.9$ and $V_{max} = 1.1$ in per unit, as depicted in Figure 3.1).

However, depending on the voltage level, voltage magnitude limits might differ from these reference values. Rules regarding acceptable ranges can be found in the EU grid code regulation [64]. It should be emphasized that the grid code's limits are hard limits to ensure the security of grid assets, but VOEs negotiation could lead to a more restrictive range of voltage magnitudes, i.e, a subset of the grid code's limits. Once VOEs are agreed on, the operator of the operational network has the responsibility to ensure that these voltage magnitude limits are respected at the child nodes during operation, while the upstream operator ensures the respect of voltage magnitude limits at the parent node.

To be able to properly operate its operational network and, in particular, to ensure that no security constraints are violated in operation, the operator requires power demand forecasts from its child networks. Therefore, as illustrated in Figure 3.1, power demand estimates are communicated from downstream to upstream networks (i.e, child networks 1, 2, and 3 provide net power demand estimates to the operational network's operator) to enable the operator to plan for suitable control actions. As the upstream operational network's operator is also required to ensure the security of its network during operation, the latter needs to receive net power demand estimates from its child networks (including the net power demand estimate from the considered network).

The net power demand forecasts coming from child networks are, by definition, only the best estimates of the power demand at a given moment prior to real-time operation and might significantly differ from the true power demand in real-time. Therefore, there is a need for flexibility. POEs can be leveraged to provide this required flexibility to child networks.

POEs are to be computed such that, whatever the power exchanges within their bounds, the security of the network can be ensured. In particular, the forecasted power exchange values should be within the POEs' bounds. Increasing the flexibility provided to child networks comes with additional control action costs. Therefore, it can be understood that there exists a trade-off between the flexibility provided to the child networks and the operational network's operation costs.

Moreover, the quality of the POEs provided to child networks not only depends on the operational network control actions but also on the POE allocated at the parent network. Therefore, the POEs are computed in a top-down manner. In Figure 3.1, this cascade computation is represented as the third step of the coordination procedure, where the POEs are computed from upstream to downstream networks. In other words, the POEs computed at the child nodes directly depend on the one imposed by its parent network at their interface.

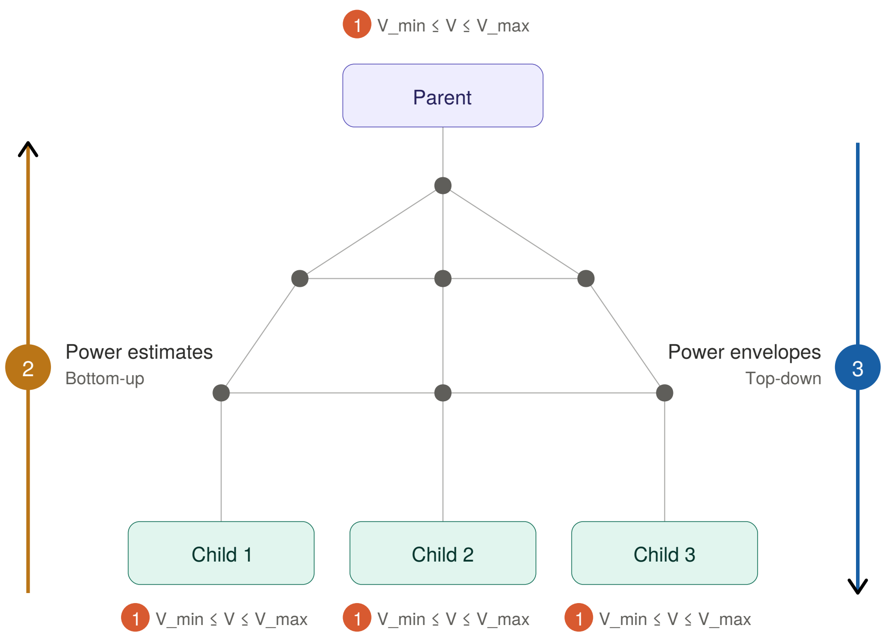

Figure 3.1: Schematic of the coordination procedure of an operational network, starting with (1) the voltage limit agreements at each parent and child nodes, followed by (2) the complex power estimates from the child networks communicated to the operational network's operator, and finally (3) the computation of POEs communicated from upstream to downstream.

The last step (i.e, the computation of POEs) is particularly challenging, as it requires accounting for network security constraints and the available control actions. To this end, the problem is formulated as an optimisation problem that each operator can solve separately. In section 3.2, the mathematical formulation to compute POEs is detailed.

For the coordination approach to be effective in practice, all operators must respect the agreed VOEs and POEs during real-time operation. Specifically, each operational network is allowed to exchange power with its parent within the limits defined by the corresponding POEs, while the parent network is responsible for maintaining interface voltages within the prescribed VOEs. As long as the POEs and VOEs are respected, there exists a set of control actions that can be activated by the operator at a maximum cost to ensure the secure operation of its network, even when power exchanges move away from their forecasted values.

In this way, the coordination procedure enables a scalable and coordinated operation of large-scale power systems, reducing the need for centralized control while preserving static security through well-defined interface agreements. This procedure is particularly suitable for TSO/DSO coordination where the TSO computes POEs for its child networks, which are the DSOs' networks.

At this stage, it is worth positioning the proposed coordination approach in perspective to the alternatives documented in the literature. As outlined in section 1.3, existing coordination approaches can be divided into four main categories: centralized, hybrid, distributed, and hierarchical approaches, as illustrated in Figure 2.1.

Compared to the existing literature, the proposed approach can be classified as decentralized and hierarchical. Decision-making is distributed across the TSO's and DSOs' operators without reliance on a single central optimizer, while a leader-followers structure governs the sequential exchange of boundary envelopes between the transmission and distribution networks.

3.2 Mathematical formulation

As mentioned in section 3.1, the computation of POEs is particularly challenging as it requires accounting for both security requirements and control actions. This section presents an optimisation problem to compute POEs. The mathematical formulation presented in this section is largely inspired by [1], a scientific article to which I participated and that is written in collaboration with researchers from the Smart Grid Lab (ULiege).

3.2.1 Electrical network model

An electrical network can be modeled as a graph, denoted by $\mathfrak{G} = (\mathcal{N}, \mathcal{E})$, where $\mathcal{N}$ is the set of nodes and $\mathcal{E} \subseteq \mathcal{N} \times \mathcal{N}$ is the set of edges. It is assumed in this thesis that networks are perfectly balanced three-phase networks. Each node $n \in \mathcal{N}$ corresponds to a network bus, such as a generator, a customer, or a substation. Each edge $(m, n) \in \mathcal{E}$ represents an electrical connection between two nodes of the set $\mathcal{N}$, commonly referred to as a line or cable.

An operational graph is a subgraph $\mathfrak{G}_o$ such that

$$\mathfrak{G}_o = (\mathcal{N}_o, \mathcal{E}_o) \subseteq \mathfrak{G},$$

where $\mathcal{N}_o \subseteq \mathcal{N}$ and

$$\mathcal{E}_o \subseteq \left(\mathcal{E} \cap \mathcal{N}_o^2\right).$$

Each operational network is connected to the rest of the electrical grid exclusively through its interface nodes $\mathcal{N}^{\mathcal{I}} \subseteq \mathcal{N}$. The set of operational networks is assumed to follow a directed-tree structure. There exists a unique root network with no parent, while every other network is connected to exactly one parent network through its unique parent node $\mathcal{N}_o^{\mathcal{P}} \subseteq \mathcal{N}^{\mathcal{I}}$ and may be connected to one or more child networks through its child nodes $\mathcal{N}_o^{\mathcal{C}} \subseteq \mathcal{N}^{\mathcal{I}}$. Interface nodes are the only nodes shared between adjacent operational networks.

3.2.2 Electrical quantities

Each node $n \in \mathcal{N}$ has an associated line voltage phasor $V_n \in \mathbb{C}$. This means that each voltage V_n is characterised by a magnitude and a phase. The vector of complex voltages of operational graph $\mathfrak{G}_o$ is denoted as $V^o \in \mathbb{C}^{|\mathcal{N}_o|}$, the vector of voltages at parent nodes $V^{\mathcal{P}} \in \mathbb{C}^{|\mathcal{N}_o^{\mathcal{P}}|}$ and the vector of voltages at child nodes $V^{\mathcal{C}} \in \mathbb{C}^{|\mathcal{N}_o^{\mathcal{C}}|}$. It should be noted that the vector $V^{\mathcal{P}}$ is only composed of one component, as there exists only one parent node for each operational network, and that the value of this component is uncertain to the operational network's operator. The operator has the guarantee that $V^{\mathcal{P}}$ lies between the bounds of the agreed VOE, without further information about its expected value. Moreover, $I^o \in \mathbb{C}^{|\mathcal{E}_o|}$ denotes the vector of complex currents in each edge.

In addition, the complex power demand (loads) at each node $n \in \mathcal{N}$ is denoted as $S_{load,n} = P_{load,n} + jQ_{load,n} \in \mathbb{C}$ and the complex power generation at each node $n \in \mathcal{N}$ is denoted as $S_{gen,n} = P_{gen,n} + jQ_{gen,n} \in \mathbb{C}$. When generators' power outputs are modified compared to their scheduled production, the effective complex power injection at each node $n \in \mathcal{N}$ is denoted as $S'_{gen,n} = P'_{gen,n} + jQ'_{gen,n} \in \mathbb{C}$. When there is no modification of the generator's output at node n, we have $S_{gen,n} = S'_{gen,n}$.

By convention, positive (active or reactive) power denotes withdrawal, and negative power denotes injection. We denote as $S^o_{load} \in \mathbb{C}^{|\mathcal{N}_o|}$ the vector of all complex power demands within the operational graph $\mathfrak{G}_o$, and as $S^o_{gen} \in \mathbb{C}^{|\mathcal{N}_o|}$ the vector of all scheduled complex power injection within this same graph $\mathfrak{G}_o$.

For an operational graph $\mathfrak{G}_o = (\mathcal{N}_o, \mathcal{E}_o)$, let us denote the complex power entering and leaving the operational graph, at each node $n \in \mathcal{N}_o$, by $S_n^+ = P_n^+ + jQ_n^+$ and by $S_n^- = P_n^- + jQ_n^-$, respectively. The entering power S_n^+ is nonzero only for parent nodes, and the leaving power S_n^- is nonzero only for child nodes. Therefore, power entering through parent nodes and leaving through child nodes are denoted as $S^{+,\mathcal{P}} \in \mathbb{C}^{|\mathcal{N}_o^{\mathcal{P}}|}$, $S^{-,\mathcal{C}} \in \mathbb{C}^{|\mathcal{N}_o^{\mathcal{C}}|}$, respectively. The vector $S^{-,\mathcal{C}}$ is uncertain to the operational network's operator. The operator has the guarantee that this vector lies between the bounds of the agreed POE at the interface with its child networks.

Active and reactive power flows through edge (m, n) are depicted as $P_{m,n} \in \mathbb{R}$ and $Q_{m,n} \in \mathbb{R}$, respectively. Without additional assumptions: $|P_{m,n}| \neq |P_{n,m}|$ and $|Q_{m,n}| \neq |Q_{n,m}|$.

3.2.3 Control Actions

Let us define u as a vector of decision variables, which model the control actions that the operator can take. The convex feasible set $\mathcal{F}$ encodes its physical bounds and constraints. Mathematically:

$$u \in \mathcal{F}.$$

Since control actions can be adjusted in response to the operating conditions, u may take a different value for each realization of the uncertain parameters ($S^{-,\mathcal{C}}$, $V^{\mathcal{P}}$). For example, modifying the generators' power outputs S'^o_{gen} is considered as a control action. This action, called re-dispatch, can be adjusted depending on the realization of the uncertain parameters ($S^{-,\mathcal{C}}$, $V^{\mathcal{P}}$).

3.2.4 Boundary conditions for decoupled operation

Mathematically, a POE is a subset of power $\overline{S}_n \subset \mathbb{C}$ that is allowed to leave or enter an operational graph at node n. Let $\overline{S}^{\mathcal{C}} \subset \mathbb{C}^{|\mathcal{N}_o^{\mathcal{C}}|}$ and $\overline{S}^{\mathcal{P}} \subset \mathbb{C}^{|\mathcal{N}_o^{\mathcal{P}}|}$ be the subsets of allowed power leaving through all child nodes and entering through the parent node, respectively. In particular, $\overline{P}^{\mathcal{C}} \subset \mathbb{R}^{|\mathcal{N}_o^{\mathcal{C}}|}$ and $\overline{Q}^{\mathcal{C}} \subset \mathbb{R}^{|\mathcal{N}_o^{\mathcal{C}}|}$ are the subsets of allowed active and reactive power leaving through all child nodes. For a given child node $n \in \mathcal{N}_o^{\mathcal{C}}$, $\overline{P}_n^{\mathcal{C}} \subset \mathbb{R}$ and $\overline{Q}_n^{\mathcal{C}} \subset \mathbb{R}$ are the subsets of allowed active and reactive power leaving through child node n.

Similarly, a VOE is a subset of voltage magnitude $\overline{V}_n \subset \mathbb{R}$ that is contractually agreed upon at a node n of the graph. The voltage magnitude guarantee at parent nodes and at the child nodes are respectively denoted by the subsets $\overline{V}^{\mathcal{C}} \subseteq \mathbb{R}^{|\mathcal{N}_o^{\mathcal{C}}|}$ and $\overline{V}^{\mathcal{P}} \subseteq \mathbb{R}^{|\mathcal{N}_o^{\mathcal{P}}|}$. These subsets are agreed upon at parent and child nodes between the different operational graphs.

Throughout all POE computation models presented in this thesis, the interface nodes, i.e, the parent node and the child nodes connecting the operational network to the rest of the grid, are modelled as follows.

Parent nodes are treated as ideal voltage sources. Their voltage magnitudes are supposed to be held constant, while the power injections $S_n^+ = P_n^+ + jQ_n^+ \in \mathbb{C}$ can vary freely within the POE imposed at the parent node. Formally, the voltage phasor at the parent node is denoted as $V^{\mathcal{P}}$, and its magnitude $|V^{\mathcal{P}}|$ is fixed and constrained to lie within the agreed VOE.

Child nodes are treated as constant-power sources: the complex power exchanged at each child node, $S_n^- = P_n^- + jQ_n^- \in \mathbb{C}$, is fixed for a given scenario and constitutes a parameter of the optimisation problem, while the corresponding vector of voltage phasors at the child nodes $V^{\mathcal{C}}$ is determined by the power flow equations and the voltage magnitudes are constrained to remain within the agreed VOE.

3.2.5 Optimisation problem: an overview

As VOEs are supposed to be contractually agreed upon, they are considered as input parameters and are thus not computed. Therefore, only POEs are to be determined for each child node of the operational graph.

In this thesis, POEs are determined by solving an optimisation problem, whose formulation depends on the choice of the network model, i.e, the type of equations used to model the power flows, and the control actions. This network model serves to evaluate whether security constraints are satisfied for a given operating state and to identify the control actions required to restore security when they are not. Since different network models lead to different instantiations of the POE computation problem, the formulation presented in this subsection is deliberately kept generic. In the rest of the thesis, any optimisation problem that seeks to compute POEs is simply referred to as a *POE computation model*. The generic POE computation model is written as:

$$\max_{\overline{S}^{\mathcal{C}}, A} U^{POE}(\overline{S}^{\mathcal{C}}) - A \tag{3.1a}$$

$$\text{s.t. } \forall S^{-,\mathcal{C}} \in \overline{S}^{\mathcal{C}},\ \forall \left|V^{\mathcal{P}}\right| \in \overline{V}^{\mathcal{P}},\ \exists\, u \in \mathcal{F}:$$

$$Security(S^{o}_{load}, S^{o}_{gen}, S^{-,\mathcal{C}}, V^{\mathcal{P}}, u) \leq 0, \tag{3.1b}$$

$$Cost(u) \leq A, \tag{3.1c}$$

$$|V^{\mathcal{C}}| \in \overline{V}^{\mathcal{C}}, \tag{3.1d}$$

$$S^{+} \in \overline{S}^{\mathcal{P}}, \tag{3.1e}$$

where U^{POE} is an arbitrary utility function representing the quality of the POEs (e.g, the volume of the POEs), and for which a possible instantiation is given in section 3.3. It must be maximized such that, for each value of $S^{-,\mathcal{C}}$ and $V^{\mathcal{P}}$, there exist certain control actions which ensure that the network can be securely operated.

More specifically, Equation 3.1b constraints some electrical variables to ensure grid security in the N-state. The N-1 security criterion is not considered in this formulation. The function in Equation 3.1b returns a non-positive value if and only if the grid operation remains secure in the N-state. This constraint is detailed in section 3.4.

In Equation 3.1c, the variable $A \in \mathbb{R}^{+}$ bounds the cost related to the network operation (e.g., re-dispatch cost) for the different values of $S^{-,\mathcal{C}}$ and $V^{\mathcal{P}}$, and is minimized in the objective function. This last constraint represents the operational constraints and is further detailed in section 3.5.

Equation 3.1d and Equation 3.1e ensure that the VOE at the child nodes and the POE at the parent node are respected, respectively.

3.2.6 Optimisation problem: a reformulation

In this thesis, POEs are defined as Cartesian products of two intervals: one for active power and one for reactive power. VOEs are defined as intervals for the voltage magnitude at interface nodes. The corresponding voltage phase angle is left unconstrained. Considering intervals offers two main advantages. First, each envelope is fully parameterised by its lower and upper bounds, which become the decision variables of the optimisation problem. Second, the envelope membership constraints (Equation 3.1d and Equation 3.1e) reduce to simple linear inequalities on these bounds.

Even with these interval definitions, the optimisation problem proposed in Equation 3.1 cannot be solved as such since all constraints should be respected, whatever the realizations of the uncertain parameters $S^{-,\mathcal{C}}$ and $V^{\mathcal{P}}$. Because of these uncertain parameters, the constraints are said to be semi-infinite [65]. Thanks to robust optimisation techniques, the constraints can be reformulated into finitely many convex constraints, under some assumptions.

Let us assume that $\overline{S}^{\mathcal{C}}$ and $\overline{V}^{\mathcal{P}}$ are bounded polyhedra with finitely many vertices. Their sets of vertices are respectively denoted by $\Psi(\overline{S}^{\mathcal{C}})$ and $\Psi(\overline{V}^{\mathcal{P}})$. We further assume that the utility function depends only on these vertex values, and that all constraints are convex functions with respect to their respective arguments. Under these assumptions, solving the generic optimisation problem Equation 3.1 is equivalent to solving the following reformulated problem:

$$\max_{\overline{S}^{\mathcal{C}},A} \quad U^{POE}\Big(\Psi(\overline{S}^{\mathcal{C}})\Big) - A \tag{3.2a}$$

$$\text{s.t.} \quad \forall S^{-,\mathcal{C}} \in \Psi(\overline{S}^{\mathcal{C}}),\ \forall \left|V^{\mathcal{P}}\right| \in \Psi(\overline{V}^{P}), \exists u \in \mathcal{F}: \tag{3.2b}$$

$$Security(S^{o}_{load}, S^{o}_{gen}, S^{-,\mathcal{C}}, V^{\mathcal{P}}, u) \leq 0, \tag{3.2c}$$

$$Cost(u) \leq A, \tag{3.2d}$$

$$|V^{\mathcal{C}}| \in \overline{V}^{\mathcal{C}}, \tag{3.2e}$$

$$S^{+} \in \overline{S}^{\mathcal{P}}. \tag{3.2f}$$

This reformulation consists of ensuring that the constraints are respected for all combined assignments of interval bound values. In other words, instead of verifying that the constraints are respected for every point within the POEs and VOEs, which would require infinitely many constraints, it is sufficient to check the constraints only at the vertices of the Cartesian product of the uncertainty sets. Each vertex corresponds to a scenario in which every child node's power exchange and every parent node's voltage magnitude takes either its minimum or maximum value simultaneously. Respecting these constraints at all such vertices implies respecting these constraints everywhere within the uncertainty sets, under the convexity assumption. The reformulation therefore reduces the number of constraints to a finite, though exponentially growing in the number of interface nodes, set of convex constraints. As illustrated in chapter 4 and chapter 5, this reformulation leads to an SOCP that can be solved using modern solvers. A proof of the equivalence of optimisation problems (the generic one and the reformulated one) is provided in [1].

In the rest of this chapter, a first instantiation of the generic POE computation model presented in Equation 3.1 is provided. This includes an instantiation of the utility function, the power flow and security constraints, and the operational constraints.

3.3 Objective function

The utility function $U^{POE}(\overline{S}^{\mathcal{C}})$ presented in Equation 3.1 should encapsulate the different criteria to select a POE. These criteria may include some measure of social fairness between child nodes, or, on the contrary, the criteria might promote certain critical child networks over others.

The utility function presented in this section is defined as a utility of POEs, as first proposed in [1]. It is assumed that each child node has a local utility and that the utility function is the aggregation of these local utilities. Mathematically, the utility function $U^{POE}(\overline{S}^{\mathcal{C}})$ can be written as:

$$U^{POE}(\overline{S}^{\mathcal{C}}) = \sum_{c \in \mathcal{N}^{\mathcal{C}}_{o}} U_c(\overline{P}^{\mathcal{C}}_c, \overline{Q}^{\mathcal{C}}_c), \tag{3.3a}$$

with:

$$U_c(\overline{P}^{\mathcal{C}}_c, \overline{Q}^{\mathcal{C}}_c) = Vol(\overline{P}^{\mathcal{C}}_c) - \gamma_P \cdot Vol(\overline{P}^{\mathcal{C}}_c)^2 - \alpha_P \cdot \Big(Bar(\overline{P}^{\mathcal{C}}_c) - \hat{P}^{-}_c\Big)^2 \tag{3.4a}$$

$$+ Vol(\overline{Q}^{\mathcal{C}}_c) - \gamma_Q \cdot Vol(\overline{Q}^{\mathcal{C}}_c)^2 - \alpha_Q \cdot \Big(Bar(\overline{Q}^{\mathcal{C}}_c) - \hat{Q}^{-}_c\Big)^2, \tag{3.4b}$$

where $U_c(\overline{P}_c^{\mathcal{C}}, \overline{Q}_c^{\mathcal{C}})$ represents the local utility. The functions $Vol(X)$ and $Bar(X)$ return the length and the center of the interval X, respectively. In other words, $Vol(X)$ is the difference between the bounds of interval X. Similarly, $Bar(X)$ is the average of the interval X bounds.

Values of parameters $\alpha_P, \alpha_Q, \gamma_P, \gamma_Q \in \mathbb{R}^+$ are to be tuned. The power exchange forecasted at child node c is denoted as $\hat{S}_c^- = \hat{P}_c^- + j\hat{Q}_c^- \in \mathbb{C}$. This value is supposed to be computed by the child network and communicated to the operational network's operator.

In this formulation, the sum of concave functions of $\overline{S}_c$ over each child node is maximized, while any deviation of the POEs from the forecasted power exchange is penalized.

In order to formulate the optimisation problem completely, this objective function formulation should be accompanied by the adapted security constraints and cost-related constraints, presented in section 3.4 and section 3.5, respectively.

3.4 Security constraints

Equation 3.1b ensures that the operational graph remains secure. To verify the security constraints, the electrical variables are computed using power flow equations, which practically correspond to additional constraints in the optimisation problem. Mathematically:

$$V^o, I^o = PowerFlow(S^o_{load},\ S^o_{gen},\ S^{-,\mathcal{C}},\ V^{\mathcal{P}},\ u). \tag{3.5a}$$

Depending on the network's characteristics, assumptions are made on the electrical variables used, which lead to different power flow models. A first power flow model is given in subsection 3.4.1, similar to the one proposed in [1].

3.4.1 Power flow equations

In order to verify the assumptions of the robust reformulation problem presented in section 3.3, power flow models must remain convex. In [1], the AC power flow equations are linearized around 1 p.u for the voltage magnitude and around 0 for the voltage phase angle. This model is called the linearized AC power flow (LACPF) model. The mathematical development used to linearize the AC power flow equations and obtain the LCAPF model is given in Appendix B. Mathematically, it is written as:

$$P_{nj} = g_{nj}(V_n - V_j) - b_{nj}(\theta_n - \theta_j), \tag{3.6a}$$

$$Q_{nj} = -b_{nj}(V_n - V_j) - g_{nj}(\theta_n - \theta_j), \tag{3.6b}$$

where P_{nj} and Q_{nj} are the active and reactive power flow on branch (n, j), V_n and V_j are the voltage magnitudes at bus n and bus j, θ_n and θ_j are the voltage angles at bus n and bus j, and g_{nj}, b_{nj} are, respectively, the conductance and susceptance of branch (n, j).

The LACP model is often considered as a reasonable trade-off between using the accurate but computationally-expensive AC power flow equations, which might make the problem NP-hard if no relaxation is considered, and the scalable but highly simplified DC power flow equations[1]. As stated in [66], the LACPF model yields a power flow solution with a higher accuracy than the DC power flow model, at a similar computational performance.

[1] The DC power flow model is further detailed in Appendix C.

Related to the power flow equations, the power balance equations should be considered as well.

For every $n \in \mathcal{N}$:

$$P_{\text{load},n} - P'_{\text{gen},n} = \sum_{(m,n)\in\mathcal{E}} P_{mn} \; + \; P_n^+ - P_n^-, \tag{3.7a}$$

$$Q_{\text{load},n} - Q'_{\text{gen},n} = \sum_{(m,n)\in\mathcal{E}} Q_{mn} \; + \; Q_n^+ - Q_n^-, \tag{3.7b}$$

where all parameters and variables are defined in subsection 3.2.2. The parent node is considered as the slack bus and is indexed as 0 by default. At this bus:

$$\theta_0 = 0.$$

3.4.2 A secure grid operation

The choice of the power flow equations limits the degrees of freedom for integrating security constraints into the optimisation model. Depending on the choice of the most suitable power flow equations (the LACPF model in this case), a set of adapted security constraints should be considered.

Network security constraints are assumed to correspond to thermal limits, i.e, the maximum rating of the line should not be exceeded, and upper and lower limits on, respectively, voltage magnitudes and voltage phase angle differences:

$$P_{mn}^2 + Q_{mn}^2 \leq \bar{S}_{mn}^2, \qquad \forall\, (m,n) \in \mathcal{E}, \tag{3.8a}$$

$$\underline{V}_n \leq |V_n| \leq \bar{V}_n, \qquad \forall\, n \in \mathcal{N}, \tag{3.8b}$$

$$\underline{\Delta\theta} \leq \theta_m - \theta_n \leq \overline{\Delta\theta}, \qquad \forall\, (m,n) \in \mathcal{E}, \tag{3.8c}$$

where the parameter $\bar{S}_{mn} \in \mathbb{R}^+$ is the line rating[2], $\underline{V}_n, \bar{V}_n \in \mathbb{R}^+$ are the minimum and maximum allowed voltage magnitudes, $\underline{\Delta\theta}, \overline{\Delta\theta} \in \mathbb{R}^+$ are the minimum and maximum voltage phase angle allowed, respectively.

Moreover, the generator capabilities should be respected as well:

For every $n \in \mathcal{N}$:

$$\underline{P}_{\text{gen},n} \leq P'_{\text{gen},n} \leq \bar{P}_{\text{gen},n}, \tag{3.9a}$$

$$\underline{Q}_{\text{gen},n} \leq Q'_{\text{gen},n} \leq \bar{Q}_{\text{gen},n}, \tag{3.9b}$$

where parameters $\underline{P}_{\text{gen},n}, \bar{P}_{\text{gen},n} \in \mathbb{R}^+$ are the minimum and maximum active power production of the generator connected at node n and $\underline{Q}_{\text{gen},n}, \bar{Q}_{\text{gen},n} \in \mathbb{R}$ are the minimum and maximum reactive power production of the generator connected at node n. $\underline{P}_{\text{gen},n} = \bar{P}_{\text{gen},n} = \underline{Q}_{\text{gen},n} = \bar{Q}_{\text{gen},n} = 0$ if there is no generator at node n.

In the proposed instantiation of the POE computation model, Equation 3.1b is respected, i.e, the function $Security(.)$ outputs a negative value, if Equation 3.8a-Equation 3.9b are respected. In order to assess whether Equation 3.8a-Equation 3.9b are respected, a power flow model is required, as described in the previous subsection.

[2] In practice, this value might vary with the season, temperatures, etc. It is assumed to be constant in this thesis.

3.5 Control Actions

The cost-related constraints (also denoted as operational constraints) are represented by Equation 3.1c in the generic POE computation model proposed in subsection 3.2.5.

One might note that power flow equations can be seen as input to these operational constraints, as the observation of the electrical state of the network is required to take actions and to modify operating points. In [1], only the re-dispatch of generators' active and reactive power is considered as a control action. Mathematically, the vector of control actions becomes $u = (S'_{\text{gen},n})_{n\in\mathcal{N}_o}$, with $\mathcal{F}$ defined by the generator capability constraints (4.7)–(4.9).

It is assumed that the power output of generators within the operational network can be adjusted at a certain cost, reflecting the deviation from the generation schedule. This cost applies only to active power, while reactive power is assumed to be freely controllable within each generator's capability limits. Accordingly, the associated cost constraint can be formulated as follows:

$$\beta \cdot \sum_{n\in\mathcal{N}} \left(P_{\text{gen},n} - P'_{\text{gen},n}\right)^2 \leq A, \tag{3.10a}$$

where variable A, defined in subsection 3.2.5, bounds the worst-case re-dispatch and is minimized in the objective function. The parameter $\beta \in \mathbb{R}^+$ is a measure of the cost of modifying a generator's setpoint.

3.6 A first POE Computation Model

As mentioned in section 3.1, the third step of the coordination procedure is to compute POEs. Based on the developments proposed in section 3.2, section 3.3, section 3.4 and section 3.5, the optimisation problem required to compute POEs can be fully formalized.

The goal is to find the largest feasible POEs, while penalising deviations of the POE's barycentre from children's active and reactive power demands, and regularizing the re-dispatch requirements. Mathematically: [3]

$$\max_{\overline{S}^{\mathcal{C}},\,A} \quad U^{POE}(\overline{S}^{\mathcal{C}}) - A \tag{3.11}$$

$$\begin{aligned} \text{s.t.} \quad & \forall\,(P^-,Q^-) \in \overline{S}^{\mathcal{C}},\ \forall\,|V^{\mathcal{P}}| \in \overline{V}^{\mathcal{P}}, \exists u \in \mathcal{F}: \\ & (3.6\text{a}) - (3.10\text{a}) \end{aligned} \tag{3.12}$$

This optimisation problem[4] presents several limitations:

1. Generator re-dispatch is the only control action considered. In practice, system operators have access to a broader set of corrective actions, many of which may be prioritized over generator re-dispatch.

[3] The reformulation of the optimisation problem can be implemented using the Pyomo optimisation modelling language [67], which is well-suited for power system optimisation.

[4] All optimisation problems presented in this thesis are written in per unit. More details about the per unit normalization are provided in Appendix A.

2. The LACPF model is a significant simplification of steady-state power flow behavior. As a linear approximation, it cannot fully capture the nonlinear nature of AC power systems and may therefore introduce inaccuracies.

3. The generator P–Q capability limits are represented using a simplified square capability region. In general, generator capability curves are more complex and may differ substantially from this approximation.

To address these limitations, the remainder of this thesis focuses on extending the optimisation model and evaluating it on test networks.

Chapter 4

Model Developments and Experimental Methodology

4.1 Preliminaries

In chapter 3, a TSO/DSO coordination approach relying on the notion of OEs is introduced. More specifically, chapter 3 introduces an optimisation problem to compute POEs. In this chapter, the POE computation model presented in chapter 3 is extended. For example, an additional control action is considered, namely the phase-shifter. This additional control action is described in subsection 4.2.1.

Additionally, a convex model of the AC power flow equations is proposed to represent the power flows. This ensures a more accurate representation of power flows than linearization, while keeping the optimisation problem convex. This power flow model, called the Quadratic Convex (QC) model, is discussed in subsection 4.2.2.

In subsection 4.2.3, a detailed representation of the PQ-capability curves of generators is provided, which concludes the extension of the POE computation model.

The extended model is validated on test networks whose description, alongside the experimental methodology and the benchmark POE computation model used for comparison, is provided in section 4.3. The corresponding results are presented and discussed in chapter 5.

4.2 Improvements of the POE computation model

4.2.1 Phase Shifters

Currently, the model used to compute POEs only considers the re-dispatch of active and reactive power of generation as control actions. However, since these actions might entail large financial compensation, they should be regarded as last-resort options. Therefore, there is a need to further develop practical control actions that the operators can implement to improve the quality of the computed POEs. A typical control action regularly exploited by transmission system operators is the modification of phase-shifters' operating set-point. In this subsection, phase shifters and their mathematical models are presented and subsequently integrated into the optimisation model.

Phase-shifters or, more precisely, phase-shifting transformers were first introduced in power systems in the 1930s. A phase-shifting transformer is a transformer-based device whose essential feature is to regulate a phase angle in a power system. It can be proven that modifying the phase shift between terminal voltage phasors helps regulate power flow through a line [68]. Phase-shifting transformers have been widely used by TSOs to manage congestion issues in their networks by redirecting power flows. They rely on mechanical switches, which can have a high response time as a result of the inertia of moving parts and a high level of maintenance due to mechanical contacts and oil deterioration.

Authors in [69] highlight that some power-electronic-based devices can be an alternative to classical phase-shifting transformers. These are called static phase-shifters and mainly rely on thyristors. The models proposed by the authors in [69] can be used to model a phase-shifting device, whatever the underlying technology. By considering only symmetrical phase shifters (i.e., the magnitude of the output and input voltages is the same), the active and reactive power flowing through the phase shifters are given by:

$$P_{ik} = -P_{ki} = \frac{V_i V_k}{X_s}\sin(\theta_{ik} + \rho), \tag{4.1a}$$

$$Q_{ik} = \frac{V_i}{X_s}\left(V_i - V_k \cos(\theta_{ik} + \rho)\right), \tag{4.1b}$$

$$Q_{ki} = \frac{V_k}{X_s}\left(V_k - V_i \cos(\theta_{ik} + \rho)\right), \tag{4.1c}$$

where $\rho \in \mathbb{R}$ is the shift angle, $P_{ik}, Q_{ik} \in \mathbb{R}$ are the active and reactive power flow going through the phase-shifter, with i, k the indices of the input and output nodes, respectively. $V_i, V_k \in \mathbb{R}^+$ are the voltage magnitudes. $X_s \in \mathbb{R}^+$ is the equivalent reactance and $\theta_{ik} \in \mathbb{R}$ is the voltage phase angle difference.

Therefore, phase-shifters can be integrated into the power flow model by simply summing up voltage phase angle differences and an additional variable, ρ, representing the phase-shifter's operating point. For example, when considering phase-shifters, the LACPF model becomes:

$$P_{nj} = g_{nj}(V_n - V_j) - b_{nj}(\theta_n - \theta_j + \rho_{nj}), \tag{2-P}$$

$$Q_{nj} = -b_{nj}(V_n - V_j) - g_{nj}(\theta_n - \theta_j + \rho_{nj}), \quad \forall (n,j) \in \mathcal{E}_o. \tag{2-Q}$$

The variable $\rho_{n,m} \in \mathbb{R}$ is non-zero only if a phase-shifter is present on line (n, j), and is bounded by:

$$\underline{\rho}_{nj} \leq \rho_{nj} \leq \overline{\rho}_{nj},$$

where parameters $\underline{\rho}_{nj}, \overline{\rho}_{nj} \in \mathbb{R}$ are the maximum and minimum allowed phase-shifts at line (n,j). Phase-shifting transformers are typically operated in the symmetric range ±30° (±25° in Belgium) [70]. Mathematically, these control actions are added to the vector u, such that $u \leftarrow \big(u,\ (\rho_{nj})_{(n,j)\in\mathcal{E}}\big)$. The joint feasible set is updated accordingly as $\mathcal{F} \leftarrow \mathcal{F} \times \prod_{(n,j)\in\mathcal{E}} \mathcal{F}_{nj}$, where each $\mathcal{F}_{nj} = [\,\underline{\rho}_{nj}, \overline{\rho}_{nj}\,]$ constitutes one additional factor in the Cartesian product defining $\mathcal{F}$.

It is further assumed that adjusting a phase-shifter's operating setpoint carries an operational cost for the network operator. Including this cost in the model serves two purposes: (i) it reflects the mechanical wear and associated maintenance expenses incurred by phase-shifting transformers during tap changes, and (ii) it acts as a regularisation term, preventing the solver from exploiting the phase-shifter in an unrealistic or excessive manner. The cost-related constraint is accordingly extended as follows:

$$\beta \sum_{n\in\mathcal{N}} \left[P_{gen,n} - P'_{gen,n}\right]^2 + \tau \sum_{(n,j)\in\mathcal{E}} \rho_{nj}^2 \ \leq\ A,$$

where A is the worst-case operational cost, minimised in the objective function. The weighting parameter $\tau \in \mathbb{R}^+$ is set significantly smaller than β, reflecting the fact that generator re-dispatch is considerably more costly than a phase-shifter setpoint adjustment.

4.2.2 QC model

Let us consider a branch $(n, j) \in \mathcal{E}$ with series admittance $y_{nj} = g_{nj} + jb_{nj} = 1/(R_{nj} + jX_{nj})$. Every branch carries a phase-shift angle ρ_{nj}; for branches without a physical phase-shifter, ρ_{nj} is fixed to zero via its bounds. The sending-end active and reactive power flows are [71–73]:

$$P_{nj} = g_{nj} V_n^2 - V_n V_j \big[g_{nj} \cos(\theta_n - \theta_j + \rho_{nj}) + b_{nj} \sin(\theta_n - \theta_j + \rho_{nj}) \big], \tag{4.2}$$

$$Q_{nj} = -b_{nj} V_n^2 - V_n V_j \big[g_{nj} \sin(\theta_n - \theta_j + \rho_{nj}) - b_{nj} \cos(\theta_n - \theta_j + \rho_{nj}) \big], \tag{4.3}$$

where V_n represents the voltage magnitude at node n. Setting $\rho_{nj} = 0$ recovers the standard equations for an ordinary branch.[1]

The branch flow equations (4.2)–(4.3) are non-convex due to bilinear products $V_n V_j \cos(\cdot)$ and $V_n V_j \sin(\cdot)$. The QC model convexifies these terms by introducing auxiliary variables and replacing each nonlinear product with a tight convex envelope [74]. To avoid any confusion with previous envelope definitions, the convex constraints on the auxiliary variables presented in this subsection are referred to as convex *bounds*.

Auxiliary Variables

For each branch $(n, j) \in \mathcal{E}$, the following auxiliary variables replace the nonlinear terms in (4.2)–(4.3):

- $v_n \approx V_n^2$: voltage magnitude squared,
- $\delta_{nj} = \theta_n - \theta_j + \rho_{nj}$: effective angle difference,
- $u_{nj} \approx V_n V_j$: voltage magnitude product,
- $c_{nj} \approx \cos \delta_{nj}$: cosine of effective angle difference,
- $s_{nj} \approx \sin \delta_{nj}$: sine of effective angle difference,
- $wr_{nj} \approx V_n V_j \cos \delta_{nj}$: active cross-product,
- $wi_{nj} \approx V_n V_j \sin \delta_{nj}$: reactive cross-product.

The symbol $\approx$ indicates that these variables are not set equal to their nonlinear counterparts, but are instead constrained to lie within convex bounds around them. Substituting into (4.2)–(4.3):

$$P_{nj} = g_{nj}(v_n - wr_{nj}) - b_{nj}\, wi_{nj}, \tag{4.4}$$

$$Q_{nj} = -b_{nj}(v_n - wr_{nj}) - g_{nj}\, wi_{nj}. \tag{4.5}$$

These expressions are now linear in the auxiliary variables. The remaining work of this subsection is to enforce, through convex constraints, that each auxiliary variable remains a valid approximation of the nonlinear expression it replaces.

Convex bounds

Let us assume that δ_{nj} is bounded by $|\delta_{nj}| \leq \theta^{\Delta}$. Five families of convex bounds are required, one for each type of nonlinear product.

Bounds for v_n:

[1] No shunt susceptance is included; the branch model is a pure series admittance y_{nj}.

The squared voltage magnitude is enclosed between a lower convex bound and a linear upper bound derived from the secant of the function over $[\underline{V}_n, \overline{V}_n]$, i.e., the line passing through the points $(\underline{V}_n, \underline{V}_n^2)$ and $(\overline{V}_n, \overline{V}_n^2)$:

$$v_n \geq V_n^2, \tag{T-lb}$$

$$v_n \leq (\underline{V}_n + \overline{V}_n)V_n - \underline{V}_n\overline{V}_n, \tag{T-ub}$$

where $\underline{V}_n, \overline{V}_n$ are the minimum and maximum acceptable voltage magnitude at node n, respectively. Mathematically, these convex bounds are noted as $v_n \in \text{CONV}(V_n)$ in the POE computation model.

McCormick bounds for u_{nj}:

The bilinear product of two voltage magnitudes is enclosed by the McCormick relaxation, which constructs four linear inequalities from the bounds $[\underline{V}_n, \overline{V}_n]$ and $[\underline{V}_j, \overline{V}_j]$:

$$u_{nj} \geq \underline{V}_n V_j + V_n \underline{V}_j - \underline{V}_n \underline{V}_j, \tag{M-lb1}$$

$$u_{nj} \geq \overline{V}_n V_j + V_n \overline{V}_j - \overline{V}_n \overline{V}_j, \tag{M-lb2}$$

$$u_{nj} \leq \overline{V}_n V_j + V_n \underline{V}_j - \overline{V}_n \underline{V}_j, \tag{M-ub1}$$

$$u_{nj} \leq \underline{V}_n V_j + V_n \overline{V}_j - \underline{V}_n \overline{V}_j. \tag{M-ub2}$$

Mathematically, the McCormick bounds are noted as $u_{nj} \in \text{McCormick}(V_n, V_j)$ in the POE computation model.

Bounds for c_{nj}:

The cosine function is bounded above by a quadratic concave upper bound and below by the chord value at the boundary of the angle interval:

$$c_{nj} \leq 1 - \frac{1 - \cos\theta^\Delta}{(\theta^\Delta)^2}\delta_{nj}^2, \tag{C-ub}$$

$$c_{nj} \geq \cos\theta^\Delta. \tag{C-lb}$$

Bounds for s_{nj}:

The sine function is enclosed between two linear bounds:

$$s_{nj} \leq \cos\left(\frac{\theta^\Delta}{2}\right)\left(\delta_{nj} - \frac{\theta^\Delta}{2}\right) + \sin\left(\frac{\theta^\Delta}{2}\right), \tag{S-ub}$$

$$s_{nj} \geq \cos\left(\frac{\theta^\Delta}{2}\right)\left(\delta_{nj} + \frac{\theta^\Delta}{2}\right) - \sin\left(\frac{\theta^\Delta}{2}\right). \tag{S-lb}$$

Mathematically, the bounds around the trigonometric functions are written as $(c_{nj}, s_{nj}) \in \text{TrigEnv}(\delta_{nj})$, in the POE computation model.

Composed bounds for wr_{nj} and wi_{nj}:

The triple products $V_n V_j \cos\delta_{nj}$ and $V_n V_j \sin\delta_{nj}$ are convexified by applying a second McCormick relaxation to the product of u_{nj} and the corresponding trigonometric auxiliary variable:

$$wr_{nj} \in \text{McCormick}(u_{nj},\ c_{nj}), \tag{M-wr}$$

$$wi_{nj} \in \text{McCormick}(u_{nj},\ s_{nj}). \tag{M-wi}$$

Jabr constraint [75]:

Finally, the following second-order cone constraint, known as the Jabr constraint, is imposed to strengthen the approximation by linking the cross-products back to the squared voltage magnitudes:

$$wr_{nj}^2 + wi_{nj}^2 \le v_n \cdot v_j, \qquad \forall (n, j) \in \mathcal{E}. \tag{4.6}$$

These bounds, as well as Equation 4.4, Equation 4.5, and the Jabr constraint, form the power flow model used in this section. These equations are a main block of the full QC-POE computation model proposed in the thesis, and fully detailed in subsection 4.2.4.

4.2.3 Generator Capability

The P–Q capability area of a generator at node n is defined by:

$$\underline{P}_{gen,n} \le P'_{gen,n} \le \overline{P}_{gen,n}, \tag{4.7}$$

$$\underline{Q}_{gen,n} \le Q'_{gen,n} \le \overline{Q}_{gen,n}, \tag{4.8}$$

$$\left(\frac{P'_{gen,n}}{\overline{P}_{gen,n}}\right)^2 + \left(\frac{Q'_{gen,n}}{\overline{Q}_{gen,n}}\right)^2 \le 1. \tag{4.9}$$

Constraint (4.9) is a convex second-order cone constraint restricting the feasible region to an ellipse centred at the origin, as illustrated in Figure 4.1. This set is particularly suitable for modelling converter-interfaced PV generators [76].

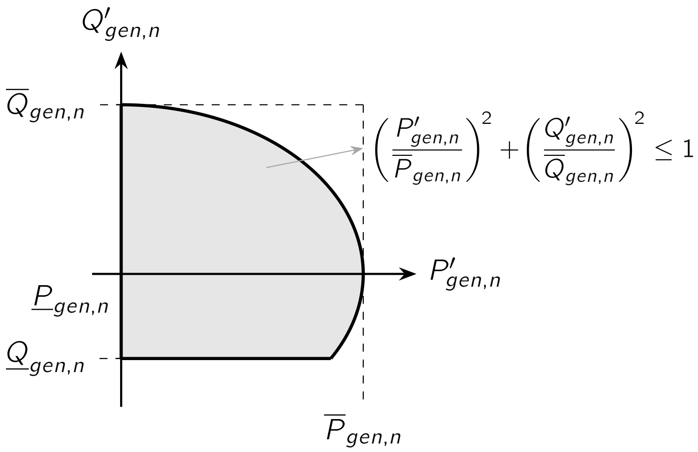

Figure 4.1: Illustration of the convex set $\mathcal{O}_g$ defining the P–Q capability area of a generator at node n. The feasible region (shaded) is the intersection of the bounding box $[\underline{P}_{gen,n}, \overline{P}_{gen,n}] \times [\underline{Q}_{gen,n}, \overline{Q}_{gen,n}]$ and the interior of ellipse (4.9).

4.2.4 Full QC-POE Model

The goal is to find the largest feasible POE volume (both in terms of active and reactive power) while penalising barycentre deviations from children's demands and regularising re-dispatch and phase-shift utilization. The QC-POE computation model can be written as:

$$
\begin{aligned}
\max_{\overline{P}^{\mathcal{C}},\overline{Q}^{\mathcal{C}},A} \quad & \sum_{n\in\mathcal{N}_o^{\mathcal{C}}}\Big[\mathrm{Vol}(\overline{P}_n^{\mathcal{C}}) - \gamma_P \mathrm{Vol}(\overline{P}_n^{\mathcal{C}})^2\Big] + \sum_{n\in\mathcal{N}_o^{\mathcal{C}}}\Big[\mathrm{Vol}(\overline{Q}_n^{\mathcal{C}}) - \gamma_Q \mathrm{Vol}(\overline{Q}_n^{\mathcal{C}})^2\Big] \\
& - \alpha_P \sum_{n\in\mathcal{N}_o^{\mathcal{C}}}\Big[\mathrm{Bar}(\overline{P}_n^{\mathcal{C}}) - \hat{P}_n^{-,c}\Big]^2 - \alpha_Q \sum_{n\in\mathcal{N}_o^{\mathcal{C}}}\Big[\mathrm{Bar}(\overline{Q}_n^{\mathcal{C}}) - \hat{Q}_n^{-,c}\Big]^2 - A && (4.10a)\\
\text{s.t.} \quad & \forall (P^-,Q^-)\in\overline{S}^{\mathcal{C}},\ \forall |V^{\mathcal{P}}|\in\overline{V}^{\mathcal{P}}, \exists u\in\mathcal{F}: \\
& \beta\sum_{n\in\mathcal{N}_o}\big[P_{gen,n} - P'_{gen,n}\big]^2 + \tau\sum_{(n,j)\in\mathcal{E}_o}\rho_{nj}^2 \le A, && (4.10b)\\
& P_{\mathrm{load},n} - P'_{\mathrm{gen},n} = \sum_{(nm)\in\mathcal{E}_o} P_{nm} + P_n^+ - P_n^-, \quad \forall n\in\mathcal{N}_o, && (4.10c)\\
& Q_{\mathrm{load},n} - Q'_{\mathrm{gen},n} = \sum_{(nm)\in\mathcal{E}_o} Q_{nm} + Q_n^+ - Q_n^-, \quad \forall n\in\mathcal{N}_o, && (4.10d)\\
& P_{nj} = g_{nj}(v_n - wr_{nj}) - b_{nj}\, wi_{nj}, \quad \forall (nj)\in\mathcal{E}_o, && (4.10e)\\
& Q_{nj} = -b_{nj}(v_n - wr_{nj}) - g_{nj}\, wi_{nj}, \quad \forall (nj)\in\mathcal{E}_o, && (4.10f)\\
& \underline{P}_{gen,n} \le P'_{gen,n} \le \overline{P}_{gen,n}, \quad \forall n\in\mathcal{N}_o, && (4.10g)\\
& \underline{Q}_{gen,n} \le Q'_{gen,n} \le \overline{Q}_{gen,n}, \quad \forall n\in\mathcal{N}_o, && (4.10h)\\
& \left(\frac{P'_{gen,n}}{\overline{P}_{gen,n}}\right)^2 + \left(\frac{Q'_{gen,n}}{\overline{Q}_{gen,n}}\right)^2 \le 1, \quad \forall n\in\mathcal{N}_o, && (4.10i)\\
& P_{nj} + P_{jn} = R_{nj}\cdot l_{nj}, \quad \forall (nj)\in\mathcal{E}_o, && (4.10j)\\
& Q_{nj} + Q_{jn} = X_{nj}\cdot l_{nj}, \quad \forall (nj)\in\mathcal{E}_o, && (4.10k)\\
& P_{nj}^2 + Q_{nj}^2 \le v_n\cdot l_{nj}, \quad \forall (nj)\in\mathcal{E}_o, && (4.10l)\\
& \delta_{nj} = \theta_n - \theta_j + \rho_{nj}, \quad \forall (nj)\in\mathcal{E}_o, && (4.10m)\\
& |\delta_{nj}| \le \overline{\Delta\theta}, \quad \forall (nj)\in\mathcal{E}_o, && (4.10n)\\
& v_n \in \mathrm{CONV}(V_n), \quad \forall n\in\mathcal{N}_o, && (4.10o)\\
& u_{nj} \in \mathrm{McCormick}(V_n, V_j), \quad \forall (nj)\in\mathcal{E}_o, && (4.10p)\\
& (c_{nj}, s_{nj}) \in \mathrm{TrigEnv}(\delta_{nj}), \quad \forall (nj)\in\mathcal{E}_o, && (4.10q)\\
& wr_{nj} \in \mathrm{McCormick}(u_{nj}, c_{nj}), \quad \forall (nj)\in\mathcal{E}_o, && (4.10r)\\
& wi_{nj} \in \mathrm{McCormick}(u_{nj}, s_{nj}), \quad \forall (nj)\in\mathcal{E}_o, && (4.10s)\\
& wr_{nj}^2 + wi_{nj}^2 \le v_n\cdot v_j, \quad \forall (nj)\in\mathcal{E}_o, && (4.10t)\\
& \underline{v}_n \le v_n \le \overline{v}_n, \quad \forall n\in\mathcal{N}_o, && (4.10u)\\
& \theta_r = 0, \quad v_r = 1 \text{ p.u.}, && (4.10v)\\
& \underline{\rho}_{nj} \le \rho_{nj} \le \overline{\rho}_{nj}, \quad \forall (nj)\in\mathcal{E}_o, && (4.10w)\\
& |V^{\mathcal{C}}| \in \overline{V}^{\mathcal{C}}, && (4.10x)\\
& S^+ \in \overline{S}^{\mathcal{P}}, && (4.10y)
\end{aligned}
$$

where Equation 4.10l is defined to strengthen the approximation of the power flow equations by using a second-order cone constraint that relies on the absolute square of line current $I_{nj} \in \mathbb{R}^{+}, \forall(nj) \in \mathcal{E}_o$, first proposed in [77]. Equation 4.10j and Equation 4.10k model the active and reactive power losses of the lines, respectively.

4.3 Experimental Methodology

In this section, the methodology to validate the POE computation model, detailed in section 4.2, is explained.

Firstly, the POE computation model is compared to another model that is considered as a benchmark. This benchmark is chosen to be a DC-based POE computation model, i.e, a POE computation model relying on the DC power flow equations. The motivation for this choice and the detailed modelling are discussed in subsection 4.3.1.

Secondly, POE computation models rely on some initial set-points of the generators. These set-points need to be determined, alongside the active and reactive forecasted power exchange at each child node. The procedure to determine the values of these parameters is given in subsection 4.3.2.

Finally, the test networks on which the POE computation models are applied are presented in detail in subsection 4.3.3.

4.3.1 DC-based POE computation problem

In order to compare the results obtained with the developed POE computation model, a benchmark model should be formalized. In this thesis, this benchmark model corresponds to an active-power-only model.

The main advantage of this choice is that the benchmark model is a model accounting solely for the thermal limits and not for voltage-related constraints, which simplifies the analysis of the results. It has another advantage of allowing for phase-shifter modelling as the voltage phase angles are accounted for in the model. An extensive description of the DC power flows is given in Appendix C.

Mathematically, the DC-based POE computation problem can be written as:

$$\max_{\overline{P}^C, A} \sum_{n \in \mathcal{N}_o^C} \left[\mathrm{Vol}(\overline{P}_n^C) - \gamma \cdot \mathrm{Vol}(\overline{P}_n^C)^2\right] - \alpha \sum_{n \in \mathcal{N}_o^C} \left[\mathrm{Bar}(\overline{P}^C) - \hat{P}_n^{-,c}\right]^2 - A \tag{4.11a}$$

$$\text{s.t. } \forall P^{-,\mathcal{C}} \in \overline{P}^{\mathcal{C}},\ \forall \left|V^{\mathcal{P}}\right| \in \overline{V}^{\mathcal{P}}:$$

$$\beta \sum_{n \in \mathcal{N}_o} \left(P_{gen,n} - P'_{gen,n}\right)^2 + \tau \sum_{(m,n) \in \mathcal{E}_o} \rho_{m,n}^2 \leq A, \tag{4.11b}$$

$$P_{m,n} = \frac{\theta_m - \theta_n + \rho_{m,n}}{X_{m,n}}, \qquad \forall (m,n) \in \mathcal{E}_o, \tag{4.11c}$$

$$P_{load,n} - P'_{gen,n} = \sum_{(m,n) \in \mathcal{E}_o} P_{m,n} + P_n^+ - P_n^-, \qquad \forall n \in \mathcal{N}_o, \tag{4.11d}$$

$$\underline{P}_{gen,n} \leq P'_{gen,n} \leq \overline{P}_{gen,n}, \qquad \forall n \in \mathcal{N}_o, \tag{4.11e}$$

$$-\overline{P}_{m,n} \leq P_{m,n} \leq \overline{P}_{m,n}, \qquad \forall (m,n) \in \mathcal{E}_o, \tag{4.11f}$$

$$\underline{\rho}_{mn} \leq \rho_{mn} \leq \overline{\rho}_{mn}, \qquad \forall (m,n) \in \mathcal{E}_o, \tag{4.11g}$$

$$\underline{\Delta\theta} \leq \theta_m - \theta_n \leq \overline{\Delta\theta}, \qquad \forall (m,n) \in \mathcal{E}_o, \tag{4.11h}$$

$$|V^{\mathcal{C}}| \in \overline{V}^{\mathcal{C}}, \tag{4.11i}$$

$$P^+ \in \overline{P}^{\mathcal{P}}, \tag{4.11j}$$

where $\overline{P}_{m,n} \in \mathbb{R}^+$ is the capacity of line (m,n). To avoid any confusion, Equation 4.11 is called the DC-POE computation model, while Equation 4.10 is called the QC-POE computation model.

It is worth noting that VOEs are trivially verified in the DC-POE computation model, since all voltage magnitudes in the operational graph are treated as parameters assumed to be equal to 1 $p.u.$ and constant.

4.3.2 Initial generator set-points and children power exchanges

Parameters $P_{gen,n}$ which correspond to the generator's active power output at node $n \in \mathcal{N}$, (before potential re-dispatch), need to be determined. For that, it is assumed in the experiments that the parameters' values are the results of a centralized OPF. More precisely, the parameters $P_{gen,n}$ required in the DC-POE computation model are obtained after solving a DC-OPF, while an AC-OPF is solved to determine the parameters $P_{gen,n}$ for the QC-POE computation model.

The DC-OPF minimizes both generators' power output (i.e, $P_{gen,n}$) and imported energy, subject to DC power flow equations and security constraints [78]:

$$\min_{P_{gen,n}, P_n^+} \sum_n \left(\alpha_n P_{gen,n}^2 + \beta_n P_{gen,n}\right) + \sum_n \left(\xi_n P_n^{+2} + \psi_n P_n^+\right) \tag{4.12a}$$

$$\text{s.t. } P_{load,n} - P_{gen,n} = \sum_{(m,n)} P_{m,n} - \sum_{(n,j)} P_{n,j} + P_n^+, \qquad \forall n \in \mathcal{N}, \tag{4.12b}$$

$$P_{n,m} = \frac{\theta_n - \theta_m}{X_{n,m}}, \qquad \forall (n,m) \in \mathcal{E}, \tag{4.12c}$$

$$\theta_{ref} = 0, \tag{4.12d}$$

$$P_{gen,\min,n} \leq P_{gen,n} \leq P_{gen,\max,n}, \qquad \forall n \in \mathcal{N}, \tag{4.12e}$$

$$-\overline{P}_{n,m} \leq P_{n,m} \leq \overline{P}_{n,m}, \qquad \forall (n,m) \in \mathcal{E}, \tag{4.12f}$$

where parameter $X_{n,m} \in \mathbb{R}$ is the reactance of line (n,m), parameters $\alpha_n, \beta_n \in \mathbb{R}^+$ are the quadratic and linear costs of the generator at node n and parameters $\xi_n, \psi_n \in \mathbb{R}^+$ are the quadratic and linear costs of imported power from the slack node n. As the slack node is assumed to be the parent node, P_n^+ is non-zero only at $n \in \mathcal{N}_o^{\mathcal{P}}$. The AC-OPF minimizes generators' output and imported energy, subject to the full AC power flow equations [78, 79]:

$$
\begin{aligned}
\min_{P_{gen,n},\, P_n^+} \quad & \sum_n \left(\alpha_n P_{gen,n}^2 + \beta_n P_{gen,n}\right) + \sum_n \left(\xi_n P_n^{+2} + \psi_n P_n^+\right) && && \text{(4.13a)}\\
\text{s.t. } & P_{\text{load},n} - P_{\text{gen},n} = \sum_{nm \in \mathcal{E}} P_{nm} + P_n^+ - P_n^-, && \forall n \in \mathcal{N}, && \text{(4.13b)}\\
& Q_{\text{load},n} - Q_{\text{gen},n} = \sum_{nm \in \mathcal{E}} Q_{nm} + Q_n^+ - Q_n^-, && \forall n \in \mathcal{N}, && \text{(4.13c)}\\
& P_{n,m} = V_n^2 G_{nm} - V_n V_m \big(G_{nm}\cos(\theta_n - \theta_m) + B_{nm}\sin(\theta_n - \theta_m)\big), && \forall (n,m) \in \mathcal{E}, && \text{(4.13d)}\\
& Q_{n,m} = -V_n^2 \big(B_{nm} + B_{nm}^{sh}\big) + V_n V_m \big(B_{nm}\cos(\theta_n - \theta_m) - G_{nm}\sin(\theta_n - \theta_m)\big), && && \text{(4.13e)}\\
& && \forall (n,m) \in \mathcal{E}, && \text{(4.13f)}\\
& \theta_{ref} = 0, \quad V_{ref} = 1, && && \text{(4.13g)}\\
& P_{gen,\min,n} \le P_{gen,n} \le P_{gen,\max,n}, && \forall n \in \mathcal{N}, && \text{(4.13h)}\\
& Q_{gen,\min,n} \le Q_{gen,n} \le Q_{gen,\max,n}, && \forall n \in \mathcal{N}, && \text{(4.13i)}\\
& V_{\min,n} \le V_n \le V_{\max,n}, && \forall n \in \mathcal{N}, && \text{(4.13j)}\\
& P_{n,m}^2 + Q_{n,m}^2 \le \overline{S}_{n,m}^2, && \forall (n,m) \in \mathcal{E}, && \text{(4.13k)}
\end{aligned}
$$

where G_{nm} and B_{nm} are the series conductance and susceptance of line (n,m), and B_{nm}^{sh} is the total shunt susceptance of line (n,m).

In practice, $P_{gen,n}$ might be the result of a market-clearing or unit commitment process, for which the results are communicated to the system operator. Other parameters need to be determined. For example:

$$\hat{P}_n^{-,c}, \hat{Q}_n^{-,c}, \quad \forall n \in \mathcal{N}_o^{\mathcal{C}},$$

which are, respectively, the active and reactive forecasted power exchange at the child node n, and are used in the utility function of the POE computation model.[2]

To determine these parameters, let us suppose that the operational network of child c, such that $c \in \mathcal{N}_o^{\mathcal{C}}$, is depicted as

$$\mathfrak{G}_c = (\mathcal{N}_c, \mathcal{E}_c) \subseteq \mathfrak{G},$$

where $\mathcal{N}_c \subseteq \mathcal{N}$ is the set of nodes within operational network of child c and $\mathcal{E}_c$ is the set of edges within operational network of child c such that

$$\mathcal{E}_c \subseteq \left(\mathcal{E} \cap \mathcal{N}_c^2\right).$$

Based on these definitions, it is supposed that the active and reactive power exchange forecasts at the interfaces between operational networks o and c are computed as follows, for each time period:

$$\hat{P}_n^{-,c} = \sum_{n' \in \mathcal{N}_c} P_{load,n'}, \quad \forall n \in \mathcal{N}_o^{\mathcal{C}},$$

$$\hat{Q}_n^{-,c} = \sum_{n' \in \mathcal{N}_c} Q_{load,n'}, \quad \forall n \in \mathcal{N}_o^{\mathcal{C}},$$

[2] Only the active power exchange $\hat{P}_n^{-,c}$ is used in the DC-POE computation model.

where both local generation and losses are neglected. It should be emphasized that the operator of a given operational network would not directly compute the loads of another operator's network. In practice, a parent network must rely on forecasts directly provided by its child networks. Since these forecasts affect the optimisation problem, regulatory oversight is required to prevent potential misuse.

4.3.3 Test Network Description

The test networks used to illustrate the POE computation approach are based on the IEEE 14-bus network and the PandaPower MultiVoltage network. These test networks are depicted in Figure 4.2 and Figure 4.3. In both cases, the system is partitioned into three subnetworks: the TSO (parent) network, highlighted in red, and the DSO (child) networks, shown in dark. The modified IEEE 14-bus network includes two distribution networks connected to the TSO, whereas the second test network features both a TSO/DSO interface and a TSO/TSO interface.

POEs are computed at the interfaces between subnetworks. Beyond the TSO/DSO interfaces considered in the modified IEEE 14-bus network, the second test case illustrates that the proposed approach can also be applied to operate separately different parts of the TSO's network for which there exists a hierarchy. For example, the parent network might be a higher-voltage network, and the child networks are lower-voltage-level networks, operated by the TSO. This decomposition serves two purposes: (i) it illustrates that POEs can be computed not only across transmission–distribution boundaries but also within networks that are willing to be operated independently, and (ii) it enables the study of an operational network in which the parent network itself has a non-zero POE.

Therefore, for the first test network (i.e, the modified IEEE 14-bus), POEs are computed at the interface between the TSO and the DSOs, which means that the operational network considered is the one encircled in red in Figure 4.2. For the second test network (i.e, the PandaPower MultiVoltage network), the considered operational network in the experiments is the one having node 3 as a parent node and node 11 as a child node. It should be emphasized that nodes 9,10 and 12 are also assumed to be child nodes.

The POE computation model relies on the network characteristics. Depending on the power flow model used, the network parameters required might differ. This might include the line resistances $R_{n,j}$, reactances $X_{n,j}$, conductances $G_{n,j}$, and/or susceptances $B_{n,j}$. For example, the DC-POE computation model relies solely on the inverse of the line reactance, whereas the QC-POE computation model relies on both the line conductances and susceptances. These parameters are provided in Appendix D for both test networks.

4.3.4 Sequence of operations

The experiments are to be performed in the following sequence:

For all test networks and, in particular, for all operational networks:

1. First step of the coordination procedure: all VOEs must be defined at the interface between the operational network and the neighboring networks. In these experiments, it is supposed that the bounds of the VOEs are 0.9 and 1.1 p.u., respectively.

2. Centralized DC-OPF and AC-OPF are performed to obtain $P_{gen,n}, \forall n \in \mathcal{N}_o$ for the DC-POE and QC-POE computation models, respectively. $\hat{P}_n^{-,c}$ and, if relevant, $\hat{Q}_n^{-,c}$ are computed as well, according to subsection 4.3.2, which corresponds to the second step of the coordination procedure.

3. Last step of the coordination procedure: computing the POEs at the interfaces. For that, the DC-POE computation model of subsection 4.3.1 and the QC-POE computation model of subsec-

tion 4.3.1 are solved to compute POEs, which concludes the coordination procedure. Using two POE computation models allows for comparing the resulting POEs depending on the power flow model used.

4. An additional step is to compute POEs when phase-shifters are discarded, and compare the results with the case where the phase-shifter is present to assess the usefulness of the phase-shifter as a control action to compute POEs.

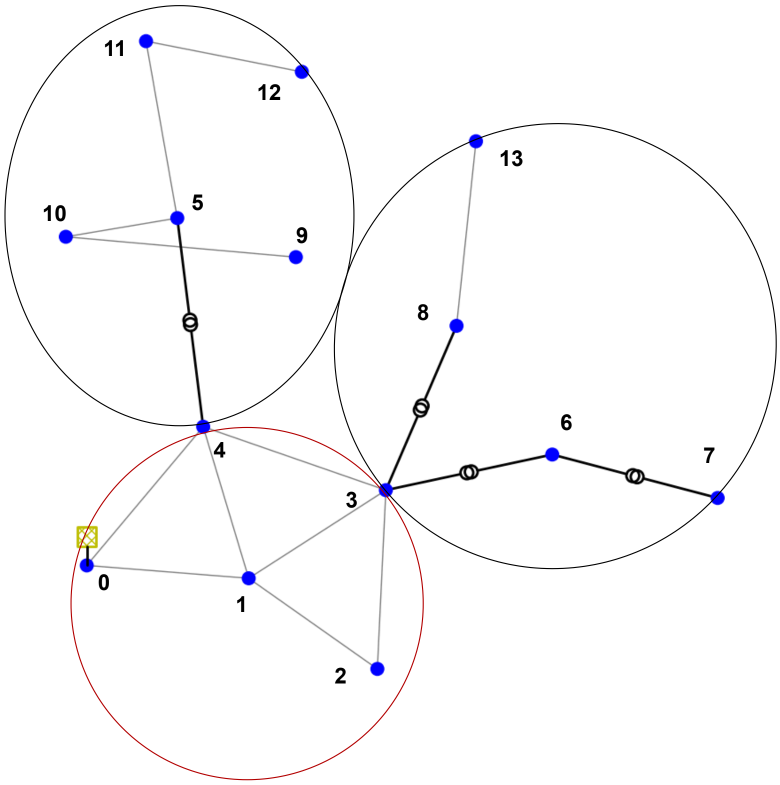

Figure 4.2: Illustration of the modified IEEE 14-bus network, divided into three operational networks.

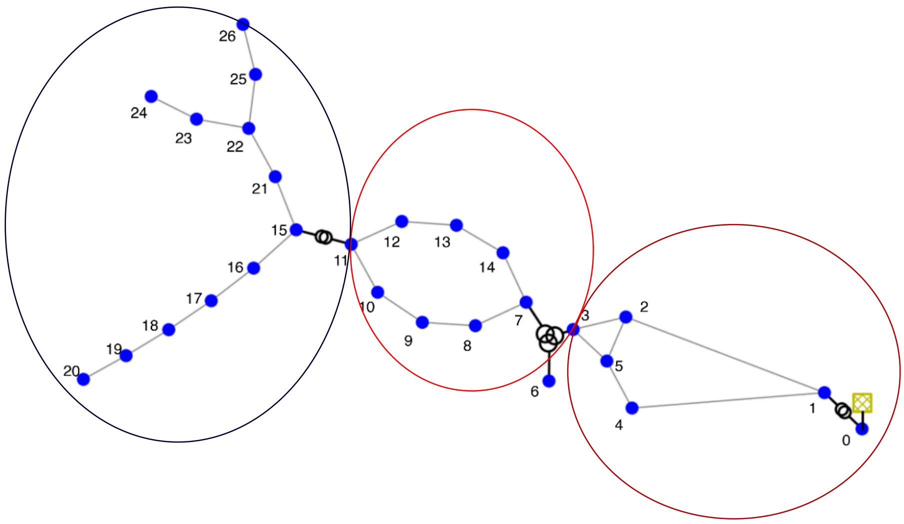

Figure 4.3: Illustration of the *Pandapower Multi-Voltage Level Network*, divided into three operational networks.

Chapter 5

Results and Discussions

5.1 Preliminaries

As explained in subsection 4.3.4, this thesis follows a precise sequence of operations to perform the coordination procedure. The first two steps are (i) determining VOEs at each interface and (ii) determining the load and generation dispatch within the operational network, as well as the forecasted power exchange at all child nodes. Step (i) is trivially satisfied in the experiments, with VOEs' bounds set to 0.9 and 1.1 p.u., respectively. Step (ii) consists in gathering the data required to solve the POE computation model, which involves solving a centralized OPF over the entire network, i.e, a DC-OPF for the DC-POE computation model and an AC-OPF for the QC-POE computation model, and extracting the generators' initial dispatch and the power exchanges at child nodes, as described in chapter 3.

The results of the DC-OPF applied to both test networks are provided in section 5.2. Based on the resulting generators' dispatch and power exchanges, the DC-POE computation model is solved, and the computed POEs are presented in section 5.3. This chapter also discusses the effect of the phase-shifter on the quality of the computed POEs. The sensitivity of the results to the model's parameters is assessed in section 5.4.

Similarly, the results of the AC-OPF applied to both test networks are provided in section 5.5. Based on the resulting generators' dispatch and power exchanges, the QC-POE computation model is solved, and the computed POEs are described in section 5.6. The influence of the model's parameters is assessed in section 5.7.

The quality of the computed POEs is assessed using three metrics:

1. The volume of the POE, hereafter referred to as the *envelope size*.
2. The deviation of the POE's barycenter from the forecast value, hereafter referred to as the *deviation from center*.
3. The worst-case cost (i.e, the value of variable A in the POE computation model), to obtain the POEs, hereafter referred to as the *worst-case cost*.

5.2 DC-OPF Results

5.2.1 DC-OPF: Modified IEEE 14-bus

The results of the DC-OPF are depicted in Figure 5.1. The dispatch of generators is provided in Table 5.1. Considering the TSO's network as the operational network, the child nodes' power exchanges with the operational network are 105.2 MW at child node 3 and 50.9 MW at child node 4.

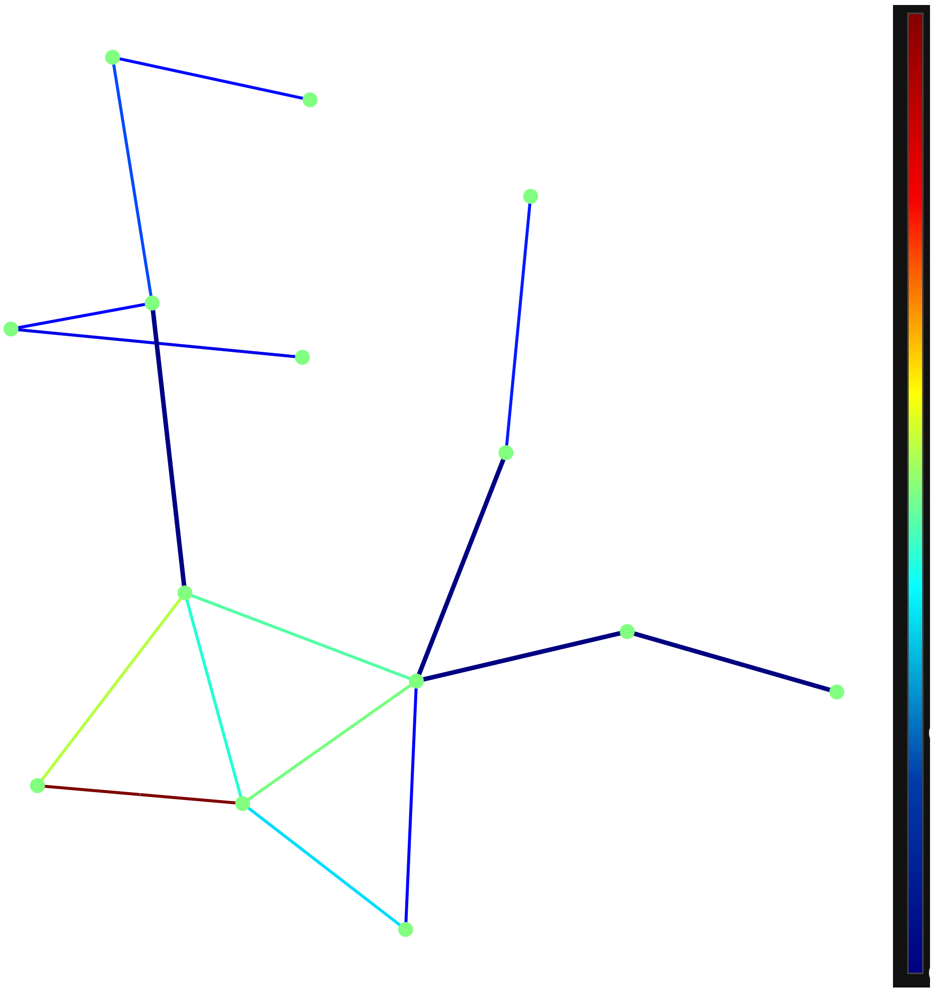

Figure 5.1: Resulting power flows of the DC-OPF applied on the entire IEEE 14-bus network. Red lines are close to congestion, and blue lines are lightly loaded.

Bus	Generation Dispatch (MW)	Load (MW)
0	165.6	10.0
1	44.6	21.7
2	71.75	94.2
3	/	47.8
4	/	7.6
5	/	11.2
6	/	5.0
7	/	8.0
8	/	29.5
9	/	9.0
10	/	3.5
11	/	6.1
12	/	13.5
13	/	14.9
Total	**282**	**282**

Table 5.1: Bus-wise generation and load values after DC-OPF in the modified IEEE 14-bus network.

5.2.2 DC-OPF: Modified PandaPower Multi-Voltage Network

The DC-OPF applied to the second test network shows that resulting flows can remain within acceptable bounds (Figure 5.2). Considering the operational network that has node 3 as the parent node, the child nodes' power exchanges are 1.58, 2.01, 2.45, and 1.64 MW at child nodes 9,10,11, and 12, respectively. The generators' dispatch is given in Table 5.2.

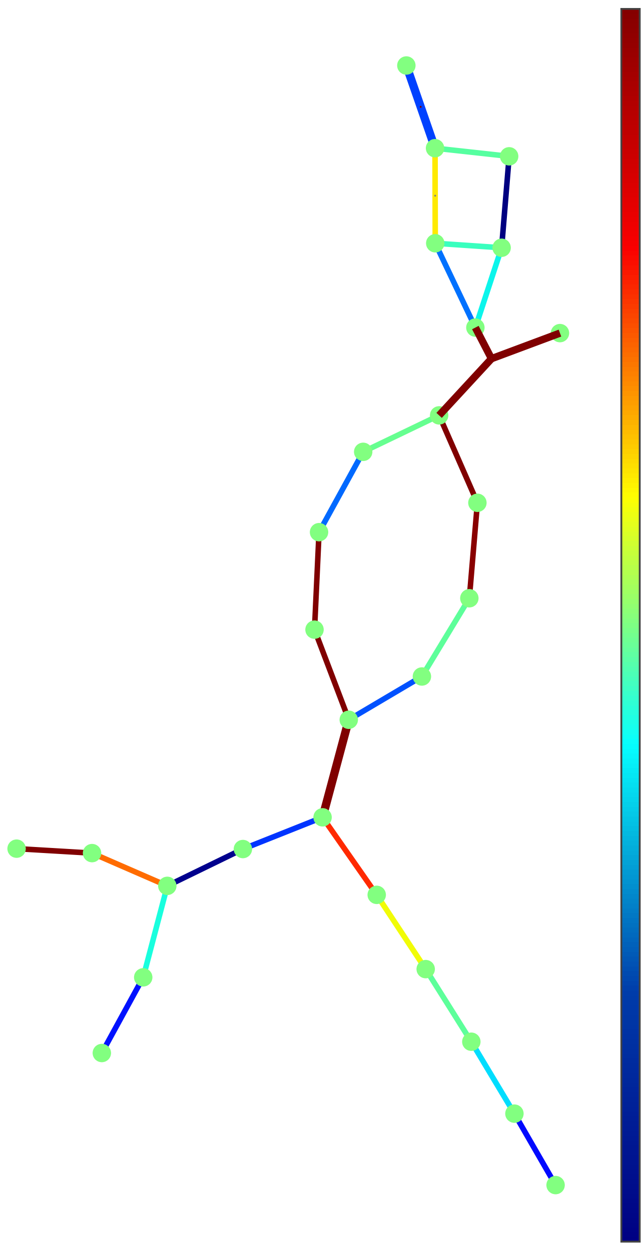

Figure 5.2: Resulting power flows of the DC-OPF applied on the entire PandaPower MultiVoltage network. Red lines are close to congestion; blue lines are lightly loaded.

5.3 DC-POE Computation Model

As mentioned in section 5.1, the impact of the phase-shifter on POEs is assessed in this section. First, POEs are computed without phase-shifters (subsection 5.3.1), while a phase-shifter is added to test networks in subsection 5.3.2.

Bus	Generation Dispatch (MW)	Load (MW)
0	91.10	/
1	330.71	166.00
2	/	138.00
3	/	162.00
4	/	148.00
5	274.18	146.00
6	92.80	68.80
7	82.01	27.20
8	6.10	6.20
9	/	5.28
10	/	6.72
11	/	7.32
12	5.48	5.48
13	18.38	6.04
14	0.00	7.08
15	/	0.36
16	0.00	0.06
17	/	0.05
18	0.00	0.03
19	/	0.06
20	/	0.04
21	/	0.04
22	/	0.05
23	0.00	0.03
24	0.05	0.06
25	0.00	0.02
26	0.15	0.04
Total	**900.96**	**900.96**

Table 5.2: Bus-wise DC-OPF generation and load (PandaPower Multi-Voltage network). A slash denotes no generation unit present; 0.00 denotes a unit present but not dispatched.

5.3.1 Without Phase-Shifter

Without phase-shifters, the POEs obtained at the child nodes are depicted in Figure 5.3 and Figure 5.4 for the IEEE 14-bus network and the PandaPower Multivoltage Network, respectively. The main metrics are given in Tables 5.3 and 5.4.

Child Node	Min (MW)	Max (MW)	Size (MW)	Midpoint Dev. (MW)
3	88.0821	122.3047	34.2226	0.0066
4	32.4093	69.3781	36.9688	0.0063

Table 5.3: POE metrics for child nodes 3 and 4 of the IEEE 14-bus network, without phase-shifter. Worst-case redispatch: 0.0458 p.u. Objective value: 0.356. Parameters: $\alpha = 10000$, $\beta = 5$, $\gamma = 0.5$.

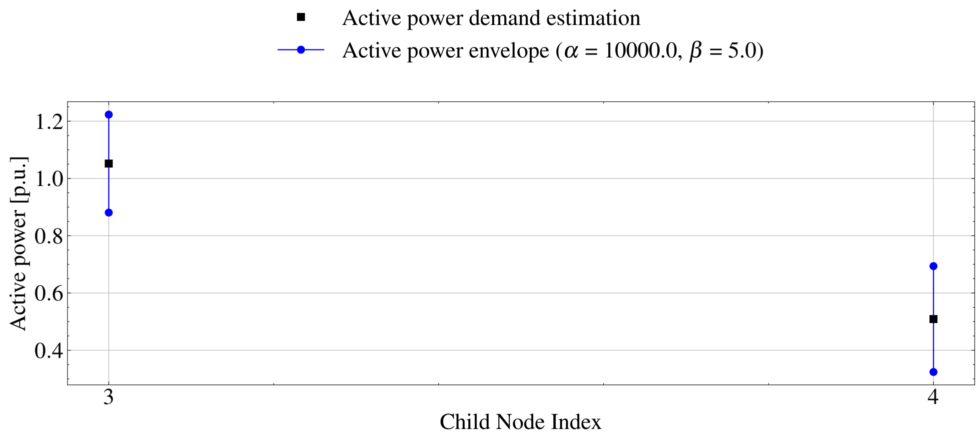

Figure 5.3: POEs obtained at child nodes 3 and 4 of the IEEE 14-bus network, without phase-shifters.

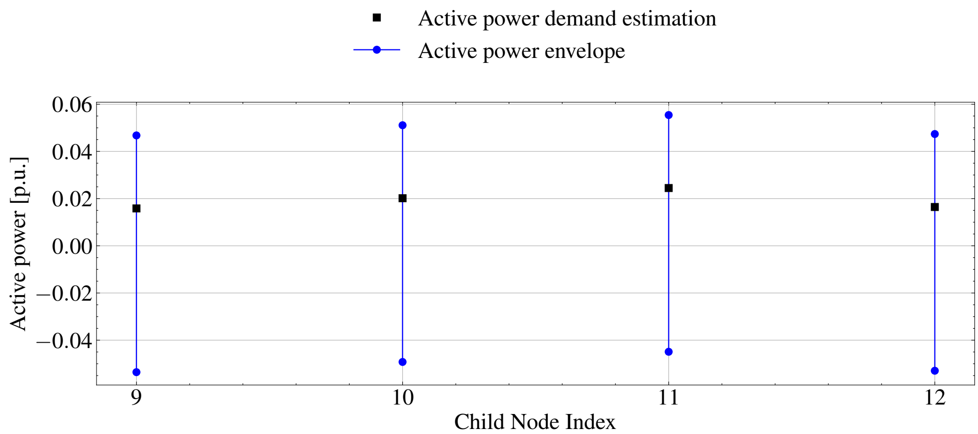

Figure 5.4: POEs obtained at child nodes 9, 10, 11, and 12 of the PandaPower MultiVoltage network, without phase-shifters. Parameters: $\alpha = 100.0$, $\beta = 3.0$, $\gamma = 0.5$.

Child Node	Min (MW)	Max (MW)	Size (MW)	Midpoint Dev. (MW)
9	-5.36	4.68	10.03	1.92
10	-4.92	5.11	10.03	1.92
11	-4.49	5.54	10.03	1.92
12	-5.29	4.74	10.03	1.92

Table 5.4: POE metrics for the multi-voltage network, without phase-shifter. Objective: 2.9987×10^{-1}. Worst-case redispatch: 0.0798 p.u. Parameters: $\alpha = 100$, $\beta = 3.0$, $\gamma = 0.5$, $P_{min} = 0.0$, $P_{max} = 0.5$.

5.3.2 With Phase-Shifter

As depicted in Figure 5.1, the most congested line in the IEEE 14-bus network is line $(0, 1)$. A phase-shifter on this line may therefore increase envelope size by redirecting flows through lines $(0, 4)$ and $(4, 1)$. In the multi-voltage network, different lines are congested, as depicted in Figure 5.2, and it is arbitrarily chosen to put a phase-shifter on line $(7, 14)$.

When a phase-shifter is installed on line $(0, 1)$, the POEs at the child nodes of the IEEE 14-bus network is depicted in Figure 5.5. Table 5.5 reports the corresponding metrics. Compared to Table 5.3, envelope size increases (+9.6% for child node 3 and +1.4% for child node 4), and the deviation from center of both envelopes drops to approximately zero. The worst-case cost, increases (+2.8%) alongside the objective function value (+5.3%).

Regarding the POEs computed for the PandaPower multi-voltage network, the results show that the phase-shifter has no significant impact on POE quality. Indeed, comparing the metrics without a phase-shifter (Table 5.4) and with one (Table 5.6), the variation in metric values is almost imperceptible (below 0.1%).

Given that phase-shifters are CAPEX-intensive, one might question whether the additional flexibility (i.e., the increase in the POE's quality) justifies the investment in this asset. The investment decision process is not formally addressed in this thesis. However, the proposed tool can serve as decision support by quantifying the potential gain in flexibility when investing in this asset. For example, while a phase-shifter might be relevant in the IEEE 14-bus network as it increases the size of the POEs, it seems completely irrelevant for the PandaPower MultiVoltage Network. It should be emphasized that a broader study should be performed to make the final investment decisions. This includes computing POEs at different time steps under different loading conditions. A full profitability assessment methodology is beyond the scope of this thesis.

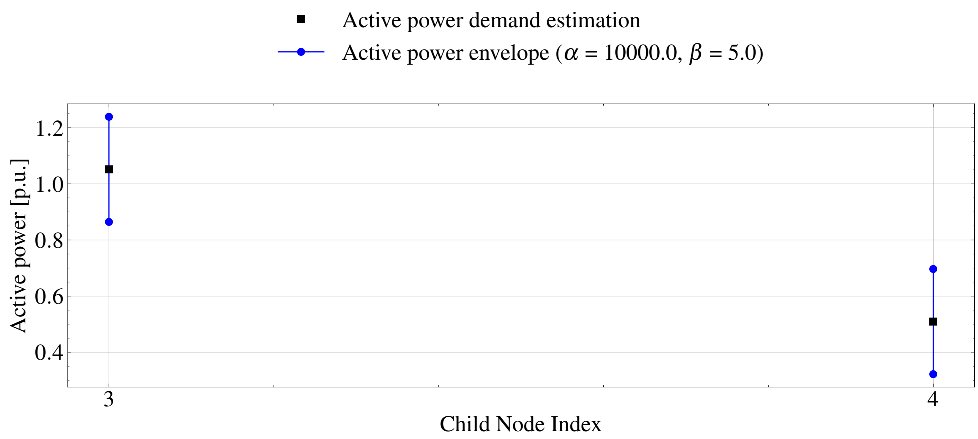

Figure 5.5: POEs obtained at child nodes 3 and 4 of the IEEE 14-bus network, with a phase-shifter on line $(0, 1)$.

Child Node	Min (MW)	Max (MW)	Size (MW)	Midpoint Dev. (MW)
3	86.45	123.95	37.5 (+9.6%)	0.0001
4	32.15	69.65	37.5 (+1.4%)	0.0001

Table 5.5: POE metrics with a phase-shifter at line $(0, 1)$. Worst-case redispatch: 0.0469 p.u (+2.4%). Objective: 0.375 (+5.3%). Parameters: $\alpha = 10000$, $\beta = 5$, $\gamma = 0.5$, $\tau = 1 \times 10^{-5}$.

Child Node	Min (MW)	Max (MW)	Size (MW)	Midpoint Dev. (MW)
9	−0.0535	0.0468	0.1003 (−0.010%)	0.0192 (−0.0004%)
10	−0.0492	0.0511	0.1004 (+0.033%)	0.0192 (−0.0002%)
11	−0.0449	0.0554	0.1003 (−0.034%)	0.0192 (+0.0022%)
12	−0.0530	0.0474	0.1003 (+0.012%)	0.0192 (−0.0001%)

Table 5.6: POE metrics for the multi-voltage network with a phase-shifter on line $(7, 14)$. Percentages indicate relative change w.r.t. the no-phase-shifter scenario. Objective: 2.9987×10^{-1} (+0.0002%). Worst-case redispatch: 0.0798 MW (+0.00003%). Parameters: $\alpha = 100$, $\beta = 3.0$, $\gamma = 0.5$, $\tau = 0.01$, $P_{min} = 0.0$, $P_{max} = 0.5$.

5.4 DC-POE computation model: Sensitivity Analysis

A sensitivity analysis is performed to assess the influence of parameters α and β on the main metrics. Results on the IEEE 14-bus network are provided in Figures 5.6–5.7. Parameter α has no noticeable influence on the main metrics, while the envelopes' volume decreases monotonously with parameter β, as expected.

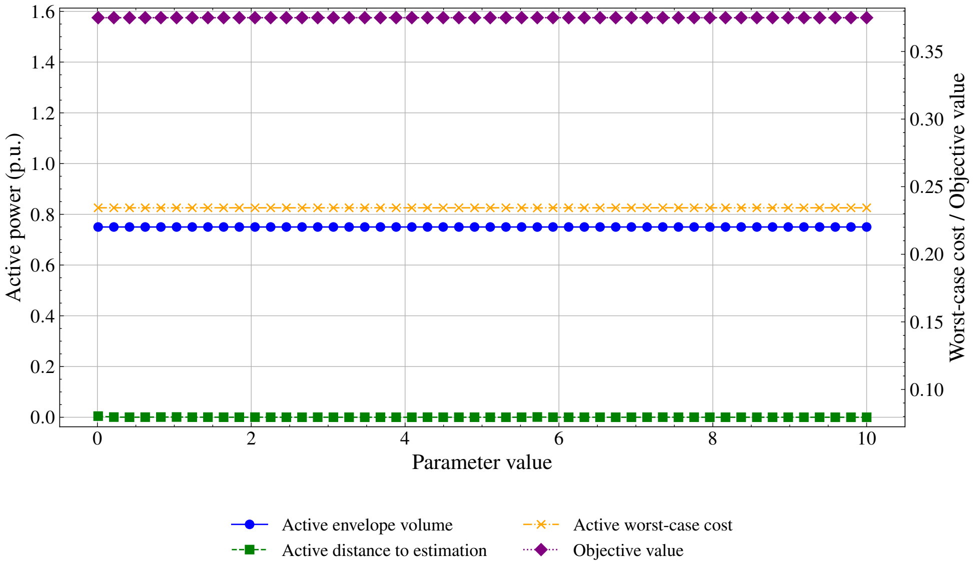

Figure 5.6: Evolution of envelope volume, worst-case dispatch, and midpoint deviation from estimation as a function of α, with $\beta = 5$ and $\tau = 1 \times 10^{-5}$.

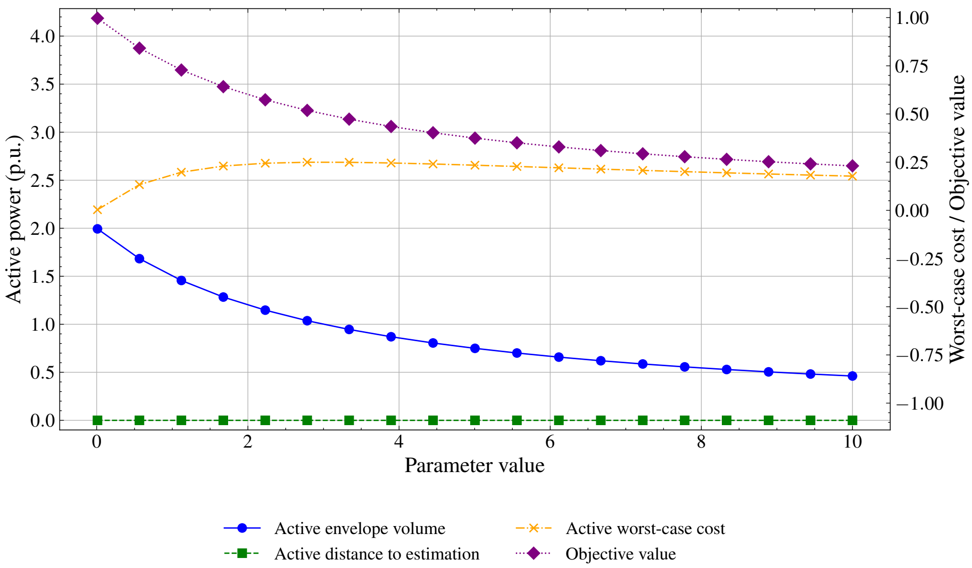

Figure 5.7: Evolution of envelope volume, worst-case dispatch, and midpoint deviation from estimation as a function of β, with $\alpha = 10000$ and $\tau = 1 \times 10^{-5}$.

5.5 AC-OPF Results

Resulting power flows and voltage magnitudes after solving the AC-OPF are depicted in Figure 5.8 and Figure 5.9 for IEEE 14-bus and PandaPower Multivoltage networks, respectively. The dispatch of generators is provided in Tables 5.7 and 5.8.

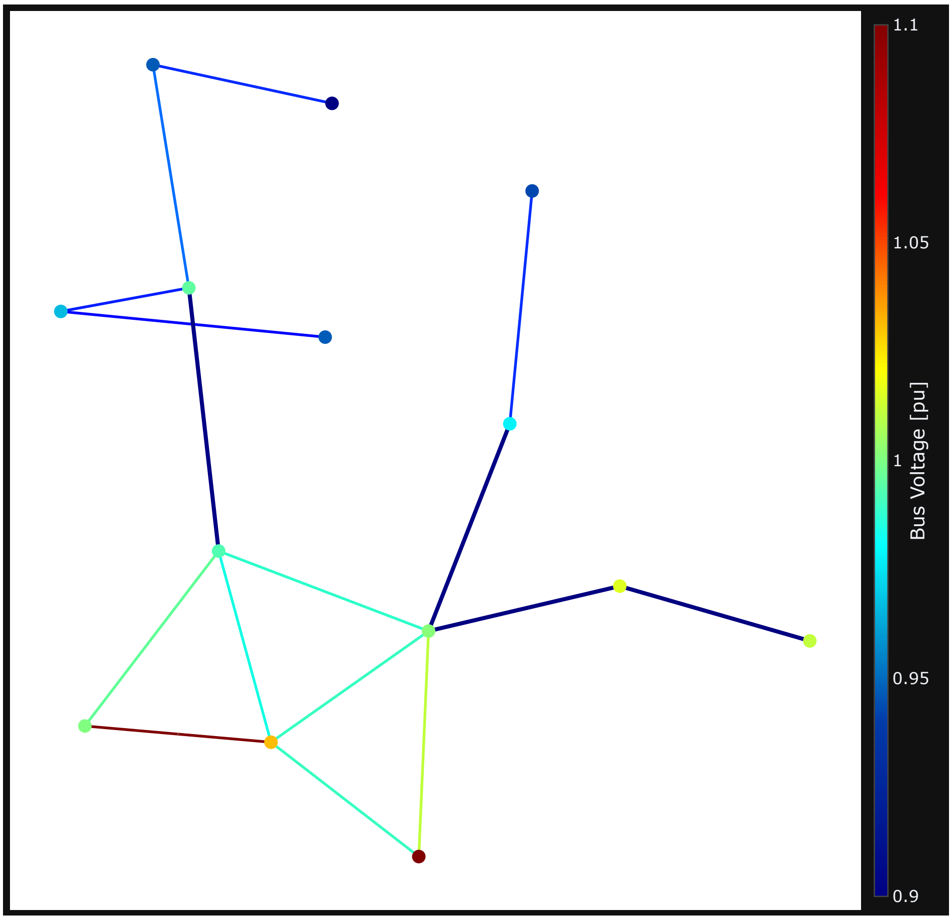

Figure 5.8: Resulting power flows of the AC-OPF applied on the modified IEEE 14-bus network. Red lines are close to congestion; blue lines are lightly loaded.

5.6 POE Computation: QC model

The POEs obtained at the child nodes using the QC model are depicted in Figures 5.10–5.13, where POEs include both an active and a reactive part. The main metric values are provided in Tables 5.9 and 5.10.

The POEs computed for the IEEE 14-bus network reveal that the reactive power component exhibits large flexibility around the forecast reactive power values (Figure 5.11), while the active power component deviates significantly from the active power forecasts (Figure 5.10). This is consistent with the objective function, which accounts for the volumes of both the active and reactive parts of the POE. Since reactive power adjustments are assumed to be costless, the solver is incentivised to reduce active power generation, at a certain cost, and thereby exploit the full reactive power capability of generators. This effect is further amplified by the generator capability curves, under which reactive power capability vanishes at maximum active power output. While such curves accurately represent inverter-based generators such as PV plants, they are not appropriate for synchronous generators, whose reactive power capability decreases as active

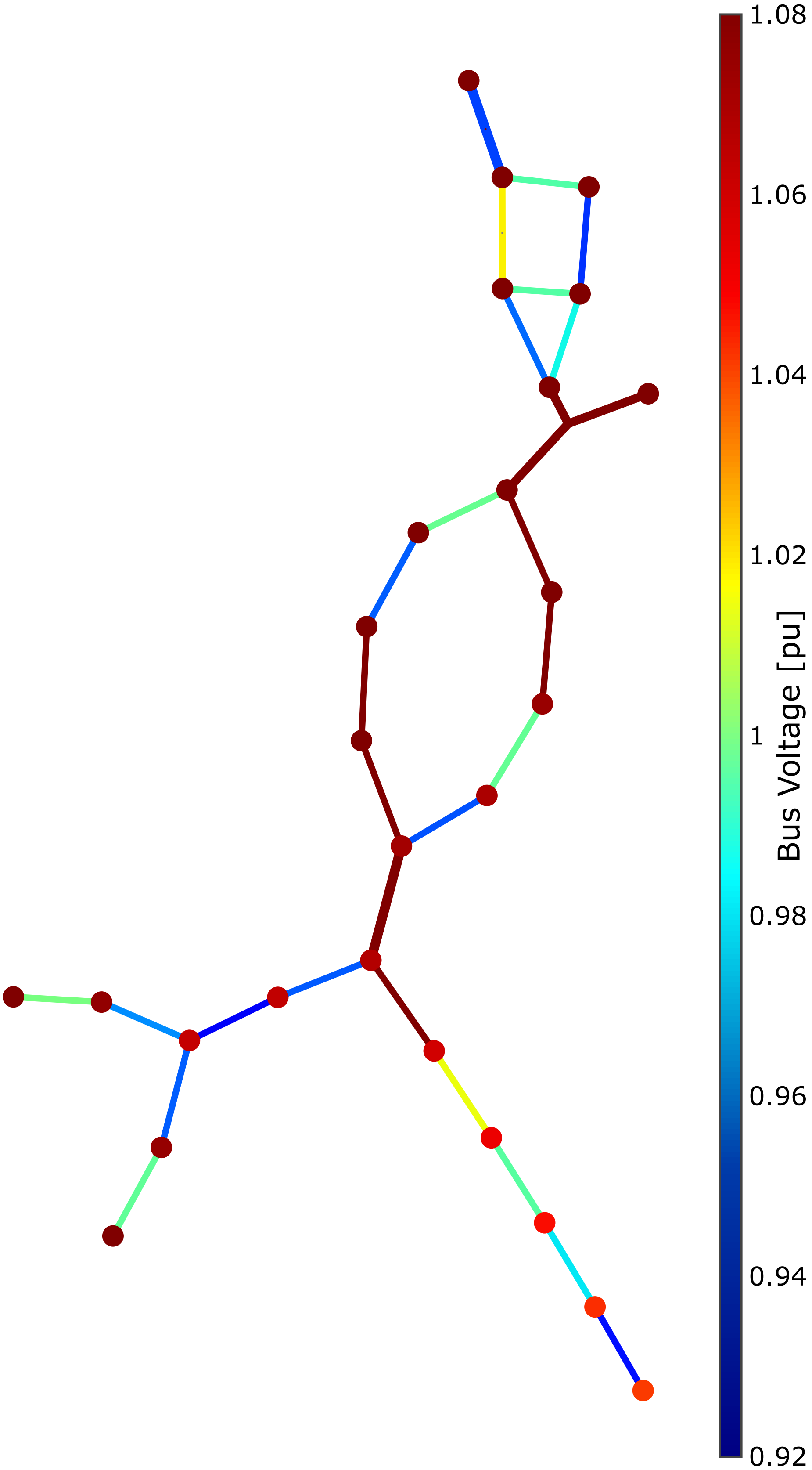

Figure 5.9: Resulting power flows of the AC-OPF applied on the PandaPower MultiVoltage network.

Bus	Gen P (MW)	Gen Q (MVAr)	Load P (MW)	Load Q (MVAr)
0	122.04	−77.84	10.0	3.0
1	45.91	58.16	21.7	12.7
2	123.77	105.39	94.2	19.0
3	/	/	47.8	−3.9
4	/	/	7.6	1.6
5	/	/	11.2	7.5
6	/	/	5.0	1.5
7	/	/	8.0	2.5
8	/	/	29.5	16.6
9	/	/	9.0	5.8
10	/	/	3.5	1.8
11	/	/	6.1	1.6
12	/	/	13.5	5.8
13	/	/	14.9	5.0
Total	**291.72**	**85.71**	**282.0**	**80.5**

Table 5.7: Bus-wise active and reactive generation and load in the modified IEEE 14-bus network (AC-OPF results).

Bus	Gen P (MW)	Gen Q (MVAr)	Load P (MW)	Load Q (MVAr)
0	94.43	−0.66	/	/
1	330.72	27.77	166.00	23.65
2	/	/	138.00	19.66
3	/	/	162.00	23.08
4	/	/	148.00	21.09
5	274.18	97.55	146.00	20.80
6	93.28	13.13	68.80	9.80
7	82.47	6.40	27.20	3.88
8	6.09	2.85	6.20	0.88
9	/	/	5.28	0.75
10	/	/	6.72	0.96
11	/	/	7.32	1.04
12	5.48	/	5.48	0.78
13	18.38	0.25	6.04	0.86
14	0.00	1.00	7.08	1.01
15	/	/	0.360	0.051
16	0.00	/	0.060	0.009
17	/	/	0.048	0.007
18	0.00	/	0.032	0.005
19	/	/	0.056	0.008
20	/	/	0.036	0.005
21	/	/	0.044	0.006
22	/	/	0.052	0.007
23	0.00	/	0.028	0.004
24	0.05	/	0.064	0.009
25	0.00	/	0.024	0.003
26	0.15	/	0.036	0.005
Total	**905.23**	**148.28**	**900.96**	**128.38**

Table 5.8: Bus-wise AC-OPF active and reactive generation and load (PandaPower Multi-Voltage network, buses 0–26). A slash denotes no generation unit present; 0.00 denotes a unit present but not dispatched.

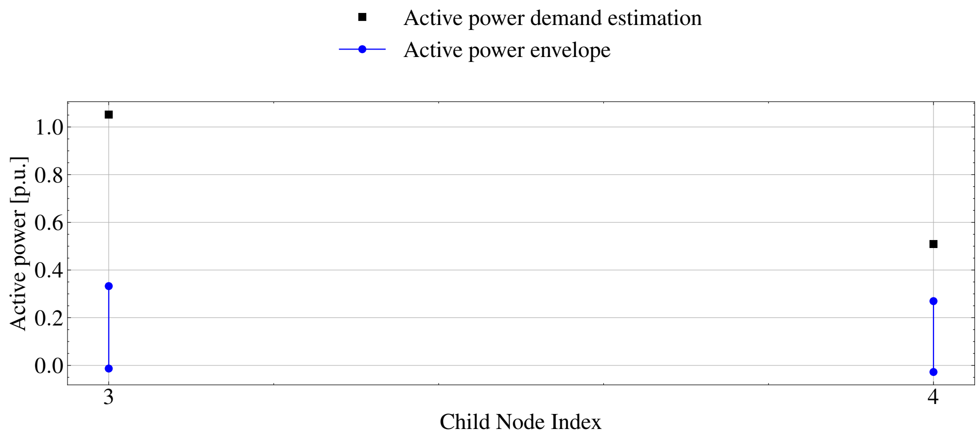

Figure 5.10: Active POEs at child nodes 3 and 4 (IEEE 14-bus, QC model, phase-shifter on line $(0,1)$). Parameters: $\overline{\Delta\theta} = 0.8$ rad, $\alpha_P = \alpha_Q = 10$, $\beta = 5.0$, $\gamma_P = \gamma_Q = 0.2$, $\tau = 1.0$.

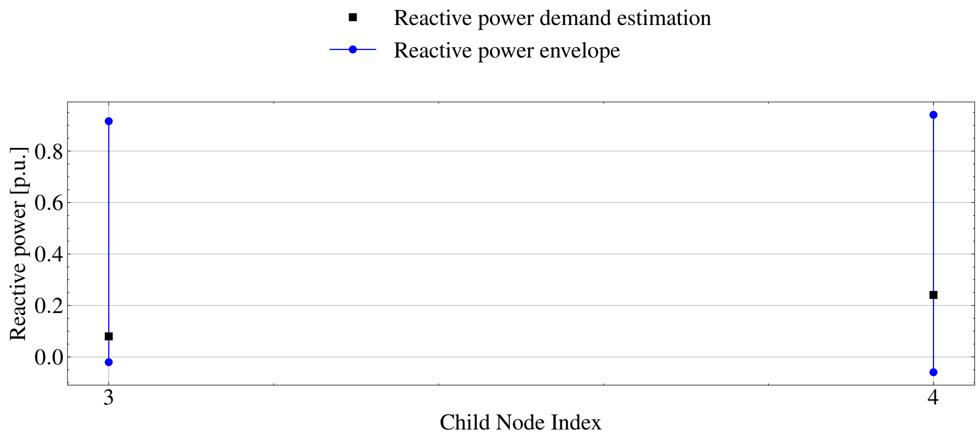

Figure 5.11: Reactive POEs at child nodes 3 and 4 (IEEE 14-bus, QC model, phase-shifter on line $(0,1)$). Same parameters as Figure 5.10.

Child Node	Qty	Min	Max	Size	Midpoint Dev.
3	P (MW)	-1.3211	33.2547	34.5758	79.6256
	Q (MVAr)	-2.0228	91.6025	93.6253	13.5358
4	P (MW)	-2.7728	26.9540	29.7269	15.0617
	Q (MVAr)	-5.9404	94.0789	100.0193	3.9877

Table 5.9: Active and reactive POE metrics (IEEE 14-bus, QC model, phase-shifter on line $(0,1)$). Worst-case cost: 5.45 p.u. Parameters: $\overline{\Delta\theta} = 0.8$ rad, $\alpha_P = \alpha_Q = 10$, $\beta = 5.0$, $\gamma_P = \gamma_Q = 0.2$, $\tau = 1.0$.

power production increases but remains non-negligible even at maximum active power output. In future work, a distinction should be made between inverter-based and synchronous generators to accurately represent their respective capability curves.

Regarding the POEs computed for the PandaPower MultiVoltage network, the main observation is a large discrepancy among child nodes: some are assigned a large POE in both active and reactive power limits, while others receive a low-quality POE, i.e, one with a relatively small size and/or whose barycenter deviates significantly from the forecast exchange. These differences arise from the varying ease with which each child node can be fed, depending on its location within the network. In the POE computation

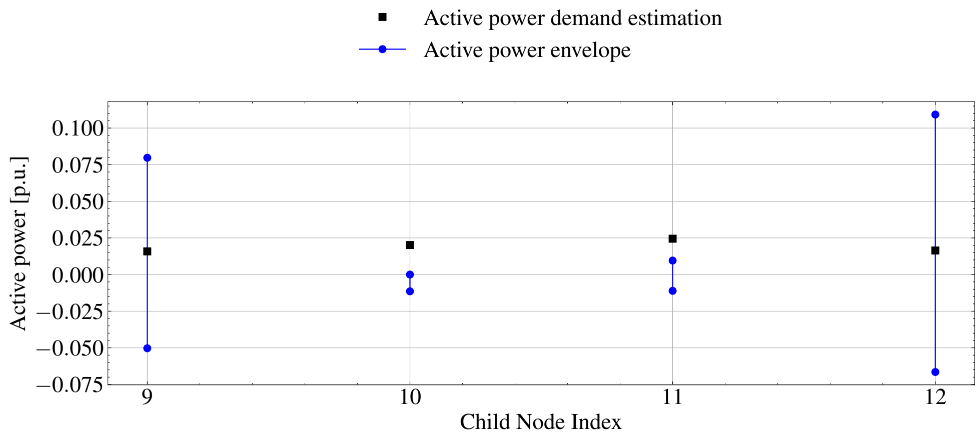

Figure 5.12: Active POEs at child nodes 9–12 (PandaPower MultiVoltage, QC model, phase-shifter on line $(7, 14)$). Parameters: $\overline{\Delta\theta} = 0.8$ rad, $\alpha_P = \alpha_Q = 5.0$, $\beta = 3.0$, $\gamma_P = \gamma_Q = 0.5$, $\tau = 0.1$, $P_{min} = Q_{min} = 0.0$, $P_{max} = Q_{max} = 0.5$.

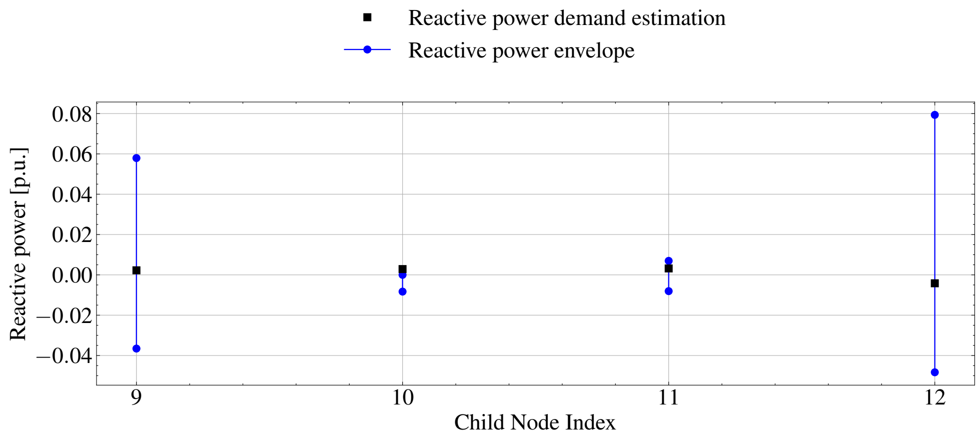

Figure 5.13: Reactive POEs at child nodes 9–12 (PandaPower MultiVoltage, QC model). Same parameters as Figure 5.12.

Child Node	Qty	Min	Max	Size	Midpoint Dev.
9	P (MW)	−5.03	7.97	13.00	0.11
	Q (MVAr)	−3.66	5.79	9.45	0.84
10	P (MW)	−1.14	0.00	1.14	2.59
	Q (MVAr)	−0.83	0.00	0.83	0.70
11	P (MW)	−1.11	0.96	2.07	2.53
	Q (MVAr)	−0.81	0.69	1.50	0.37
12	P (MW)	−6.65	10.92	17.57	0.49
	Q (MVAr)	−4.83	7.93	12.77	1.97

Table 5.10: Active and reactive POE metrics (PandaPower MultiVoltage, QC model, phase-shifter on line $(7, 14)$). Objective: 4.1317×10^{-1}. Curtailable active-power budget: 0.1239 MW. Same parameters as Figure 5.12.

model, the objective sums local utilities across all child nodes without any fairness constraint, providing no incentive to distribute POEs equitably. A solution to this fairness issue is discussed in chapter 6.

The phase-shift variables remain virtually zero (of the order of 10^{-10} p.u.) when solving the QC-POE computation model on both test cases, indicating that the phase-shifter is not activated. This suggests that the usefulness of a phase-shifter depends not only on the network characteristics and loading scenarios but also on the type of power flow equations used. Depending on the characteristics of the studied network (e.g., meshed or radial, high-voltage or low-voltage,...), appropriate power flow equations and network representations should be selected.

Knowing that some parameters of the POE computation model have a significant impact on the result quality. Parameter tuning is therefore required to better understand these influences and, in particular, to avoid large deviations between the computed POEs and the actual power requirements forecast by the DSOs. Parameter sensitivity is examined in section 5.7.

5.7 QC-POE computation model: Parameter Sensitivity Analysis

To avoid numerical issues during the solving of the QC-POE model, the parameters are fixed to $\alpha_P = \alpha_Q = 10$ and $\tau = 1$. The sensitivity of the main metrics with respect to each remaining parameter is illustrated in Figures 5.14–5.18. As a reminder, parameters α_P and α_Q penalise the deviation of the active and reactive POE barycentres from their respective forecast values, γ_P and γ_Q are quadratic regularisation parameters on the active and reactive POE volumes. The term $\text{Vol} - \gamma\,\text{Vol}^2$ is maximised at $\text{Vol} = 1/(2\gamma)$, so larger values of γ yield smaller optimal envelope sizes. β penalises generator re-dispatch and τ penalises the use of phase-shifter.

Regarding parameter α_P, it can be seen on Figure 5.14 that all metrics are decreasing, i.e, active and reactive components of the POEs and their distance to forecasts. This seems coherent as the optimal POEs tend to become closer to the forecasted values if their deviation is increasingly penalized, at a cost of having a reduced size.

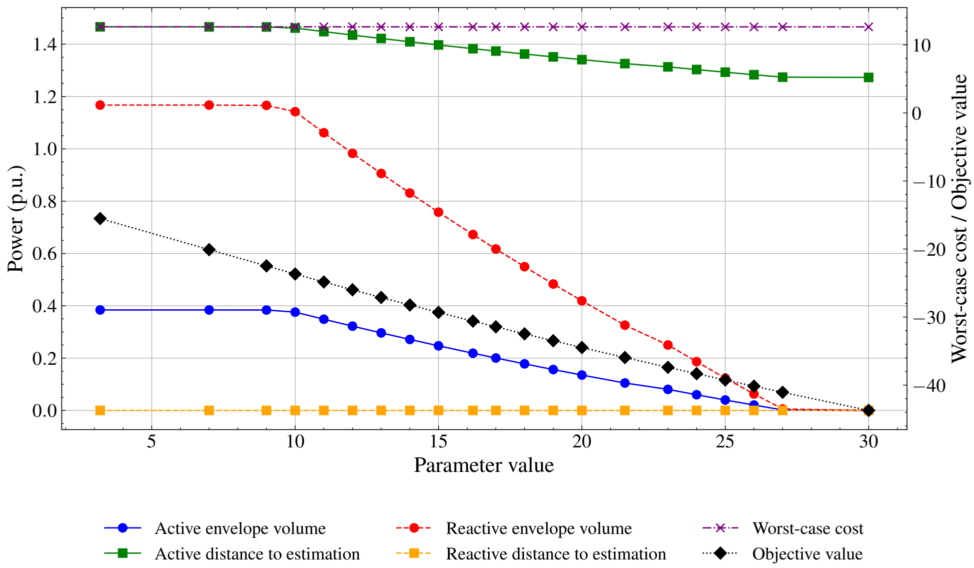

Figure 5.14: Evolution of the active and reactive POE volume, barycenter deviation from forecast, worst-case redispatch cost, and objective value within the IEEE 14-bus network (QC-POE model, phase-shifter on line $(0, 1)$), as a function of parameter α_P. Fixed parameters: $\alpha_Q = 10$, $\beta = 5.0$, $\gamma_P = \gamma_Q = 0.2$, $\tau = 1.0$.

In Figure 5.15, less intuitive dynamics are taking place. As the reactive envelope's distance to estimation is already close to zero, modifying the value of parameter α_Q modifies the solution without impacting the objective function significantly. Parameters α_P and α_Q have no noticeable impact on the worst-case cost.

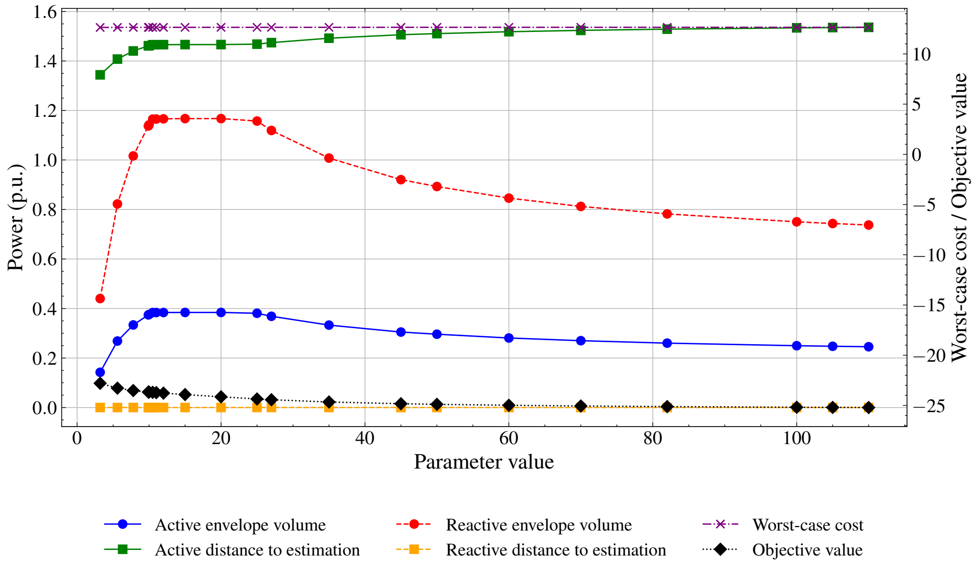

Figure 5.15: Evolution of the active and reactive POE volume, barycenter deviation from forecast, worst-case redispatch cost, and objective value within the IEEE 14-bus network (QC-POE model, phase-shifter on line $(0, 1)$), as a function of parameter α_Q. Fixed parameters: $\alpha_P = 10$, $\beta = 5.0$, $\gamma_P = \gamma_Q = 0.2$, $\tau = 1.0$.

Regarding the influence of parameter β, depicted in Figure 5.16, it seems coherent that the envelopes' size decreases, as the re-dispatch decreases. However, this decrease in re-dispatch remains relatively low as the worst-case cost increases when β is increasing.

Finally, the influence of parameters γ_P and γ_Q is depicted in Figure 5.17 and Figure 5.18, respectively. It can be observed that, within the parameter range studied, i.e, $\gamma_P, \gamma_Q \in [0, 1]$, there is no significant variation in the metrics' values.

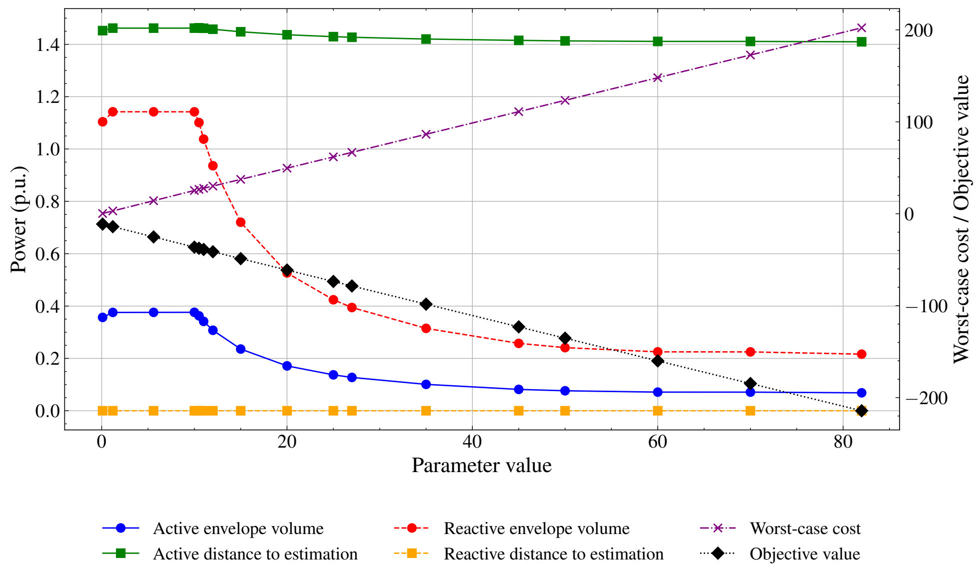

Figure 5.16: Evolution of the active and reactive POE volume, barycenter deviation from forecast, worst-case redispatch cost, and objective value within the IEEE 14-bus network (QC-POE model, phase-shifter on line $(0, 1)$), as a function of the redispatch cost parameter β. Fixed parameters: $\alpha_P = \alpha_Q = 10$, $\gamma_P = \gamma_Q = 0.2$, $\tau = 1.0$.

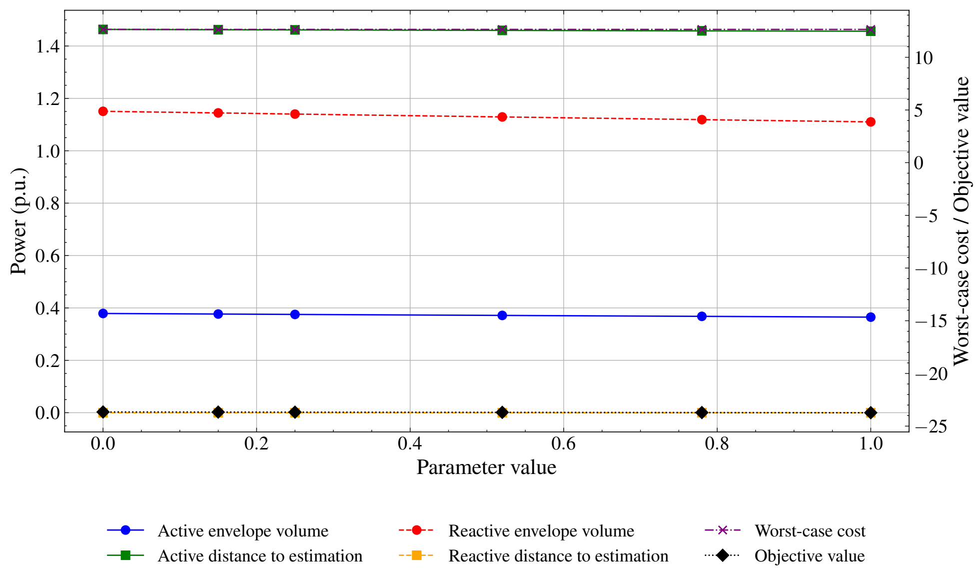

Figure 5.17: Evolution of the active and reactive POE volume, barycenter deviation from forecast, worst-case redispatch cost, and objective value within the IEEE 14-bus network (QC-POE model, phase-shifter on line $(0, 1)$), as a function of parameter γ_P. Fixed parameters: $\alpha_P = \alpha_Q = 10$, $\beta = 5.0$, $\gamma_Q = 0.2$, $\tau = 1.0$.

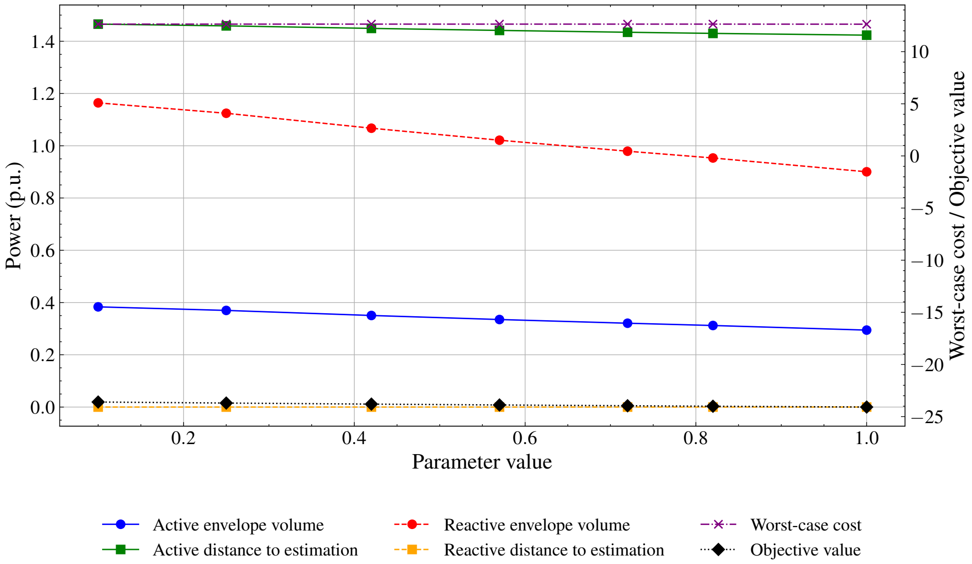

Figure 5.18: Evolution of the active and reactive POE volume, barycenter deviation from forecast, worst-case redispatch cost, and objective value within the IEEE 14-bus network (QC-POE model, phase-shifter on line $(0, 1)$), as a function of parameter γ_Q. Fixed parameters: $\alpha_P = \alpha_Q = 10$, $\beta = 5.0$, $\gamma_P = 0.2$, $\tau = 1.0$.

Chapter 6

Future Perspectives

6.1 Preliminaries

The coordination procedure and, in particular, the POE computation model, rely on several simplifying assumptions that constitute its main limitations. These include a restricted set of control actions, the absence of N-1 contingency requirements, a sum-of-utilities objective that provides no fairness guarantee across child nodes, and the lack of a mechanism to reallocate POEs once computed. Addressing these limitations also raises regulatory questions.

This chapter explores research directions to tackle each of these limitations. In section 6.2, extensions of the control action space are discussed. In section 6.3, N-1 security requirements are addressed, while section 6.4 surveys additional power flow models developed in the literature and that could be suitable for computing POEs. In section 6.5, a fair POE computation formulation is introduced, while section 6.6 proposes a secondary market for POE reallocation. Finally, section 6.7 highlights the regulatory implications of the proposed framework.

6.2 Control actions

Current POE computation models consider two control actions: (i) generator re-dispatch and (ii) phase-shifter setpoint adjustment. In practice, system operators have access to a broader set of control actions. However, many of these involve discrete decision variables. These include, among others, topology reconfiguration [80, 81], the connection and disconnection of shunt reactors and capacitor banks [82, 83], and on-load tap-changers' setpoint modification [84, 85]. Including such actions into the POE computation model is, however, incompatible with the robust reformulation proposed in subsection 3.2.5, which requires all constraints to be convex. The introduction of integer variables would violate this requirement. Therefore, continuous control actions should be first considered to extend the POE computation model. For example, static VAR compensator and synchronous condensers can be modeled using continuous variables.

The static var compensator (SVC) is a shunt-connected var compensator used primarily to maintain bus voltage magnitude, as mentioned in [86]. It continuously compensates for variations in reactive power demand and can increase the transfer capacity of an electrical line. An SVC typically consists of a reactor and multiple shunt capacitor banks, which are rapidly controlled using power electronic devices. This enables the dynamic generation or absorption of reactive power, allowing for fast voltage regulation, as detailed in [87].

Similarly, synchronous condensers (SC) are synchronous machines whose goal is to support system voltage. It is essentially composed of a motor to which no load is connected [88]. The condenser is said to be overexcited when behaving like a capacitor, i.e, producing reactive power, and underexcited when behaving like an inductor, i.e, consuming reactive power [89].

Whether the underlying technology consists of an SVC or an SC, the model is similar and can be written as follows, as proposed in [90]:

$$\underline{Q_n^S} \leq Q_n^S \leq \overline{Q_n^S},$$

where parameters $\underline{Q_n^S}, \overline{Q_n^S} \in \mathbb{R}$ depict the reactive power capacity limits of the SVC or SC connected to node n, if any. The decision variable Q_n^S is the reactive power output of this device connected to node n. If no such device is connected to node n, this variable is equal to zero. As this action affects reactive power flow in the system, it cannot be implemented for the DC-POE computation model, which neglects reactive power flows, but rather in the QC-POE computation model, described in subsection 3.4.1. In particular, the reactive power balance constraint becomes:

$$Q_{\text{load},n} - Q'_{\text{gen},n} = \sum_{(nm)\in\mathcal{E}} Q_{nm} + Q_n^+ - Q_n^- + Q_n^S, \qquad \forall n \in \mathcal{N}_o. \tag{6.1a}$$

Although discrete control actions cannot be directly included in the POE models, research on mixed-integer AC-OPF formulations has produced methods to handle such variables. These approaches typically proceed in two stages: (i) the integer variables are first relaxed to continuous ones and the resulting model is solved, and (ii) the relaxed solution is then projected onto the nearest feasible integer values. Notable examples include the *relax–round–resolve* framework of [91] and the homotopy-based relaxation for discrete control variables proposed in [92]. Originally developed for AC-OPF, such methods could potentially be adapted to include discrete actions into POE computation models.

6.3 N-1 criterion

A particularly critical criterion when operating a power system, especially in a transmission network, is the N-1 criterion. This criterion ensures the resilience of the network, and, in particular, that it can still be operated in a secure way after a contingency occurs. The current POE computation models only account for security in the N-state. In order to account for the N-1 criterion, all security constraints, i.e, voltage magnitude limits and thermal limits, should be respected even if one grid element is lost. This implies that all constraints should be verified for all N-1 contingency cases.

Let $\Omega_{N\text{-}1}$ denote the set of all N-1 contingencies, where each $c \in \Omega_{N\text{-}1}$ corresponds to the loss of a single grid element (line, transformer, or generator). The base case (N-state) is denoted c_0, and the full contingency set is $\Omega = \{c_0\} \cup \Omega_{N\text{-}1}$. The generic POE optimisation model should become:

$$\max_{\overline{S}^{\mathcal{C}},\, A} U^{POE}(\overline{S}^{\mathcal{C}}) - A \tag{6.2a}$$

$$\text{s.t. } \forall S^{-,\mathcal{C}} \in \overline{S}^{\mathcal{C}},\ \forall |V^{\mathcal{P}}| \in \overline{V}^{\mathcal{P}},\ \forall c \in \Omega,\ \exists\, u \in \mathcal{F}:$$

$$Security(S^o_{load}, S^o_{gen}, S^{-,\mathcal{C}}, V^{\mathcal{P}}, u, c) \leq 0, \tag{6.2b}$$

$$Cost(u) \leq A, \tag{6.2c}$$

$$|V^{\mathcal{C}}| \in \overline{V}^{\mathcal{C}}, \tag{6.2d}$$

$$S^+ \in \overline{S}^{\mathcal{P}}. \tag{6.2e}$$

It should be noted that the robust reformulation of subsection 3.2.5 extends naturally to this formulation. However, the vertex enumeration now runs over all three uncertain sets, i.e, $\Psi(\overline{S}^{\mathcal{C}})$, $\Psi(\overline{V}^{\mathcal{P}})$, and Ω, which increases the number of constraints and can therefore significantly increase the computational burden. In general, accounting for all possible outages might lead to a high computational burden. Typical approaches to avoid this burden consider only a subset of possible relevant outages [93].

6.4 Power flow models

The power flow models presented in this thesis, i.e, the LACPF, DC, and QC models, already provide a variety of options for POE computation models. Each model is suited to specific network characteristics. As a reminder, DC power flow equations are particularly appropriate for transmission networks but completely neglect voltage magnitude constraints, since reactive power flows are neglected. Moreover, the DC assumptions are generally not satisfied in distribution networks.

Additional power flow models could nonetheless be exploited depending on network characteristics and the accuracy required. Beyond the already-presented LACPF, DC, and QC models, the DistFlow model and a hybrid DC/DistFlow model might be leveraged.

6.4.1 DistFlow model.

The DistFlow model is derived from the branch flow model, first introduced in [94], by neglecting the phase angles of voltages and currents. This formulation is particularly suitable for radial networks, for which the relaxation is always exact, but may not be exact for meshed networks [95]. Authors in [96] illustrate its use in distribution system expansion planning. The DistFlow equations are:

$$P'_n = \sum_{(m,n)\in\mathcal{E}_o} P_{m,n} - \sum_{(n,j)\in\mathcal{E}_o} \big(P_{n,j} + R_{nj}\, I^{sq}_{nj}\big) + P^+_n - P^-_n, \qquad \forall\, n \in \mathcal{N}_o, \tag{6.3a}$$

$$Q'_n = \sum_{(m,n)\in\mathcal{E}_o} Q_{m,n} - \sum_{(n,j)\in\mathcal{E}_o} \big(Q_{n,j} + X_{nj}\, I^{sq}_{nj}\big) + Q^+_n - Q^-_n, \qquad \forall\, n \in \mathcal{N}_o, \tag{6.3b}$$

$$V^{sq}_n - V^{sq}_j = 2\big(R_{nj}\, P_{nj} + X_{nj}\, Q_{nj}\big) + Z^2_{nj}\, I^{sq}_{nj}, \qquad \forall\, (n,j) \in \mathcal{E}_o, \tag{6.3c}$$

$$P^2_{nj} + Q^2_{nj} \;\le\; V^{sq}_n\, I^{sq}_{nj}, \qquad \forall\, (n,j) \in \mathcal{E}_o, \tag{6.3d}$$

where R_{nj}, X_{nj}, and $Z_{nj} = \sqrt{R^2_{nj} + X^2_{nj}}$ are the resistance, reactance, and impedance magnitude of branch (n,j), respectively, and V^{sq}_n, I^{sq}_{nj} denote the squared voltage and current magnitudes. Since the DistFlow model does not represent voltage phase angles, phase-shifters cannot be included as a control action with this model.

6.4.2 Hybrid DC/DistFlow model.

Authors in [97] propose a hybrid model applicable to both transmission and distribution systems, combining the voltage magnitude and current equations of the DistFlow model with the phase-angle equations of the DC power flow model. This allows both voltage magnitude and phase-angle bound constraints to be enforced simultaneously. Phase-shifters (ρ_{nj}) and static var compensators (Q^S_n) are included as control actions:

$$P'_n = \sum_{(m,n)\in\mathcal{E}_o} P_{m,n} - \sum_{(n,j)\in\mathcal{E}_o} \left(P_{n,j} + R_{nj}\, I^{sq}_{nj}\right) + P^+_n - P^-_n\,, \qquad \forall\, n \in \mathcal{N}_o, \tag{6.4a}$$

$$Q'_n = \sum_{(m,n)\in\mathcal{E}_o} Q_{m,n} - \sum_{(n,j)\in\mathcal{E}_o} \left(Q_{n,j} + X_{nj}\, I^{sq}_{nj}\right) + Q^+_n - Q^-_n + Q^S_n, \qquad \forall\, n \in \mathcal{N}_o, \tag{6.4b}$$

$$P^2_{nj} + Q^2_{nj} \;\le\; V^{sq}_n\, I^{sq}_{nj}, \qquad \forall\,(n,j) \in \mathcal{E}_o, \tag{6.4c}$$

$$V^{sq}_n - V^{sq}_j = 2\left(R_{nj}\, P_{nj} + X_{nj}\, Q_{nj}\right) + Z^2_{nj}\, I^{sq}_{nj}, \qquad \forall\,(n,j) \in \mathcal{E}_o, \tag{6.4d}$$

$$P_{nj} = \frac{\theta_n - \theta_j + \rho_{nj}}{X_{nj}}, \qquad \forall\,(n,j) \in \mathcal{E}_o, \tag{6.4e}$$

$$\underline{\rho} \;\le\; \rho_{nj} \;\le\; \overline{\rho}, \qquad \forall\,(n,j) \in \mathcal{E}_o, \tag{6.4f}$$

$$\underline{\theta} \;\le\; \theta_n \;\le\; \overline{\theta}, \qquad \forall\, n \in \mathcal{N}_o, \tag{6.4g}$$

$$\theta_{\text{ref}} = 0, \tag{6.4h}$$

$$\underline{V}^2_n \;\le\; V^{sq}_n \;\le\; \overline{V}^2_n, \qquad \forall\, n \in \mathcal{N}_o, \tag{6.4i}$$

$$0 \;\le\; I^{sq}_{nj} \;\le\; \overline{I}^2_{nj}, \qquad \forall\,(n,j) \in \mathcal{E}_o. \tag{6.4j}$$

6.4.3 Additional models.

Future library developments should include further well-established convex relaxations of the AC power flow equations, enabling a broader comparison of models and a wider choice for users depending on their network characteristics. A particularly relevant relaxation is the Semidefinite Programming (SDP) relaxation.

The SDP relaxation of the AC power flow equations is performed as follows. The complex voltage vector $v \in \mathbb{C}^{|\mathcal{N}|}$ is lifted into a Hermitian matrix $W = vv^H \in \mathbb{C}^{|\mathcal{N}|\times|\mathcal{N}|}$, which is rank-1 and positive semidefinite by construction. The power flow equations, which are quadratic in the voltages, become linear in W. Relaxing the rank-1 constraint to $W \succeq 0$ yields a convex SDP. Under certain network conditions, the relaxation is exact, i.e, the optimal W has rank 1 and the true AC solution can be recovered, as established by the zero duality gap result of [98]. The SDP relaxation is generally tighter than the convex Distflow model, but it incurs a significantly higher computational cost [99].

6.5 A Fair POE Computation Model

As observed in chapter 5, the quality of the computed POEs can vary significantly across child nodes. From a regulatory standpoint, such an approach may not be acceptable in practice without fairness guarantees for all child nodes. Several methods have been proposed in the literature to consider fairness in optimisation problems. A particularly well-suited approach is the lexicographic max-min optimisation, which has been widely studied in multi-objective optimisation [100].

Lexicographic approaches rank objective functions by order of importance rather than aggregating them through weights. Once ranked, the most important objective is solved first as a single-objective problem. The second objective is then optimised subject to the additional constraint that the first objective value is not degraded. This process is repeated iteratively. At each step, the optimal value of the previous objective is fixed as a new constraint, and the next objective is optimised [101].

To compute fair POEs, the proposed formulation applies this principle to the local utilities $U_c(\overline{S}_c)$ of child nodes. The variable $\psi \in \mathbb{R}^+$ acts as a lower bound on the minimum local utility across all child nodes, so that maximising ψ raises the utility of the least-favoured node. Mathematically:

$$\max_{\overline{S}^{\mathcal{C}},\, A} \psi - A \tag{6.5a}$$

$$\text{s.t. } \forall S^{-,\mathcal{C}} \in \overline{S}^{\mathcal{C}},\ \forall |V^{\mathcal{P}}| \in \overline{V}^{\mathcal{P}},\ \exists\, u \in \mathcal{F}:$$

$$\psi \ \leq\ U_c(\overline{S}_c), \quad \forall\, c \in \mathcal{N}_o^{\mathcal{C}}. \tag{6.5b}$$

$$Security(S^o_{load},\, S^o_{gen},\, S^{-,\mathcal{C}},\, V^{\mathcal{P}},\, u) \leq 0, \tag{6.5c}$$

$$Cost(u) \leq A, \tag{6.5d}$$

$$|V^{\mathcal{C}}| \in \overline{V}^{\mathcal{C}}, \tag{6.5e}$$

$$S^+ \in \overline{S}^{\mathcal{P}}. \tag{6.5f}$$

This problem is solved iteratively. At each iteration, ψ is maximised, effectively raising the utility of the least-favoured child node. The resulting optimal value ψ^* is then fixed as a lower bound in the subsequent iteration, during which the child node(s) achieving ψ^* are removed from constraint (6.5b) and their POEs are fixed. The process terminates once all child nodes' POEs have been determined.

6.6 Market-Based Reallocation of Operating Envelopes

POE allocations may not satisfy all DSOs, even when a fair allocation model is used. In particular, the robust formulation requires that network security be guaranteed for all simultaneous realisations of power exchanges within the POE bounds, including when all child nodes inject or withdraw at their extreme values at the same time. This worst-case requirement becomes increasingly constraining as the number of child nodes grows, resulting in tighter individual envelopes.

This motivates the introduction of a secondary market where DSOs connected to the TSO can trade POE bounds among themselves. Any exchange on this market must maintain network security, introducing a security-constrained market-clearing problem.

Each DSO, connected at a TSO's child node $c \in \mathcal{N}_o^{\mathcal{C}}$, is initially allocated a POE. Assuming that only the active power bounds of the POE are exchanged, each DSO can submit an order to trade these bounds. A buy order requests an expansion of the envelope, while a sell order proposes a reduction in exchange for payment. The active power bounds of a POE allocated at child node c are depicted as $[\underline{P}_c,\, \overline{P}_c]$, while $[\underline{P}'_c,\, \overline{P}'_c]$ depicts the new bounds after market clearing.

Let $\mathcal{O}$ denote the set of all submitted orders. Orders are partitioned along two independent dimensions: by direction into buy orders $\mathcal{B} \subset \mathcal{O}$ and sell orders $\mathcal{S} \subset \mathcal{O}$, and by the bound they concern into lower-bound orders $\mathcal{L} \subset \mathcal{O}$ and upper-bound orders $\mathcal{U} \subset \mathcal{O}$. Each order $o \in \mathcal{O}$ is characterised by the submitting DSO $c_o \in \mathcal{N}_o^{\mathcal{C}}$ and a maximum traded quantity $\Delta P_o \in \mathbb{R}^+$. Buyers $b \in \mathcal{B}$ additionally specify a limit price $\pi_b \in \mathbb{R}^+$, representing the maximum price they are willing to pay per unit, while sellers $s \in \mathcal{S}$ specify a limit price $\pi_s \in \mathbb{R}^+$, representing the minimum price they are willing to accept per unit. Upon clearing, each buyer and seller is assigned an accepted quantity a_b and a_s, respectively.

It is assumed that each order can be partially cleared to maximise social welfare. The accepted quantity a_o for each order o can be determined by solving Equation 6.6. This formulation is adapted from [102], where Seculex, a capacity exchange market between customers sharing the same feeder, is presented:

$$\max_{a} \quad \sum_{b\in\mathcal{B}} \pi_b\, a_b - \sum_{s\in\mathcal{S}} \pi_s\, a_s \tag{6.6a}$$

$$\text{s.t.} \quad 0 \leq a_o \leq \Delta P_o, \qquad \forall\, o \in \mathcal{O}, \tag{6.6b}$$

$$\underline{P}'_c = \underline{P}_c + \sum_{\substack{s\in\mathcal{S}\cap\mathcal{L}:\\ c_s=c}} a_s - \sum_{\substack{b\in\mathcal{B}\cap\mathcal{L}:\\ c_b=c}} a_b, \qquad \forall\, c \in \mathcal{N}_o^{\mathcal{C}}, \tag{6.6c}$$

$$\overline{P}'_c = \overline{P}_c - \sum_{\substack{s\in\mathcal{S}\cap\mathcal{U}:\\ c_s=c}} a_s + \sum_{\substack{b\in\mathcal{B}\cap\mathcal{U}:\\ c_b=c}} a_b, \qquad \forall\, c \in \mathcal{N}_o^{\mathcal{C}}, \tag{6.6d}$$

$$\underline{P}'_c \leq \overline{P}'_c, \qquad \forall\, c \in \mathcal{N}_o^{\mathcal{C}}, \tag{6.6e}$$

$$\overline{P}^{\prime,\mathcal{C}} = [\underline{P}', \overline{P}'], \tag{6.6f}$$

$$\forall S^{-,\mathcal{C}} \in \overline{S}^{\prime,\mathcal{C}},\ \forall |V^{\mathcal{P}}| \in \overline{V}^{\mathcal{P}},\ \exists\, u \in \mathcal{F}:$$

$$Security(S^o_{load}, S^o_{gen}, S^{-,\mathcal{C}}, V^{\mathcal{P}}, u) \leq 0, \tag{6.6g}$$

$$Cost(u) \leq A^*, \tag{6.6h}$$

$$|V^{\mathcal{C}}| \in \overline{V}^{\mathcal{C}}, \tag{6.6i}$$

$$S^+ \in \overline{S}^{\mathcal{P}}, \tag{6.6j}$$

where $A^* \in \mathbb{R}^+$ is the optimal worst-case cost determined by the TSO after solving the POE computation model.

The objective function maximizes social welfare as the difference between the aggregate willingness-to-pay of buyers and the aggregate compensation required by sellers. Constraint (6.6b) enforces partial clearing bounds. Constraints (6.6c)–(6.6d) update the lower and upper POE bounds of each child node based on the accepted quantities: a seller of a lower (resp. upper) bound tightens (resp. loosens) the envelope, while a buyer of a lower (resp. upper) bound loosens (resp. tightens) it. Constraint (6.6e) ensures that each updated active POE $[\underline{P}'_c, \overline{P}'_c]$ remains non-degenerate, and the updated active POE set $\overline{P}^{\prime,\mathcal{C}}$ is assembled in constraint (6.6f).

The final constraints require that, for all power exchanges within the updated POEs and all voltage realizations within the VOEs, there exists a set of control actions ensuring both network security and a worst-case operational cost no greater than A^*. This guarantees that any reallocation of POE bounds remains jointly feasible with the TSO's existing operational plan. Solving this problem yields the updated POE set $\overline{P}^{\prime,\mathcal{C}}$ and the residual order book $\mathcal{O}' \subset \mathcal{O}$ containing the uncleared quantities[1].

[1] This formulation only accounts for active power bounds, whereas reactive power bounds are assumed to remain constant. A more developed market-based formulation could account for both active and reactive power bounds.

6.7 Regulatory Aspects

6.7.1 A novel coordination paradigm.

As reviewed in section 1.3, existing approaches generally rely on extensive data exchange, shared network models, or centralised optimisation problems requiring full network visibility across operators. In contrast, the proposed approach limits all inter-operator communication to a minimal set of interface variables, i.e, POEs and VOEs, which preserves the operational independence of each entity. This decoupled architecture has important regulatory implications. Since no sensitive network data needs to be shared beyond the interface, the approach is inherently compatible with the strict confidentiality requirements that govern regulated network operators under European law.

6.7.2 Respecting the independence of grid operators and regulators.

A key feature of the POE framework is that it preserves the independence of all participating entities at every level. The TSO computes POEs without requiring knowledge of DSOs' internal network topologies, generation portfolios, or load profiles. Symmetrically, DSOs operate within their assigned POEs without needing visibility into the TSO's network and its operating conditions. This structural independence is consistent with the unbundling requirements established under European law, which mandate clear operational separation between transmission and distribution system operators.

Beyond operator independence, the POE approach is particularly well-suited to Belgium's multi-level regulatory architecture, in which energy regulation is distributed across European, federal, and regional authorities, each with distinct and non-overlapping competences. This structure is preserved naturally by the POE framework, since each regulatory layer only needs to oversee the interface variables relevant to its own jurisdiction.

At the European level, the Agency for the Cooperation of Energy Regulators (ACER), coordinates national regulatory authorities on cross-border matters and network codes. Any new coordination product involving inter-system power flows, such as POEs, must be compatible with these European network codes, and in particular with the System Operation Guideline (SOGL) [64], which defines the operational security requirements that TSOs must satisfy. ACER would therefore need to assess whether the POE framework is compatible with existing codes or whether amendments are required. A European coordination would be particularly critical if the proposed POE-based framework is to be generalized for the coordination of TSOs, which need to be operated independently [103].

At the federal level, the Commission de Régulation de l'Électricité et du Gaz (CREG) is the Belgian federal energy regulator. CREG oversees Elia, the Belgian TSO, and regulates the wholesale electricity market. Any product that modifies the operational interface between the transmission and distribution systems, which would be the case of POEs and VOEs, falls within CREG's regulatory purview. CREG would need to define the rules governing POE computation, allocation, and potential reallocation, as well as the obligations of the TSO to provide non-discriminatory access to these products across all connected DSOs.

At the regional level, three regulators oversee distribution network operations in Belgium's three regions: VREG in Flanders, CWaPE in Wallonia, and BRUGEL in Brussels. Each would be independently responsible for ensuring that DSOs comply with their assigned POEs and that they operate their networks securely within those bounds at a reasonable cost.

A critical observation is that the POE approach respects this multi-level structure: each operator remains accountable exclusively to its own regulator, and no regulator would need access to another regulator's jurisdiction to fulfill its role. The interface between regulatory layers is fully characterized by the POEs and VOEs, which serve as the contractual boundary between regulatory domains. This compartmentalization is a significant advantage over centralized coordination approaches, which would require cross-regulatory data sharing and potentially blur the boundary between federal and regional competencies.

6.7.3 Market-based reallocation and the risk of market power.

While the secondary market proposed in section 6.6 offers a promising mechanism for redistributing POE bounds in a welfare-improving manner, it also introduces risks that must be addressed through appropriate regulation.

The most significant concern is excessive market power. In the proposed market, DSOs with large initial POE allocations hold a structural advantage as sellers. They can offer flexibility that other DSOs urgently need, potentially setting high prices. This issue is worsened due to the lack of liquidity on this potential market, as only a small number of participants (i.e, DSOs) would bid on this market. Moreover, DSOs with congested interfaces or large and variable loads may be systematically dependent on the market to obtain sufficient operational flexibility, placing them in a structurally weak position. This asymmetry can lead to welfare-reducing outcomes that the social welfare maximisation objective alone cannot prevent.

Regulatory responses to this risk should include at minimum: (i) *price caps* on sell orders to prevent exploitation of structural advantages; (ii) *minimum POE guarantees* imposed on the TSO, ensuring that each DSO receives a baseline allocation before the market opens; (iii) *transparency and reporting obligations* requiring all market participants to disclose their order books to the regulator; and (iv) *market monitoring* by an independent authority to detect and sanction anti-competitive behaviour.

Chapter 7

Conclusions

This thesis addresses the challenge of coordinating transmission and distribution system operators in the context of growing distributed energy resource penetration, which increasingly leads to security constraint violations across multiple electrical networks. To tackle this challenge, a coordination framework is proposed, in which power and voltage magnitude ranges, referred to as power operating envelopes (POEs) and voltage operating envelopes (VOEs), are agreed upon at the interfaces between hierarchically organized network parts, called operational networks.

Two main contributions are delivered. The first contribution is the coordination procedure for TSO/DSO coordination, which was developed in the context of this thesis and is formalised in [1], a scientific article to which I contributed as co-author. In this thesis, a variant of this coordination procedure is presented in detail and positioned with respect to the existing literature. The procedure establishes how VOEs are first agreed bilaterally at network interfaces, how power exchange forecasts are communicated bottom-up, and how POEs are subsequently computed top-down to guarantee that, for any operating point within the envelope, the operator can maintain the static security of its network through available corrective actions.

The second contribution is the extension of the POE computation model introduced in [1] in several directions. Phase-shifters are included as an additional control action. Experiments on test networks show that their inclusion increases active POE size by up to 9.6%. A detailed representation of generator P-Q capability curves is also introduced, replacing the simplified box constraints of the original model. Finally, the linearised AC power flow model is replaced by a quadratic convex model, which provides a more accurate convex representation of AC power flows. This POE computation model is called the QC-POE model.

The quadratic convex power flow equations allow for a better modelling than the linearized version provided in [1]. The power flow equations are also modeled using the DC power flow equations, which yield only active POEs. This POE computation model is called the DC-POE model and serves as a benchmark. Active POEs are computed using the DC-POE computation model, while the QC-POE model extends the analysis to active and reactive power simultaneously.

When both active and reactive power are considered, the experiments show that reactive POEs are systematically larger and better centred around the forecasted power exchanges than their active counterparts. This asymmetry stems from two effects. First, while the objective function assigns equal weight to active and reactive POE volumes, reactive power adjustments are assumed costless, whereas active re-dispatch incurs a penalty through parameter β in the cost constraint. The solver, therefore, freely expands reactive envelopes without incurring any additional cost.

Second, the elliptical P-Q capability constraints create a direct coupling between active and reactive operating ranges: reducing active power output unlocks additional reactive capacity, and the ellipse geometry ensures that reactive capacity vanishes entirely at maximum active output. This tends to push the solver in the same direction, i.e, reducing generators' active setpoints to exploit the full reactive power range, and therefore producing large and well-centred reactive POEs at the expense of tighter active ones.

Another observation from the experiments is that POE quality might vary considerably across child nodes, which is the consequence of the sum-of-utilities objective, which lacks fairness incentives. As proposed in chapter 6, different POE computation formulations might be leveraged to include fairness.

Several limitations of this work motivate future research directions, detailed in chapter 6. On the modelling side, the POE computation model currently considers only generator re-dispatch and phase-shifter adjustments as control actions, excludes N-1 contingency requirements, and relies on an elliptical capability curve that does not accurately represent synchronous generators. Moreover, the sum-of-utilities objective provides no fairness guarantee across child nodes.

Finally, deploying this framework in practice raises significant regulatory challenges, as OEs do not yet constitute a recognized product under existing European and national energy legislation. Addressing these limitations simultaneously across modelling and regulation dimensions will be necessary for the framework to reach full operational deployment. Nevertheless, by limiting inter-operator data exchange and preserving the independence of each participating entity, the coordination procedure proposed in this thesis provides a foundation for practical TSO/DSO coordination.

Bibliography

[1] A. Bolland, A. Maio, T. Richard, M. Vassallo, A. Bahmanyar, R. Fonteneau, J. Callec, D. Fourniret, and D. Ernst, “Coordinating secure and distributed operation of electrical networks through bilateral agreements on voltage and power envelopes,” 04 June 2026. [Online]. Available: https://orbi.uliege.be/handle/2268/345742

[2] A. G. Givisiez, K. Petrou, and L. F. Ochoa, “A review on TSO-DSO coordination models and solution techniques,” *Electric Power Systems Research*, vol. 189, p. 106659, 2020.

[3] T. Alazemi, M. Darwish, and M. Radi, “Tso/dso coordination for res integration: A systematic literature review,” *Energies*, vol. 15, no. 19, p. 7312, 2022.

[4] M. Vassallo, A. Bolland, A. Bahmanyar, R. Fonteneau, A. Maio, J. Callec, D. Fourniret, and D. Ernst, “A multidimensional analysis of existing limitations for tso-dso coordination,” 2026. [Online]. Available: https://orbi.uliege.be/handle/2268/345652

[5] C. Ziesemann, F. Gaumnitz, C. Köhnen, and I. Stoyanova, “Challenges and barriers to the implementation of tso-dso coordination concepts: Discussion paper,” RWTH Aachen University, Discussion Paper, 2023. [Online]. Available: https://publications.rwth-aachen.de/record/861280/files/861280.pdf

[6] D. P. Loucks, “Chapter 2 - impacts of climate change on economies, ecosystems, energy, environments, and human equity: A systems perspective,” in *The Impacts of Climate Change*, T. M. Letcher, Ed. Elsevier, 2021, pp. 19–50. [Online]. Available: https://www.sciencedirect.com/science/article/pii/B9780128223734000161

[7] IPCC, “Sections. In: Climate Change 2023: Synthesis Report. Contribution of Working Groups I, II and III to the Sixth Assessment Report of the Intergovernmental Panel on Climate Change [Core writing Team, H. Lee and J. Romero (eds.)]. IPCC, Geneva, Switzerland, pp. 35-115,” 2023. [Online]. Available: https://www.ipcc.ch/report/ar6/syr/downloads/report/IPCC_AR6_SYR_LongerReport.pdf

[8] ENTSO-E Expert Panel, “28 april 2025 blackout in spain and portugal: Factual report,” European Network of Transmission System Operators for Electricity (ENTSO-E), Brussels, Belgium, Tech. Rep., 10 2025, report on the Iberian Peninsula blackout of 28 April 2025. [Online]. Available: https://www.entsoe.eu/publications/blackout/

[9] A. Maio, “Grid incident in spain and portugal on 28 april 2025: A focus on oscillations,” 2026. [Online]. Available: https://orbi.uliege.be/handle/2268/341566

[10] H. W. Dommel and W. F. Tinney, “Optimal power flow solutions,” *IEEE Transactions on Power Apparatus and Systems*, vol. 87, no. 10, pp. 1866–1876, 1968.

[11] J. K. Skolfield and A. R. Escobedo, “Operations research in optimal power flow: A guide to recent and emerging methodologies and applications,” *European Journal*

of Operational Research, vol. 300, no. 2, pp. 387–404, 2022. [Online]. Available: https://www.sciencedirect.com/science/article/pii/S0377221721008481

[12] M. Garcia-Sanz, M. Marden, I. Cvetkovic, H. Oh, E. LoCicero, and S. Khalid, "Grid fragility, blackouts, and control co-design solutions," *Advanced control for applications.*, vol. 7, no. 3, 2025.

[13] X. Chen, W. Wu, and B. Zhang, "Robust capacity assessment of distributed generation in unbalanced distribution networks incorporating ANM techniques," *IEEE Transactions on Sustainable Energy*, vol. PP, 09 2017.

[14] B. Wang, C. Zhang, Z. Y. Dong, and X. Li, "Improving hosting capacity of unbalanced distribution networks via robust allocation of battery energy storage systems," *IEEE Transactions on Power Systems*, vol. 36, pp. 2174–2185, 2021. [Online]. Available: https://api.semanticscholar.org/CorpusID:226613788

[15] M. S. S. Abad and J. Ma, "Photovoltaic hosting capacity sensitivity to active distribution network management," *IEEE Transactions on Power Systems*, vol. 36, no. 1, pp. 107–117, 2021.

[16] B. Uzum, Y. Yoldas, S. Bahceci, and A. Onen, "Comprehensive review of transmission system operators–distribution system operators collaboration for flexible grid operations," *Electric Power Systems Research*, vol. 227, p. 109976, 2024. [Online]. Available: https://www.sciencedirect.com/science/article/pii/S0378779623008647

[17] G. Migliavacca, M. Rossi, D. Six, M. Džamarija, S. Horsmanheimo, C. Madina, I. Kockar, and J. M. Morales, "Smartnet: H2020 project analysing tso–dso interaction to enable ancillary services provision from distribution networks," *CIRED*, vol. 2017, pp. 1998–2002, 2017. [Online]. Available: https://digital-library.theiet.org/doi/abs/10.1049/oap-cired.2017.0104

[18] H. Gerard, E. I. Rivero Puente, and D. Six, "Coordination between transmission and distribution system operators in the electricity sector: A conceptual framework," *Utilities Policy*, vol. 50, pp. 40–48, 2018. [Online]. Available: https://www.sciencedirect.com/science/article/pii/S0957178717301285

[19] F. Najibi, D. Apostolopoulou, and E. Alonso, "Tso-dso coordination schemes to facilitate distributed resources integration," *Sustainability*, vol. 13, no. 14, p. 7832, 2021. [Online]. Available: https://doi.org/10.3390/su13147832

[20] H. Le Cadre, I. Mezghani, and A. Papavasiliou, "A game-theoretic analysis of transmission-distribution system operator coordination," *European Journal of Operational Research*, vol. 274, no. 1, pp. 317–339, 2019. [Online]. Available: https://www.sciencedirect.com/science/article/pii/S0377221718308257

[21] A. Papavasiliou and I. Mezghani, "Coordination schemes for the integration of transmission and distribution system operations," in *2018 Power Systems Computation Conference (PSCC)*, 2018, pp. 1–7.

[22] D. Koraki and K. Strunz, "Wind and solar power integration in electricity markets and distribution networks through service-centric virtual power plants," *IEEE Transactions on Power Systems*, vol. 33, no. 1, p. 473 – 485, 2018, cited by: 305. [Online]. Available: https://www.scopus.com/inward/record.uri?eid=2-s2.0-85046026967&doi=10.1109%2fTPWRS.2017.2710481&partnerID=40&md5=057a34dadd682a2211d2a507e74023ad

[23] H. Hinners, D. M. Gonzalez, J. Myrzik, and C. Rehtanz, "Multivariable control of active distribution networks for tso-dso-coordinated operation in wide-area power systems," *at - Automatisierungstechnik*, vol. 67, no. 11, pp. 904–911, 2019. [Online]. Available: https://doi.org/10.1515/auto-2019-0066

[24] K. Yoon, J. Leem, S. H. Lee, and J.-W. Park, "Cooperative control of TSO and DSO: management of line congestion and frequency response," *IEEE Access*, vol. PP, pp. 1–1, 01 2024.

[25] D. S. Stock, F. Sala, A. Berizzi, and L. Hofmann, "Optimal control of wind farms for coordinated tso–dso reactive power management," *Energies*, vol. 11, no. 1, p. 173, 2018.

[26] D. Sieraszewsk, O. K. Olsen, D. Ivanko, I. Oleinikova, and H. Farahmand, "Multi-period hybrid AC/DC-OPF model for flexibility market clearing with seamless TSO-DSO coordination," *IEEE Access*, vol. 11, pp. 40 093–40 106, 2023.

[27] S. Meinecke, D. S. Stock, and M. Braun, "New distributed optimization method for TSO–DSO coordinated grid operation preserving power system operator sovereignty," *Energies*, vol. 16, no. 12, 2023.

[28] A. Kargarian, J. Mohammadi, J. Guo, S. Chakrabarti, M. Barati, G. Hug, S. Kar, and R. Baldick, "Toward distributed/decentralized dc optimal power flow implementation in future electric power systems," *IEEE Transactions on Smart Grid*, vol. 9, no. 4, pp. 2574–2594, 2018.

[29] M. A. Bragin and Y. Dvorkin, "Tso-dso operational planning coordination through "l_1-proximal" surrogate lagrangian relaxation," *IEEE Transactions on Power Systems*, vol. 37, no. 2, pp. 1274–1285, 2022.

[30] T. Soares, L. Carvalho, H. Morais, R. J. Bessa, T. Abreu, and E. Lambert, "Reactive power provision by the dso to the tso considering renewable energy sources uncertainty," *Sustainable Energy, Grids and Networks*, vol. 22, p. 100333, 2020. [Online]. Available: https://www.sciencedirect.com/science/article/pii/S2352467719304886

[31] A. Nawaz and H. Wang, "Distributed stochastic security constrained unit commitment for coordinated operation of transmission and distribution system," *CSEE Journal of Power and Energy Systems*, vol. 7, no. 4, pp. 708–718, 2021.

[32] J. Liu, H. Cheng, P. Zeng, L. Yao, C. Shang, and Y. Tian, "Decentralized stochastic optimization based planning of integrated transmission and distribution networks with distributed generation penetration," *Applied Energy*, vol. 220, pp. 800–813, 2018. [Online]. Available: https://www.sciencedirect.com/science/article/pii/S0306261918303453

[33] C. Lou, L. Zhang, W. Tang, J. Yang, and L. Min, "A coordinated restoration method of three-phase ac unbalanced distribution network with dc connections and mobile energy storage systems," *International Journal of Electrical Power & Energy Systems*, vol. 157, p. 109895, 2024. [Online]. Available: https://www.sciencedirect.com/science/article/pii/S0142061524001169

[34] E. Raheli, Q. Wu, M. Zhang, and C. Wen, "Optimal coordinated operation of integrated natural gas and electric power systems: A review of modeling and solution methods," *Renewable and Sustainable Energy Reviews*, vol. 145, p. 111134, 2021. [Online]. Available: https://www.sciencedirect.com/science/article/pii/S1364032121004226

[35] CoordiNet Consortium, "Roadmap towards a new market design including the implementation of standardised products for system services," CoordiNet Project (Horizon 2020), Tech. Rep., 2022. [Online]. Available: https://www.edsoforsmartgrids.eu/eu-projects/coordinet/

[36] SmartNet Project, *TSO-DSO coordination for acquiring ancillary services from distribution grids*, G. Migliavacca, Ed. Florence School of Regulation, 2019. [Online]. Available: https://smartnet-project.eu/wp-content/uploads/2019/05/SmartNet-Booktlet.pdf

[37] I. Losa, A. Monti, M. Ginocchi, V. Croce, F. Bosco, E. de Luca, G. Fedele, D. Stratogiannis, and B. Petters, "PLATONE: towards a new open DSO platform for digital smart grid services and operation," in *CIRED*, Sep. 2021, pp. 2974–2978.

[38] International Renewable Energy Agency, "Innovation landscape brief: co-operation between transmission and distribution system operators," International Renewable Energy Agency (IRENA), Tech. Rep., 2020. [Online]. Available: https://www.irena.org/publications/2020/Jul/System-Operation-Innovation-Landscape-briefs

[39] A. Wickramasinghe, M. Vilathgamuwa, G. Nourbakhsh, and P. Corry, "A review of dynamic operating envelopes: Computation, applications and challenges," *Modelling*, vol. 6, no. 2, p. 29, 2025. [Online]. Available: https://doi.org/10.3390/modelling6020029

[40] M. M. Hoque, M. Khorasany, M. I. Azim, R. Razzaghi, and M. Jalili, "Dynamic operating envelope-based local energy market for prosumers with electric vehicles," *IEEE Transactions on Smart Grid*, vol. 15, no. 2, pp. 1712–1724, 2024.

[41] ——, "A framework for prosumer-centric peer-to-peer energy trading using network-secure export–import limits," *Applied Energy*, vol. 361, p. 122906, 2024. [Online]. Available: https://www.sciencedirect.com/science/article/pii/S0306261924002897

[42] Z. Jiang, Y. Guo, and J. Wang, "Dynamic operating envelopes embedded peer-to-peer-to-grid energy trading," *Applied Energy*, vol. 377, p. 124554, 2025. [Online]. Available: https://www.sciencedirect.com/science/article/pii/S0306261924019378

[43] M. Azim, G. Lankeshwara, W. Tushar, R. Sharma, M. Alam, T. Saha, M. Khorasany, and R. Razzaghi, "Dynamic operating envelope-enabled p2p trading to maximise financial returns of prosumers," *IEEE Transactions on Smart Grid*, vol. 15, no. 2, pp. 1978–1990, Mar. 2024, publisher Copyright: IEEE.

[44] M. Azim, M. Hoque, M. Khorasany, R. Razzaghi, M. Jalili, and D. Hill, "Dynamic operating envelope-integrated cooperative energy trading: A fair allocation approach," *IEEE Transactions on Power Systems*, vol. 40, no. 4, pp. 2845–2859, Jul. 2025, publisher Copyright: © 1969-2012 IEEE.

[45] A. R. Jordehi, "Optimisation of demand response in electric power systems, a review," *Renewable and Sustainable Energy Reviews*, vol. 103, pp. 308–319, 2019. [Online]. Available: https://www.sciencedirect.com/science/article/pii/S1364032118308566

[46] G. Lankeshwara, R. Sharma, M. Alam, R. Yan, and T. Saha, "Development and validation of a dynamic operating envelopes-enabled demand response scheme in low-voltage distribution networks," *Applied Energy*, vol. 382, p. 125150, 03 2025.

[47] H. Moring and J. L. Mathieu, "Inexactness of second order cone relaxations for calculating operating envelopes," in *Proceedings of the IEEE International Conference on Communications, Control, and Computing Technologies for Smart Grids (SmartGridComm)*. Glasgow, UK: IEEE, 2023.

[48] Y. Yi and G. Verbič, "Fair operating envelopes under uncertainty using chance constrained optimal power flow," *Electric Power Systems Research*, vol. 213, p. 108465, 2022.

[49] G. Lankeshwara, "A real-time control approach to maximise the utilisation of rooftop pv using dynamic export limits," in *Proceedings of the IEEE PES Innovative Smart Grid Technologies Asia (ISGT Asia)*. Brisbane, Australia: IEEE, Dec. 2021, 5–8 December 2021.

[50] B. Liu and J. H. Braslavsky, "Robust dynamic operating envelopes for der integration in unbalanced distribution networks," *IEEE Transactions on Power Systems*, vol. 39, no. 2, pp. 3921–3936, 2024.

[51] B. Liu, J. H. Braslavsky, and N. Mahdavi, “Linear OPF-based robust dynamic operating envelopes with uncertainties in unbalanced distribution networks,” *Journal of Modern Power Systems and Clean Energy*, vol. 12, pp. 1320–1326, 2023.

[52] A. Koirala, F. Geth, and T. Van Acker, “Day-ahead dynamic operating envelopes using stochastic unbalanced optimal power flow,” *Sustainable Energy, Grids and Networks*, vol. 40, p. 101528, 2024. [Online]. Available: https://www.sciencedirect.com/science/article/pii/S2352467724002571

[53] M. Laughton, I. Crow, H. Watson, W. Rizk, E. Goldwag, and L. Mahon, “26 - prime movers,” in *Electrical Engineer's Reference Book (Sixteenth Edition)*, sixteenth edition ed., M. Laughton and D. Warne, Eds. Oxford: Newnes, 2003, pp. 26–1–26–42. [Online]. Available: https://www.sciencedirect.com/science/article/pii/B9780750646376500265

[54] M. L. Crow and N. Shetty, “Electric power measurements and variables,” in *Encyclopedia of Energy*, C. J. Cleveland, Ed. New York: Elsevier, 2004, pp. 245–254. [Online]. Available: https://www.sciencedirect.com/science/article/pii/B012176480X005076

[55] O. S. E. Atwa, “Chapter 2 - substations,” in *Practical Power System and Protective Relays Commissioning*, O. S. E. Atwa, Ed. Academic Press, 2019, pp. 9–21. [Online]. Available: https://www.sciencedirect.com/science/article/pii/B9780128168585000022

[56] R. Montgomery and R. McDowall, “Chapter 2 - basics of electricity,” in *Fundamentals of HVAC Control Systems*, R. Montgomery and R. McDowall, Eds. Oxford: Elsevier, 2008, pp. 30–60. [Online]. Available: https://www.sciencedirect.com/science/article/pii/B9780080552330000029

[57] B. Khan, “Chapter 1 - electrical distribution network: An introduction,” in *Active Electrical Distribution Network*, S. Padmanaban, B. Khan, O. P. Mahela, H. H. Alhelou, and S. Rajkumar, Eds. Academic Press, 2022, pp. 3–14. [Online]. Available: https://www.sciencedirect.com/science/article/pii/B9780323851695000162

[58] C. Bayliss and B. Hardy, “Chapter 13 - switchgear,” in *Transmission and Distribution Electrical Engineering (Fourth Edition)*, fourth edition ed., C. Bayliss and B. Hardy, Eds. Oxford: Newnes, 2012, pp. 467–541. [Online]. Available: https://www.sciencedirect.com/science/article/pii/B9780080969121000137

[59] C. Booth and K. Bell, “3 - protection of transmission and distribution (td) networks,” in *Electricity Transmission, Distribution and Storage Systems*, ser. Woodhead Publishing Series in Energy, Z. Melhem, Ed. Woodhead Publishing, 2013, pp. 75–107. [Online]. Available: https://www.sciencedirect.com/science/article/pii/B9781845697846500032

[60] W. Bolton, “Chapter 13 - control systems,” in *Instrumentation and Control Systems (Third Edition)*, third edition ed., W. Bolton, Ed. Newnes, 2021, pp. 297–328. [Online]. Available: https://www.sciencedirect.com/science/article/pii/B9780128234716000137

[61] D. Botelho, B. Dias, L. de Oliveira, T. Soares, I. Rezende, and T. Sousa, “Innovative business models as drivers for prosumers integration - enablers and barriers,” *Renewable and Sustainable Energy Reviews*, vol. 144, p. 111057, 2021. [Online]. Available: https://www.sciencedirect.com/science/article/pii/S1364032121003464

[62] P. Kundur, J. Paserba, V. Ajjarapu, G. Andersson, A. Bose, C. Canizares, N. Hatziargyriou, D. Hill, A. Stankovic, C. Taylor, T. Van Cutsem, and V. Vittal, “Definition and classification of power system stability IEEE/CIGRE joint task force on stability terms and definitions,” *IEEE Transactions on Power Systems*, vol. 19, no. 3, pp. 1387–1401, 2004.

[63] E. A. Hailu, G. N. Nyakoe, and C. M. Muriithi, "Techniques of power system static security assessment and improvement: a literature survey," *Heliyon*, vol. 9, no. 3, p. e14524, 2023.

[64] European Commission, "Commission regulation (eu) 2017/1485 of 2 august 2017 establishing a guideline on electricity transmission system operation," pp. 1–120, 2017, text with EEA relevance. [Online]. Available: https://eur-lex.europa.eu/eli/reg/2017/1485/oj

[65] I. M. Bomze and M. Gabl, "Optimization under uncertainty and risk: Quadratic and copositive approaches," *European Journal of Operational Research*, vol. 310, no. 2, pp. 449–476, 2023. [Online]. Available: https://www.sciencedirect.com/science/article/pii/S0377221722008773

[66] Y. Huang, T. Ding, P. Wang, W. Jia, C. Ju, X. He, H. Zhang, Z. Zhang, and Y. Sun, "Linearized ac power flow model based interval total transfer capability evaluation with uncertain renewable energy integration," *International Journal of Electrical Power & Energy Systems*, vol. 154, p. 109440, 2023. [Online]. Available: https://www.sciencedirect.com/science/article/pii/S0142061523004970

[67] W. E. Hart, J.-P. Watson, and D. L. Woodruff, "Pyomo: modeling and solving mathematical programs in python," *Mathematical Programming Computation*, vol. 3, no. 3, pp. 219–260, 2011.

[68] T. Okon and K. Wilkosz, "Phase shifter models for steady state analysis," in *2016 17th International Scientific Conference on Electric Power Engineering (EPE)*, 2016, pp. 1–6.

[69] A. Gabrijel and B. Mihalic, "Phase-shifting transformers in a structure-preserving energy function," *Electric Power Systems Research*, vol. 74, no. 2, pp. 323–330, 2005. [Online]. Available: https://www.sciencedirect.com/science/article/pii/S0378779605000611

[70] K. Van den Bergh, E. Delarue, and W. D'haeseleer, "Dc power flow in unit commitment models," KU Leuven, Energy Institute, TME Branch, Working Paper WP EN2014-12, 2014. [Online]. Available: https://www.mech.kuleuven.be/en/tme/research/energy_environment/pdf/wpen2014-12.pdf

[71] J. D. Glover, M. S. Sarma, and T. J. Overbye, *Power Systems Analysis and Design*, 5th ed. Cengage Learning, 2012.

[72] Z. Yuan, "Formulations and approximations of branch flow model for general power networks," *Journal of Modern Power Systems and Clean Energy*, vol. 10, no. 5, pp. 1110–1126, 2022.

[73] M. Farivar and S. H. Low, "Branch flow model: Relaxations and convexification—part i," *IEEE Transactions on Power Systems*, vol. 28, no. 3, pp. 2554–2564, 2013.

[74] C. Coffrin, H. L. Hijazi, and P. Van Hentenryck, "The qc relaxation: A theoretical and computational study on optimal power flow," *IEEE Transactions on Power Systems*, vol. 31, no. 4, pp. 3008–3018, 2016.

[75] R. Jabr, "Radial distribution load flow using conic programming," *Power Systems, IEEE Transactions on*, vol. 21, pp. 1458 – 1459, 09 2006.

[76] M. Glavic and S. Greene, "Voltage stability in future power systems," in *Encyclopedia of Electrical and Electronic Power Engineering*. Elsevier, 2023. [Online]. Available: https://orbi.uliege.be/handle/2268/302373

[77] M. Farivar, C. Clarke, S. Low, and K. Chandy, "Inverter var control for distribution systems with renewables," in *2011 IEEE International Conference on Smart Grid Communications (SmartGridComm)*, oct 2011, pp. 457–462.

[78] R. D. Zimmerman, C. E. Murillo-Sanchez, and R. J. Thomas, "Matpower's extensible optimal power flow architecture," in *2009 IEEE Power Energy Society General Meeting*, 2009, pp. 1–7.

[79] R. D. Zimmerman, C. E. Murillo-Sánchez, and R. J. Thomas, "Matpower: Steady-state operations, planning, and analysis tools for power systems research and education," *IEEE Transactions on Power Systems*, vol. 26, no. 1, pp. 12–19, 2011.

[80] R. Fatima, H. Z. Butt, and X. Li, "Optimal dynamic reconfiguration of distribution networks," in *2023 North American Power Symposium (NAPS)*, 2023, pp. 1–6.

[81] M. Subramanian, J. Viebahn, S. H. Tindemans, B. Donnot, and A. Marot, "Exploring grid topology reconfiguration using a simple deep reinforcement learning approach," in *2021 IEEE Madrid PowerTech*. IEEE, 2021, p. 1–6. [Online]. Available: http://dx.doi.org/10.1109/PowerTech46648.2021.9494879

[82] S. Hoberg, I. Voloh, and T. Ernst, "Review of capacitor bank control practices," in *Proceedings of the Western Protective Relay Conference (WPRC)*. Spokane, WA, USA: WPRC Archives, October 2019. [Online]. Available: https://wprcarchives.org/wp-content/uploads/2024/04/ernst_thomas_Review-of-Capacitor_2019.pdf

[83] Z. Gajić, B. Hillström, and F. Mekić, "Hv shunt reactor secrets for protection engineers," in *Proceedings of the 30th Western Protective Relay Conference (WPRC)*. Spokane, WA, USA: WPRC Archives, October 2003. [Online]. Available: https://wprcarchives.org/wp-content/uploads/2024/07/Zoran-Gajic_Shunt-Reactor-Protection_2003.pdf

[84] M. M. Haque and P. Wolfs, "A review of high pv penetrations in lv distribution networks: Present status, impacts and mitigation measures," *Renewable and Sustainable Energy Reviews*, vol. 62, pp. 1195–1208, 2016. [Online]. Available: https://www.sciencedirect.com/science/article/pii/S1364032116300429

[85] C. Bayliss and B. Hardy, "Chapter 14 - power transformers," in *Transmission and Distribution Electrical Engineering (Fourth Edition)*, fourth edition ed. Oxford: Newnes, 2012, pp. 543–614. [Online]. Available: https://www.sciencedirect.com/science/article/pii/B9780080969121000149

[86] D. Mondal, A. Chakrabarti, and A. Sengupta, "Chapter 3 - models of power network and relevant power equipments," in *Power System Small Signal Stability Analysis and Control*, D. Mondal, A. Chakrabarti, and A. Sengupta, Eds. Boston: Academic Press, 2014, pp. 41–84. [Online]. Available: https://www.sciencedirect.com/science/article/pii/B9780128005729000032

[87] E. Bompard, A. Mazza, and L. Toma, "Chapter 3 - classical grid control: Frequency and voltage stability," in *Converter-Based Dynamics and Control of Modern Power Systems*, A. Monti, F. Milano, E. Bompard, and X. Guillaud, Eds. Academic Press, 2021, pp. 31–65. [Online]. Available: https://www.sciencedirect.com/science/article/pii/B9780128184912000031

[88] J. Manwell, "Hybrid energy systems," in *Encyclopedia of Energy*, C. J. Cleveland, Ed. New York: Elsevier, 2004, pp. 215–229. [Online]. Available: https://www.sciencedirect.com/science/article/pii/B012176480X003600

[89] M. Kamran, "Chapter 3 - power grids," in *Fundamentals of Smart Grid Systems*, M. Kamran, Ed. Academic Press, 2023, pp. 71–131. [Online]. Available: https://www.sciencedirect.com/science/article/pii/B9780323995603000053

[90] P. Li, H. Ji, H. Yu, and C. Wang, "Chapter 2 - components and modeling of flexible distribution networks," in *Flexible Distribution Networks*, P. Li, H. Ji, H. Yu, and C. Wang, Eds. Elsevier, 2024, pp. 13–64. [Online]. Available: https://www.sciencedirect.com/science/article/pii/B9780128238905000052

[91] S. Tong, M. A. Boateng, M. Tanneau, and P. V. Hentenryck, "Volt/var optimization in transmission networks with discrete-control devices," 2026. [Online]. Available: https://arxiv.org/abs/2601.22080

[92] T. McNamara, A. Pandey, A. Agarwal, and L. Pileggi, "Two-stage homotopy method to incorporate discrete control variables into ac-opf," *Electric Power Systems Research*, vol. 212, p. 108283, 2022. [Online]. Available: https://www.sciencedirect.com/science/article/pii/S0378779622004722

[93] A. Shokri Gazafroudi, F. Neumann, and T. Brown, "Topology-based approximations for n1 contingency constraints in power transmission networks," *International Journal of Electrical Power Energy Systems*, vol. 137, p. 107702, 2022. [Online]. Available: https://www.sciencedirect.com/science/article/pii/S0142061521009297

[94] M. E. Baran and F. F. Wu, "Network reconfiguration in distribution systems for loss reduction and load balancing," *IEEE Power Engineering Review*, vol. 9, no. 4, pp. 101–102, 1989.

[95] M. Farivar and S. H. Low, "Branch flow model: Relaxations and convexification—part i," *IEEE Transactions on Power Systems*, vol. 28, no. 3, pp. 2554–2564, 2013.

[96] J. F. Franco, M. J. Rider, and R. Romero, "A mixed-integer quadratically-constrained programming model for the distribution system expansion planning," *International Journal of Electrical Power & Energy Systems*, vol. 62, pp. 265–272, 2014. [Online]. Available: https://www.sciencedirect.com/science/article/pii/S0142061514002439

[97] A. Esmaeel Nezhad, P. H. Nardelli, M. S. Javadi, S. Jowkar, T. Tavakkoli Sabour, and F. Ghanavati, "A hybrid optimal power flow model for transmission and distribution networks," *Electric Power Systems Research*, vol. 245, p. 111638, 2025. [Online]. Available: https://www.sciencedirect.com/science/article/pii/S0378779625002305

[98] J. Lavaei and S. Low, "Zero duality gap in optimal power flow problem," *IEEE Transactions on Power Systems*, vol. 27, 02 2012.

[99] X. Bai, H. Wei, K. Fujisawa, and Y. Wang, "Semidefinite programming for optimal power flow problems," *International Journal of Electrical Power Energy Systems*, vol. 30, no. 6, pp. 383–392, 2008. [Online]. Available: https://www.sciencedirect.com/science/article/pii/S0142061507001378

[100] J. S. Arora, "Chapter 18 - multi-objective optimum design concepts and methods," in *Introduction to Optimum Design (Fourth Edition)*, fourth edition ed. Boston: Academic Press, 2017, pp. 771–794. [Online]. Available: https://www.sciencedirect.com/science/article/pii/B9780128008065000184

[101] K.-H. Chang, "Chapter 19 - multiobjective optimization and advanced topics," in *e-Design*. Boston: Academic Press, 2015, pp. 1105–1173. [Online]. Available: https://www.sciencedirect.com/science/article/pii/B9780123820389000193

[102] M. Vassallo, S. Khaskheli, L. Dong, A. H. Thuc, A. Anvari-Moghaddam, P. P. Vergara, L. Duchesne, S. Gerard, and D. Ernst, "A new paradigm for bilateral trading of dynamic operating envelopes in electricity distribution networks," 2025. [Online]. Available: https://orbi.uliege.be/handle/2268/331735

[103] L. J. de Vries, J. de Joode, and R. Hakvoort, *The regulation of electricity transmission networks and its impact on governance.*, ser. European review of energy markets Vol 3, 2009, issue 3. S.l: European Energy Institute, 2009.

[104] B. Taheri and D. K. Molzahn, "Ac-informed dc optimal transmission switching problems via parameter optimization," 2025. [Online]. Available: https://arxiv.org/abs/2411.10528

[105] T. J. Overbye, "The dc power flow equations," n.d., lecture notes for EE 553. [Online]. Available: https://home.engineering.iastate.edu/~jdm/ee553-Old/DCPowerFlowEquations.pdf

[106] C. Domínguez, Álvaro Porras, S. Pineda, and J. M. Morales, "Optimal power flow under uncertainty," in *Encyclopedia of Electrical and Electronic Power Engineering*, J. García, Ed. Oxford: Elsevier, 2023, pp. 765–776. [Online]. Available: https://www.sciencedirect.com/science/article/pii/B9780128212042001070

[107] A. Maio, T. Richard, M. Vassallo, A. Bolland, V. Barbesant, J. Callec, S. Haye, D. Fourniret, and D. Ernst, "Improving tso-dso coordination through dynamic operating envelopes allocation," 2025. [Online]. Available: https://orbi.uliege.be/handle/2268/336605

[108] A. Bolland, A. Maio, T. Richard, M. Vassallo, A. Bahmanyar, and D. Ernst, "Breaking down the complexity of network operation," 2025. [Online]. Available: https://orbi.uliege.be/handle/2268/337108

Appendices

Appendix A

Per-unit normalization

All optimisation problem parameters are normalized to per-unit quantities. The base voltage at each bus is taken as the nominal phase-to-phase voltage V_B, while a common system base apparent power of $S_B = 100$ MVA is considered for both test networks. The per-unit conversion formulae are as follows:

$$
\begin{aligned}
P_{n,pu} &= \frac{P_n}{S_B} \\
Q_{n,pu} &= \frac{Q_n}{S_B} \\
Z_B &= \frac{V_B^2}{S_B} \\
I_B &= \frac{S_B}{\sqrt{3}\,V_B} \\
r_{e,pu} &= \frac{r_e}{Z_B} = \frac{r_e S_B}{V_B^2} \\
x_{e,pu} &= \frac{x_e}{Z_B} = \frac{x_e S_B}{V_B^2} \\
I_{e,\max,pu} &= \frac{I_{e,\max}}{I_B} = \frac{\sqrt{3}\,I_{e,\max} V_B}{S_B} \\
G_{e,pu} &= \frac{r_{e,pu}}{r_{e,pu}^2 + x_{e,pu}^2} \\
B_{e,pu} &= -\frac{x_{e,pu}}{r_{e,pu}^2 + x_{e,pu}^2} \\
V_{n,pu} &= \frac{V_n}{V_{B,n}}
\end{aligned}
$$

where $P_{n,pu}$ and $Q_{n,pu}$ are the per-unit active and reactive power demand at node n, with P_n in MW and Q_n in MVAr, Z_B is the impedance base and I_B the base current, each varying with the local nominal voltage V_B. $r_{e,pu}$ and $x_{e,pu}$ are the per-unit series resistance and reactance of edge e, $I_{e,\max,pu}$ is the per-unit thermal current limit, $G_{e,pu}$ and $B_{e,pu}$ are the per-unit conductance and susceptance, $V_{n,pu}$ is the per-unit voltage magnitude at node n.

Appendix B

Linearisation of the AC power flow equations

The linearisation of the power flow equations can be performed in different steps. The power flow equations considered take into account phase-shifters. For sake of clarity, the following table defines all parameters and variables used in the linearisation:

Symbol	Definition
$\mathcal{N}$	Set of buses; bus 0 is the slack (reference)
$\mathcal{E}$	Set of directed branches (n, j)
$V_n \in \mathbb{R}$	Voltage magnitude at bus n [p.u.]
$\theta_n \in \mathbb{R}$	Voltage angle at bus n [rad]; $\theta_0 = 0$
P_{nj}, Q_{nj}	Active and reactive power flow on branch (n, j) [p.u.]
$P_{\text{gen},n}$, $Q_{\text{gen},n}$	Active and reactive generation at bus n [p.u.]
ρ_{nj}	Phase-shift angle on branch (n, j) [rad]
P_n^+, P_n^-, Q_n^+, Q_n^-	Active and reactive power entering/leaving the network at bus n
g_{nj}, b_{nj}	Conductance and susceptance of branch (n, j) [p.u.]
$P_{\text{load},n}$, $Q_{\text{load},n}$	Active and reactive demand at bus n [p.u.]
$\bar{S}_{nj}$	Apparent power thermal limit on branch (n, j) [p.u.]
$\underline{V}_n$, $\bar{V}_n$	Voltage magnitude bounds at bus n [p.u.]
$\underline{\rho}_{nj}$, $\bar{\rho}_{nj}$	Phase-shift limits; both zero for non-shifter branches

As a reminder, the branch flow equations are written as follows:

$$P_{nj} = g_{nj}V_n^2 - V_nV_j\big[g_{nj}\cos(\theta_n - \theta_j + \rho_{nj}) + b_{nj}\sin(\theta_n - \theta_j + \rho_{nj})\big], \tag{B.1}$$

$$Q_{nj} = -b_{nj}V_n^2 - V_nV_j\big[g_{nj}\sin(\theta_n - \theta_j + \rho_{nj}) - b_{nj}\cos(\theta_n - \theta_j + \rho_{nj})\big]. \tag{B.2}$$

Nominal Operating Point and Nominal Flows The linearization is performed around the set-point: $V_n^0 = 1$ p.u. and $\theta_n^0 = 0$ for all buses, and $\rho_{nj}^0 = 0$ for all branches. At this point, the effective angle difference is $\delta_{nj}^0 = \theta_n^0 - \theta_j^0 + \rho_{nj}^0 = 0$, so the nominal branch flows are:

$$P_{nj}^0 = (V_n^0)^2\, g_{nj} - V_n^0V_j^0\big[g_{nj}\cos 0 + b_{nj}\sin 0\big] = g_{nj} - g_{nj} = 0,$$

$$Q_{nj}^0 = -(V_n^0)^2\, b_{nj} - V_n^0V_j^0\big[g_{nj}\sin 0 - b_{nj}\cos 0\big] = -b_{nj} + b_{nj} = 0.$$

Because the nominal flows vanish, the first-order Taylor expansion gives the total flows directly:

$$P_{nj} = \left.\frac{\partial P_{nj}}{\partial V_n}\right|_{\substack{V^0=1\\ \delta^0=0}} \Delta V_n + \left.\frac{\partial P_{nj}}{\partial V_j}\right|_{\substack{V^0=1\\ \delta^0=0}} \Delta V_j + \left.\frac{\partial P_{nj}}{\partial \theta_n}\right|_{\substack{V^0=1\\ \delta^0=0}} \Delta \theta_n + \left.\frac{\partial P_{nj}}{\partial \theta_j}\right|_{\substack{V^0=1\\ \delta^0=0}} \Delta \theta_j + \left.\frac{\partial P_{nj}}{\partial \rho_{nj}}\right|_{\substack{V^0=1\\ \delta^0=0}} \Delta \rho_{nj},$$

and identically for Q_{nj}. The perturbations are $\Delta V_n = V_n - 1$, $\Delta V_j = V_j - 1$, $\Delta\theta_n = \theta_n$, $\Delta\rho_{nj} = \rho_{nj}$. In what follows, V_n and V_j denote these voltage deviations from 1 p.u., and we drop the Δ notation hereafter.

Partial Derivatives Let $\delta_{nj} = \theta_n - \theta_j + \rho_{nj}$ denote the effective angle difference. Differentiating (4.2)–(4.3) with respect to each variable and evaluating at the set-point $V_n^0 = V_j^0 = 1$ p.u., $\theta_n^0 = \theta_j^0 = 0$ rad, $\rho_{nj}^0 = 0$ rad (so $\delta_{nj}^0 = 0$):

With respect to V_n, the partial derivatives become:

$$\left.\frac{\partial P_{nj}}{\partial V_n}\right|_{\substack{V^0=1\\ \delta^0=0}} = 2V_n^0\, g_{nj} - V_j^0\left[g_{nj}\cos\delta_{nj}^0 + b_{nj}\sin\delta_{nj}^0\right] = 2g_{nj} - g_{nj} = g_{nj},$$

$$\left.\frac{\partial Q_{nj}}{\partial V_n}\right|_{\substack{V^0=1\\ \delta^0=0}} = -2V_n^0\, b_{nj} - V_j^0\left[g_{nj}\sin\delta_{nj}^0 - b_{nj}\cos\delta_{nj}^0\right] = -2b_{nj} + b_{nj} = -b_{nj}.$$

With respect to V_j, the partial derivatives become:

$$\left.\frac{\partial P_{nj}}{\partial V_j}\right|_{\substack{V^0=1\\ \delta^0=0}} = -V_n^0\left[g_{nj}\cos\delta_{nj}^0 + b_{nj}\sin\delta_{nj}^0\right] = -g_{nj},$$

$$\left.\frac{\partial Q_{nj}}{\partial V_j}\right|_{\substack{V^0=1\\ \delta^0=0}} = -V_n^0\left[g_{nj}\sin\delta_{nj}^0 - b_{nj}\cos\delta_{nj}^0\right] = b_{nj}.$$

With respect to θ_n (note $\partial\delta_{nj}/\partial\theta_n = +1$), the partial derivatives become:

$$\left.\frac{\partial P_{nj}}{\partial \theta_n}\right|_{\substack{V^0=1\\ \delta^0=0}} = V_n^0 V_j^0\left[g_{nj}\sin\delta_{nj}^0 - b_{nj}\cos\delta_{nj}^0\right] = -b_{nj},$$

$$\left.\frac{\partial Q_{nj}}{\partial \theta_n}\right|_{\substack{V^0=1\\ \delta^0=0}} = -V_n^0 V_j^0\left[g_{nj}\cos\delta_{nj}^0 + b_{nj}\sin\delta_{nj}^0\right] = -g_{nj}.$$

With respect to θ_j (note $\partial\delta_{nj}/\partial\theta_j = -1$), the partial derivatives become:

$$\left.\frac{\partial P_{nj}}{\partial \theta_j}\right|_{\substack{V^0=1\\ \delta^0=0}} = -V_n^0 V_j^0\left[g_{nj}\sin\delta_{nj}^0 - b_{nj}\cos\delta_{nj}^0\right] = b_{nj},$$

$$\left.\frac{\partial Q_{nj}}{\partial \theta_j}\right|_{\substack{V^0=1\\ \delta^0=0}} = V_n^0 V_j^0\left[g_{nj}\cos\delta_{nj}^0 + b_{nj}\sin\delta_{nj}^0\right] = g_{nj}.$$

With respect to ρ_{nj} (note $\partial\delta_{nj}/\partial\rho_{nj} = +1$), the partial derivatives become:

$$\left.\frac{\partial P_{nj}}{\partial \rho_{nj}}\right|_{\substack{V^0=1\\ \delta^0=0}} = \left.\frac{\partial P_{nj}}{\partial \theta_n}\right|_{\substack{V^0=1\\ \delta^0=0}} = -b_{nj},$$

$$\left.\frac{\partial Q_{nj}}{\partial \rho_{nj}}\right|_{\substack{V^0=1\\ \delta^0=0}} = \left.\frac{\partial Q_{nj}}{\partial \theta_n}\right|_{\substack{V^0=1\\ \delta^0=0}} = -g_{nj}.$$

With the convention $\delta_{nj} = \theta_n - \theta_j + \rho_{nj}$, the phase-shift has exactly the same sensitivity as θ_n. Physically, a positive ρ_{nj} increases the effective angle difference and therefore increases P_{nj} (since $b_{nj} < 0$ for inductive branches, $-b_{nj} > 0$).

Substituting the partial derivatives into the Taylor expansion, branch flow equations become:

$$P_{nj} = g_{nj}(V_n - V_j) - b_{nj}(\theta_n - \theta_j + \rho_{nj}), \tag{2-P}$$

$$Q_{nj} = -b_{nj}(V_n - V_j) - g_{nj}(\theta_n - \theta_j + \rho_{nj}). \tag{2-Q}$$

Branches without a phase-shifter satisfy $\underline{\rho}_{nj} = \bar{\rho}_{nj} = 0$, which forces $\rho_{nj} = 0$ and recovers the standard linearised AC flow equations. A single unified pair of equations covers the entire network.

Appendix C

DC power flow equations

The DC formulation is one of the most widely used linear power flow models for real power flow analysis. It has been exploited in different contexts, among others, unit commitment [70] and the transmission switching problem [104]. High-voltage electrical networks often respect the required assumptions to apply the DC formulation:

1. voltage angles differences between adjacent nodes are small;
2. the voltage profile is flat, meaning all voltage magnitudes are assumed equal;
3. the line resistances $R_{n,j}$ are negligible compared to the reactances $X_{n,j}$, which implies that the line susceptances $B_{n,j}$ can be approximated by: $|B_{n,j}| \approx \frac{1}{|X_{n,j}|}, \forall (n,j) \in \mathcal{E}_o$.

Under these assumptions, branch flow equations (Appendix B) can be approximated as:

$$P_{n,m} = B_{n,m} \cdot (\theta_n - \theta_m) \qquad \forall (n,m) \in \mathcal{E}_o, \tag{C.1a}$$
$$\tag{C.1b}$$

where θ_n is the voltage phase angle at a node n, $P_{n,m}$ is the power flowing through an edge (n,m).

It is worth mentioning that, by applying the DC power flow assumptions on the linearized AC power flow equations developed in Appendix B, i.e, voltage angles differences between adjacent nodes are small, the voltage profile is flat, meaning all voltage magnitudes are assumed equal, the line resistances $R_{n,j}$ are negligible compared to the reactances $X_{n,j}$, we can recover: $P_{nj} \approx -b_{nj}(\theta_n - \theta_j)$, and $Q_{nj} \approx 0$.

Launching DC load flows thus consists of solving the following linear set of equations [79]:

$$P_{n,m} = \frac{\theta_n - \theta_m}{X_{n,m}}, \qquad \forall (n,m) \in \mathcal{E}_o, \tag{C.2a}$$
$$\theta_{ref} = 0, \tag{C.2b}$$
$$P_{load,n} - P_{gen,n} = \sum_{(m,n)\in\mathcal{E}_o} P_{m,n} - \sum_{(n,j)\in\mathcal{E}_o} P_{n,j} + P_n^+, \qquad \forall n \in \mathcal{N}_o, \tag{C.2c}$$

where $P_{load,n}, P_{gen,n} \in \mathbb{R}$ are the load demand and generation at node n. $P_n^+ \in \mathbb{R}$ is non-zero only at the slack bus. θ_n is the voltage phase angle and $X_{n,m}$ the reactance of line (n,m). DC power flow models are further detailed in [105, 106].

Appendix D

Test Network Parameters

The DC and AC-OPF models rely on costs for generator dispatch, highlighting that some units are more expensive to use than others. In the formulations proposed in this thesis, both quadratic and linear costs are associated with the active power output of a given unit: parameter α_n is the quadratic cost and β_n is the linear cost. These costs are provided for the generators of the IEEE 14-bus network and the PandaPower MultiVoltage network in Table D.1 and Table D.2, respectively. Each generator has active and reactive power limits, provided in Table D.3 and Table D.4 for each test network.

The power flow models used in this thesis account for the electrical characteristics of the grid elements. These characteristics include, among others, the line resistances and reactances (or line conductance and susceptance), and the shunt susceptances. Their values are provided in Table D.5, Table D.6, Table D.7 and Table D.8.

Bus	α_n	β_n
0	0.043	20
1	0.25	20
2	0.01	40

Table D.1: Quadratic (α_n) and linear (β_n) cost coefficients of generators.

Bus	α_n	β_n
0	0.0000	30.0000
1_{G_1}	0.0040	10.0000
1_{G_2}	0.0147	18.5821
5_{G_1}	0.0060	14.0000
5_{G_2}	0.0060	14.0000
6_{G_1}	0.0100	18.0000
6_{G_2}	0.0448	29.4750
7_{G_1}	0.0180	24.0000
7_{G_2}	0.0366	20.9573
8	0.0250	32.0000
12	0.0427	25.3179
13_{G_1}	0.0400	48.0000
13_{G_2}	0.0333	23.4086
14	0.0550	65.0000
16	0.0000	79.1209
18	0.0000	76.7936
23	0.0000	73.3515
24	0.0000	55.8392
25	0.0000	64.0016
26	0.0000	51.3141

Table D.2: Quadratic (α_n, €/MW^2) and linear (β_n, €/MW) cost coefficients of all generators. The constant term $\gamma_n = 0$ for all units. Subscripts G_1 and G_2 distinguish the two generators connected to the same bus; buses 1, 5, 6, 7, and 13 each host two generation units. Buses 16–26 contain small generators with purely linear costs ($\alpha_n = 0$).

Bus	P_{min} (MW)	P_{max} (MW)	Q_{min} (MVAr)	Q_{max} (MVAr)
0	0.0	332.4	−150	150
1	0.0	140.0	−80	80
2	0.0	150.0	−90	90

Table D.3: Active and reactive power limits of generators in the modified IEEE 14-bus network.

Bus	P_{min} (MW)	P_{max} (MW)	Q_{min} (MVAr)	Q_{max} (MVAr)
0	0.0	2500.000	−2000.000	2000.000
1	0.0	330.721	−191.969	191.969
5	0.0	274.177	−157.215	157.215
6	0.0	125.651	−69.108	69.108
7	0.0	141.842	−78.013	78.013
8	0.0	60.000	−30.000	30.000
12	0.0	78.537	−43.196	43.196
13	0.0	121.516	−64.334	64.334
14	0.0	40.000	−20.000	20.000
16	0.0	3.925	−1.570	1.570
18	0.0	4.037	−1.615	1.615
23	0.0	1.077	−0.431	0.431
24	0.0	2.527	−1.011	1.011
25	0.0	2.169	−0.867	0.867
26	0.0	4.670	−1.868	1.868

Table D.4: Active and reactive power limits of generators in the PandaPower MultiVoltage network.

#	n	m	R_{nm} (Ω)	X_{nm} (Ω)	C_{nm} (nF)
0	0	1	3.532005	10.783732	768.4848
1	0	4	9.846967	40.649040	716.0881
2	1	2	8.563928	36.080033	637.4931
3	1	3	10.590547	32.134320	494.8576
4	1	4	10.379138	31.689630	503.5904
5	2	3	12.212573	31.170217	186.2993
6	3	4	2.433038	7.674548	0
7	5	10	4.1×10^{-5}	8.6×10^{-5}	0
8	5	11	5.3×10^{-5}	1.11×10^{-4}	0
11	8	13	5.5×10^{-5}	1.17×10^{-4}	0
12	9	10	3.5×10^{-5}	8.3×10^{-5}	0
13	11	12	9.6×10^{-5}	8.6×10^{-5}	0

Table D.5: Line parameters of the modified IEEE 14-bus network (series resistance, reactance, and capacitance). The horizontal rule separates HV transmission lines from near-zero-impedance internal connections.

#	n	m	R_{nm} (Ω)	X_{nm} (Ω)	C_{nm} (nF)
0	1	2	1.885200	4.80000	264.00
1	2	3	1.256800	3.20000	176.00
2	3	5	1.885200	4.80000	264.00
3	2	5	0.942600	2.40000	132.00
4	4	5	1.571000	4.00000	220.00
5	1	4	1.885200	4.80000	264.00
6	7	8	0.096600	0.07020	409.50
7	8	9	0.096600	0.07020	409.50
8	9	10	0.096600	0.07020	409.50
9	10	11	0.096600	0.07020	409.50
10	11	12	0.096600	0.07020	409.50
11	12	13	0.096600	0.07020	409.50
12	13	14	0.096600	0.07020	409.50
13	7	14	0.096600	0.07020	409.50
14	15	16	0.007200	0.00256	21.12
15	16	17	0.007200	0.00256	21.12
16	17	18	0.007200	0.00256	21.12
17	18	19	0.007200	0.00256	21.12
18	19	20	0.007200	0.00256	21.12
19	15	21	0.010800	0.00384	31.68
20	21	22	0.010800	0.00384	31.68
21	22	23	0.090091	0.01680	1.32
22	23	24	0.090091	0.01680	1.32
23	22	25	0.090091	0.01680	1.32
24	25	26	0.090091	0.01680	1.32

Table D.6: Line parameters of the PandaPower MultiVoltage network.

#	n	m	G_{nm} (S)	B_{nm} (S)	B^{sh}_{nm} (S)
0	0	1	2.743×10^{-2}	-8.375×10^{-2}	2.414×10^{-4}
1	0	4	5.629×10^{-3}	-2.324×10^{-2}	2.250×10^{-4}
2	1	2	6.228×10^{-3}	-2.624×10^{-2}	2.003×10^{-4}
3	1	3	9.252×10^{-3}	-2.807×10^{-2}	1.555×10^{-4}
4	1	4	9.334×10^{-3}	-2.850×10^{-2}	1.582×10^{-4}
5	2	3	1.090×10^{-2}	-2.781×10^{-2}	5.853×10^{-5}
6	3	4	3.754×10^{-2}	-1.184×10^{-1}	0
7	5	10	4.517×10^{3}	-9.474×10^{3}	0
8	5	11	3.503×10^{3}	-7.336×10^{3}	0
11	8	13	3.291×10^{3}	-7.001×10^{3}	0
12	9	10	4.313×10^{3}	-1.023×10^{4}	0
13	11	12	5.780×10^{3}	-5.178×10^{3}	0

Table D.7: Per-line admittances of the modified IEEE 14-bus network: series conductance $G_{nm} = R_{nm}/(R^2_{nm} + X^2_{nm})$, series susceptance $B_{nm} = -X_{nm}/(R^2_{nm} + X^2_{nm})$, and shunt susceptance $B^{\mathrm{sh}}_{nm} = 2\pi f\, c_{nm}\, \ell_{nm}$ ($f = 50$ Hz).

#	n	m	G_{nm} (S)	B_{nm} (S)	B^{sh}_{nm} (S)
0	1	2	7.089×10^{-2}	-1.805×10^{-1}	8.294×10^{-5}
1	2	3	1.063×10^{-1}	-2.707×10^{-1}	5.529×10^{-5}
2	3	5	7.089×10^{-2}	-1.805×10^{-1}	8.294×10^{-5}
3	2	5	1.418×10^{-1}	-3.610×10^{-1}	4.147×10^{-5}
4	4	5	8.507×10^{-2}	-2.166×10^{-1}	6.912×10^{-5}
5	1	4	7.089×10^{-2}	-1.805×10^{-1}	8.294×10^{-5}
6	7	8	6.774×10^{0}	-4.923×10^{0}	1.286×10^{-4}
7	8	9	6.774×10^{0}	-4.923×10^{0}	1.286×10^{-4}
8	9	10	6.774×10^{0}	-4.923×10^{0}	1.286×10^{-4}
9	10	11	6.774×10^{0}	-4.923×10^{0}	1.286×10^{-4}
10	11	12	6.774×10^{0}	-4.923×10^{0}	1.286×10^{-4}
11	12	13	6.774×10^{0}	-4.923×10^{0}	1.286×10^{-4}
12	13	14	6.774×10^{0}	-4.923×10^{0}	1.286×10^{-4}
13	7	14	6.774×10^{0}	-4.923×10^{0}	1.286×10^{-4}
14	15	16	1.233×10^{2}	-4.384×10^{1}	6.635×10^{-6}
15	16	17	1.233×10^{2}	-4.384×10^{1}	6.635×10^{-6}
16	17	18	1.233×10^{2}	-4.384×10^{1}	6.635×10^{-6}
17	18	19	1.233×10^{2}	-4.384×10^{1}	6.635×10^{-6}
18	19	20	1.233×10^{2}	-4.384×10^{1}	6.635×10^{-6}
19	15	21	8.220×10^{1}	-2.923×10^{1}	9.953×10^{-6}
20	21	22	8.220×10^{1}	-2.923×10^{1}	9.953×10^{-6}
21	22	23	1.073×10^{1}	-2.000×10^{0}	4.147×10^{-7}
22	23	24	1.073×10^{1}	-2.000×10^{0}	4.147×10^{-7}
23	22	25	1.073×10^{1}	-2.000×10^{0}	4.147×10^{-7}
24	25	26	1.073×10^{1}	-2.000×10^{0}	4.147×10^{-7}

Table D.8: Per-line admittances of the PandaPower MultiVoltage network. Horizontal rules separate high-voltage, medium-voltage, and low-voltage sections.

Appendix E

Internship and Collaboration

This thesis was carried out as part of a Master's internship within the Smart Grid Lab of the Montefiore Institute at the University of Liège, under the supervision of Professor Damien Ernst. The Montefiore Institute is the Department of Electrical Engineering and Computer Science of the Faculty of Applied Sciences, and is one of Belgium's leading research centres in power systems, machine learning, and artificial intelligence. The Smart Grid Lab, which is part of this institute, hosts about 20 doctoral and post-doctoral researchers.

The research activity of the Smart Grid Lab covers two different fields. The first is the energy transition, with a focus on the integration of distributed energy resources, and the application of optimisation and machine learning techniques to power system control and planning. The second, more recently developed, direction concerns the application of artificial intelligence to the defense sector.

The work presented in this thesis was conducted in the context of active collaborations with industrial partners. As mentioned in the preface, the research was carried out in close partnership with Réseau de Transport d'Électricité (RTE), the French transmission system operator, and Gérédis Deux-Sèvres, a French distribution system operator.

The sustained engagement of the Smart Grid Lab with industrial actors is a defining feature of its research culture. In this spirit, a spotlight presentation of the work developed during this internship was delivered to the R&D team of RTE during an internal PhD day organised by the company [107]. This occasion provided a valuable opportunity to initiate discussions on the practical deployment challenges associated with TSO/DSO coordination frameworks.

At the academic level, this work also benefited from the longstanding collaboration between the Smart Grid Lab and the Intelligent Electrical Power Grids (IEPG) group at Delft University of Technology (TU Delft, Netherlands). This partnership, rooted in shared research interests in power system control and optimisation, provided complementary scientific perspectives that contributed to the development of the coordination framework presented in this thesis. A presentation offering insights into the mathematical formulation developed during this internship was delivered in this context and is referenced in [108].